

A NOVEL WEIGHTED AVERAGE CURRENT CONTROL METHOD WITH  
EMBEDDED ACTIVE DAMPING FOR GRID TIED INVERTERS WITH LCL  
FILTER

by

Arunodai Chanda

A thesis submitted to the faculty of  
The University of North Carolina at Charlotte  
in partial fulfillment of the requirements  
for the degree of Master of Science in  
Electrical Engineering

Charlotte

2019

Approved by:

---

Dr. Madhav Manjrekar

---

Dr. Robert Cox

---

Dr. Valentina Cecchi

©2019  
Arunodai Chanda  
ALL RIGHTS RESERVED

## ABSTRACT

ARUNODAI CHANDA. A Novel weighted average current control method with embedded active damping for grid tied inverters with LCL filter. (Under the direction of DR. MADHAV MANJREKAR)

Various kind of filters have been used to interconnect PWM inverters to the utility grid. Among those filters, LCL filter is widely used for many applications because it can reduce more harmonics of an injected grid current, as compared to other filters. However, it has a poor impact on the stability of the system. Furthermore, it increases the level of difficulty in designing the controller of the system, if only grid current is used for the feedback control. To improve the system controller design, the Weighted Average Current Control (WACC) method has been proposed, where the weighted average of the inverter-side current and the grid-side current is used as a control parameter. This method reduces the order of the system to a first order. However, this method stabilizes the weighted average current instead of an injected grid current. The injected grid current is shown to be only marginally stable. In order to make the system more robust and stable, various damping methods have been introduced such as passive and active damping.

In passive damping method, a resistor is connected in series with the LCL capacitor, which helps in damping the LCL resonance. Whereas, in active damping method, an extra-feedback of capacitor voltage or current state are utilized to increase the damping behavior of the system. Due to power losses issue in passive damping method, efficiency of the system decreases. Hence, the WACC with passive damping method is not desirable. Likewise, the WACC with active damping method also has a drawback of a more complex controller design because of the use of an extra-feedback loop in the controller. In order to

overcome these limitations in both damping methods, a new current control method has been proposed and implemented, which has been investigated in this dissertation. By applying this new method, the gain of an inverter-side current is shown to be higher than that of the grid-side current. In this method, the current gains help in providing damping to the system, which improves system stability. Therefore, the system with this new method is actively damped with no additional feedback loop. Hence, this new method is named as the Weighted Average Current Controller with Embedded Active Damping (WACC\_EAD) method. The robustness of the system under various conditions is also analyzed for WACC\_EAD method. The dynamic stiffness of a system for various current control methods have been derived to analyze the stiffness of injected grid current. Simulations using MATLAB Simulink and Typhoon and hardware experimental results using PICCOLO-F28035 controller have been demonstrated to validate the theoretical analysis.

## TABLE OF CONTENTS

LIST OF TABLES	viii
LIST OF FIGURES	ix
CHAPTER 1: INTRODUCTION	1
1.1. Introduction	1
1.2. Filters and current control methods	2
1.3. Organization of thesis	5
CHAPTER 2: LITERATURE REVIEW	8
2.1. Introduction	8
2.2. LCL Filters	9
2.3. Conventional Current Control Method	12
2.4. Weighted Average Current Control Method	15
2.5. Damping Methods	20
CHAPTER 3: WEIGHTED AVERAGE CURRENT CONTROL METHOD WITH EMBEDDED ACTIVE DAMPING	29
3.1. Introduction	29
3.2. Graphical analysis of $K_1$ and $K_2$	30
CHAPTER 4: MATHEMATICAL ANALYSIS	32
4.1. Introduction	32
4.2. New expressions of $K_1$ and $K_2$ and its stability analysis	33
4.3. Comparative assessment of the transfer functions of WACC, WACC with Active Damping and WACC_EAD methods.	37
CHAPTER 5: MODELING AND SIMULATION RESULTS	42
5.1. Introduction	42

5.2. MATLAB Simulink and Typhoon model of an undamped WACC Method and their simulation results	43
5.3. MATLAB Simulink and Typhoon model of a WACC with Passive Damping Method and their simulation result.	50
5.4. MATLAB Simulink and Typhoon model of a WACC with Active Damping Method and their simulation result	53
5.5. MATLAB Simulink and Typhoon model of a WACC_EAD Method and their simulation result.	57
CHAPTER 6: EXPERIMENTAL VERIFICATION	60
6.1. Introduction	60
6.2. Experimental Setup	61
6.3. Hardware Results	63
CHAPTER 7: ROBUSTNESS OF A SYSTEM	68
7.1. Introduction	68
7.2. Test of robustness of a system for various grid conditions	69
7.3. Test of robustness of a system for various damping factor, $K_d$	74
CHAPTER 8: DYNAMIC STIFFNESS	80
8.1. Introduction	80
8.2. Dynamic stiffness characteristic of a WACC method	80
8.3. Dynamic stiffness characteristic of a WACC with Active Damping method	82
8.4. Dynamic stiffness characteristic of a WACC_EAD method	83
CHAPTER 9: CONCLUSION AND FUTURE WORK	84
9.1. Introduction	84
9.2. Contributions	85
9.3. Future Work	86

REFERENCES	87
APPENDIX	92

## LIST OF TABLES

TABLE 1: Parameters of the Three-Phase Grid-Tied Inverter	13
TABLE 2: Harmonics (THD) of injected grid current for various current control Method from simulations	59
TABLE 3: Harmonics (THD) of injected grid current for various types of current control methods from hardware experiments	67
TABLE 4: Performance of a system under strong and weak grid conditions	74
TABLE 5: Performance of a system for various damping factor, $K_d$	79

## LIST OF FIGURES

FIGURE 1: Simplified schematic of a three-phase grid-tied inverter with LCL filter	3
FIGURE 2: Simplified circuit schematic of L filter	9
FIGURE 3: Simplified circuit schematic of LCL filter	10
FIGURE 4: Control schematic of Conventional Current Control Method	13
FIGURE 5: Pole-Zero map of a three-phase grid-tied LCL filtered inverter - CCC method	14
FIGURE 6: Step Response of a three-phase grid-tied LCL filtered inverter - CCC method	15
FIGURE 7: Control schematic of Weighted Average Current Control Method - Undamped	18
FIGURE 8: Pole-Zero map of a three-phase grid-tied LCL filtered inverter - WACC (Undamped) method	19
FIGURE 9: Step Response of a three-phase grid-tied LCL filtered inverter - WACC (Undamped) method	19
FIGURE 10: Bode plot of a closed loop three-phase grid-tied LCL filtered inverter system - WACC (Undamped) method	20
FIGURE 11: Simplified schematic of a three-phase grid-tied inverter with LCL filter – Passive Damping	21
FIGURE 12: Control schematic of Weighted Average Current Control Method – Passive Damping	21
FIGURE 13: Pole-Zero map of a three-phase grid-tied LCL filtered inverter - WACC (Passive Damping) method	22
FIGURE 14: Step Response of a three-phase grid-tied LCL filtered inverter - WACC (Passive Damping) method	23
FIGURE 15: Bode plot of a closed loop three-phase grid-tied LCL filtered inverter system - WACC (Passive Damping) method	23
FIGURE 16: Control schematic of Weighted Average Current Control Method - Active Damping	25

FIGURE 17: Pole-Zero map of a three-phase grid-tied LCL filtered inverter – WACC (Active Damping) method	26
FIGURE 18: Step Response of a three-phase grid-tied LCL filtered inverter – WACC (Active Damping) method	26
FIGURE 19: Bode plot of a closed loop three-phase grid-tied LCL filtered inverter system - WACC (Active Damping) method	27
FIGURE 20: Graph of Current Gains	30
FIGURE 21: Control schematic of Weighted Average Current Controller with Embedded Active Damping Method	33
FIGURE 22: Pole-Zero map of a three-phase grid-tied LCL filtered inverter – WACC_EAD method	34
FIGURE 23: Step Response of a three-phase grid-tied LCL filtered inverter – WACC_EAD method	35
FIGURE 24: Bode plot of a closed loop three-phase grid-tied LCL filtered inverter system – WACC_EAD method	35
FIGURE 25: Graph of current gains for the parameter values of table 2.1	36
FIGURE 26: MATLAB Simulink model of a three-phase LCL filtered grid-tied inverter – WACC	44
FIGURE 27: Weighted Average Current of each phase in MATLAB Simulink	45
FIGURE 28: Controller design of a WACC method (Undamped) in MATLAB Simulink	45
FIGURE 29: Grid Voltage and Grid Current – WACC (Undamped)	46
FIGURE 30: THD of a Grid Current – WACC	46
FIGURE 31: Typhoon model of a three-phase LCL filtered grid-tied inverter – WACC	47
FIGURE 32: Weighted Average Current of each phase in Typhoon	48
FIGURE 33: Controller design of a WACC method (Undamped) in Typhoon	48
FIGURE 34: Grid Voltage and Grid Current – WACC (Undamped)	49

FIGURE 35: MATLAB Simulink model of a three-phase LCL filtered grid-tied inverter – WACC (Passive Damping)	50
FIGURE 36: Grid Voltage and Grid Current – WACC with Passive Damping	51
FIGURE 37: THD of a Grid Current – WACC (Passive Damping)	51
FIGURE 38: Typhoon model of a three-phase LCL filtered grid-tied inverter – WACC (Passive Damping)	52
FIGURE 39: Grid Voltage and Grid Current – WACC with Passive Damping	52
FIGURE 40: Controller design of a WACC with Active Damping method in MATLAB Simulink	53
FIGURE 41: Grid Voltage and Grid Current – WACC with Active Damping	54
FIGURE 42: THD of a Grid Current – WACC (Active Damping)	54
FIGURE 43: Weighted Average Current of each phase	55
FIGURE 44: Controller design of a WACC with Active Damping method	56
FIGURE 45: Grid Voltage and Grid Current – WACC with Active Damping	56
FIGURE 46: Grid Voltage and Grid Current – WACC_EAD	57
FIGURE 47: THD of a Grid Current – WACC_EAD	58
FIGURE 48: Grid Voltage and Grid Current – WACC_EAD	58
FIGURE 49: Experimental setup of Typhoon HIL 603 interfaced with the PICCOLO-F28035 controller	61
FIGURE 50: PICCOLO-F28035 Controller	62
FIGURE 51: Grid Voltage and Grid Current – WACC	63
FIGURE 52: Grid Voltage and Grid Current – WACC with Passive Damping	64
FIGURE 53: Grid Voltage and Grid Current – WACC with Active Damping	65
FIGURE 54: Grid Voltage and Grid Current – WACC_EAD	66
FIGURE 55: Graph of current gains for strong grid	70

FIGURE 56: Pole-Zero plot - Strong Grid	71
FIGURE 57: Grid Voltage and Grid Current- Strong Grid	71
FIGURE 58: Graph of current gains for a weak grid	72
FIGURE 59: Pole-Zero plot - Weak Grid	73
FIGURE 60: Grid Voltage and Grid Current – Weak Grid	73
FIGURE 61: Graph of current gains for higher $K_d$	75
FIGURE 62: Pole-Zero plot for higher $K_d$	76
FIGURE 63: Grid Voltage and Grid Current – Higher $K_d$	76
FIGURE 64: Graph of current gains for lower $K_d$	77
FIGURE 65: Pole-Zero plot for a lower $K_d$	78
FIGURE 66: Grid Voltage and Grid Current – Lower $K_d$	78
FIGURE 67: Dynamic stiffness (Magnitude plot) of a three-phase grid-tied LCL filtered inverter system – WACC (Undamped)	81
FIGURE 68: Dynamic stiffness (Magnitude plot) of a three-phase grid-tied LCL filtered inverter system – WACC with Active Damping	82
FIGURE 69: Dynamic stiffness (Magnitude plot) of a three-phase grid-tied LCL filtered inverter system – WACC_EAD	83

## CHAPTER 1: INTRODUCTION

### 1.1. Introduction

To substitute the conventional sources of energy such as petroleum, nuclear and thermal power and so on, renewable energy has been determined to be the most sustainable form of energy [1]. Renewable power generation highly depends on the renewable energy resources [2]. The use of renewable energy resources has been encouraged by the change in global climate and the current fossil-based generation system [3]. The efficient use of these resources depends on factors such as sunlight, wind etc. To interconnect the renewable energy and the grid, inverter have been used, which convert DC power produced by renewable energy sources into AC power used in domestic and residential areas [4]. Grid-tied inverter is also used to track the maximum DC power that can be extracted from the PV array [5]. To supply power to residential areas in the unavailability of energy, grid-tied inverter facilitates utility power pulling from the grid [6].

As inverter is used to interconnect renewable energy to the AC utility grid, the harmonics of current flowing into the grid increases. Hence, various filters have been used, in order to minimize those harmonics. In this chapter, various current control methods of the three-phase grid-tied inverter system have been discussed to know the advantages and disadvantages of all the methods. A new current control method has been introduced in order to make the system stable, robust, efficient and less complex.

## 1.2. Filters and Current Control Methods

The PWM inverters are used to interconnect renewable energy and the utility grid [7]. However, such inverters produce unwanted current harmonics, which flow into the grid. To reduce those harmonics, filters like L, LC and LCL have been used. Among these filters, LCL filter is a third order filter and it provides better attenuation of high-frequency current harmonics [8]-[10] flowing into the grid. Thus, converters with high switching frequency and filters with high inductance values are not required [11]. This makes the LCL filter, a better and an extensively used filter for many applications. However, it is vulnerable to stability issues in the system [12] because it triggers the resonance between the inverter and the grid [13]. The transfer function of an LCL filtered system from inverter output to the grid current contains complex conjugate poles at the resonant frequency [14]. Under such conditions, if an injected grid current is used for the feedback control then the controller design of the system becomes complex because of its higher order. In order to overcome this shortcoming, Weighted Average Current Control Method (WACC) has been introduced. In this method, the weighted average of the inverter-side current and the grid-side current is employed to perform the feedback control [15]-[17]. The transfer function of an LCL filtered system from inverter output to the weighted average current is of first order instead of a third order [18]. Therefore, this method makes the controller design of the system simpler and it also improves the dynamic performance of the system [19]. However, the WACC method not only controls the weighted average current but it also controls the grid current indirectly. By using this method, the grid-side current is marginally stable even though the weighted average current may be easily stabilized [20]. The complex conjugate poles at the resonance frequency still exist in the injected grid

current [21]. Thus, the WACC method simplifies the controller design of the system but it doesn't make the system stable [15]. In order to make the system stable, various damping methods like passive damping, active damping etc. have been implemented [22], [23]. Thus, the weighted average current control method has been improved by applying these damping methods [21].

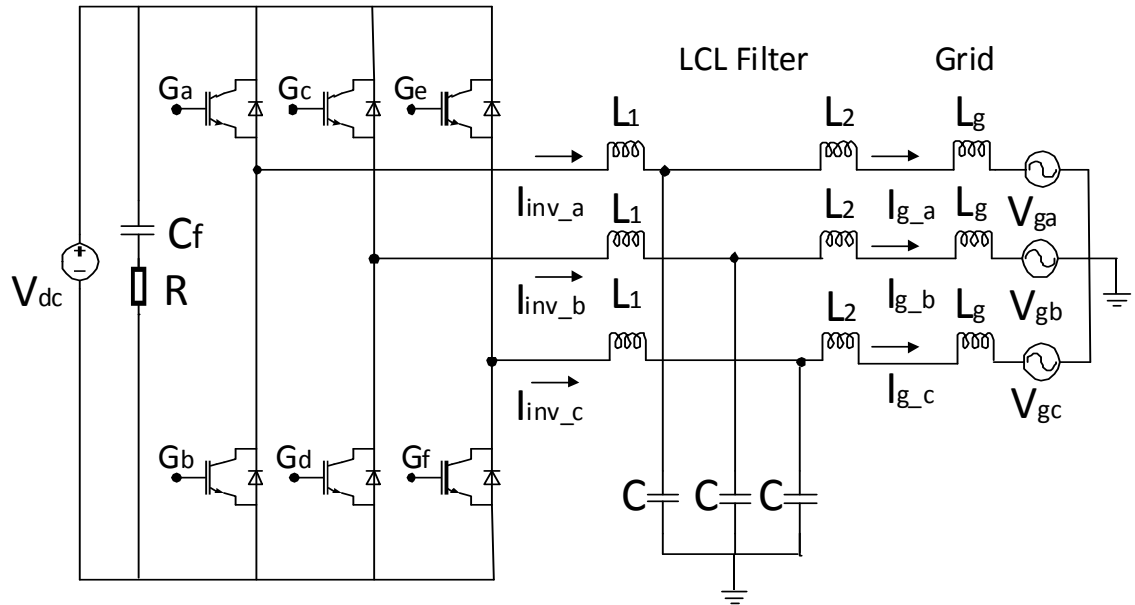


**Figure 1.1: Simplified schematic of a three-phase grid-tied inverter with LCL filter**

In passive damping method, a resistor is connected in series with the capacitor of an LCL filter [24]. As we increase this resistance value, the gain at resonant frequency will get suppressed [25], which increases the stability of the system. Implementation of this method is very simple as there is no alteration required in the controller design of the system. However, it also increases the losses in the system, which decreases systems efficiency [26]. Thus, this method is not reliable to use [27]. To overcome these limitations, an active damping method has been proposed. In this method, an extra-feedback of capacitor current or voltage state is employed in damping the LCL resonance [28], [29]. In

the literature, the current flowing through the capacitor of an LCL filter is used as an extra feedback, in order to restrain the harmonics of an injected grid current [30]-[32]. This method is more efficient than the passive damping method because it alters the controller design of the system instead of a power circuit [33]. However, it increases the complexity in the controller design of the system [34]-[36].

Since there is an issue of efficiency in a passive damping method and an issue of complex controller design in an active damping method, a new current control method has been proposed. In this new method, an active damping has been embedded into a weighted average current controller. That's why it has been called as the Weighted Average Current Controller with Embedded Active Damping (WACC\_EAD) method. In this method, a new equation of both the inverter-side current gain and the grid-side current gain has been derived. With the help of this new equation, the gain of the inverter-side current will always be higher than that of the grid-side current. This makes the system stable without using any external damping methods. Thus, no modification has been made in the power circuit and no extra-feedback has been implemented in the controller design of the system. This makes the overall system more efficient and less complex. In order to test the robustness of the system with WACC\_EAD method, the system stability has been analyzed under strong and weak grid conditions. The equation of the gain of both the inverter-side current and the grid-side current contains a damping factor. With the increases of this damping factor, the inverter-side current gain increases and the grid-side current gain decreases. Thus, the testing of the robustness of the system has also been done by varying the damping factor value.

For designing the controller of the system of all the current control methods (discussed in this book), F28035 PICCOLO Experimenter's Kit have been used. The coding for the controller design has been done in Code Composer Studio using C language. After designing the controller, the PICCOLO has been interfaced with the Typhoon Hardware-in-loop (HIL), where a three-phase grid-tied inverter is designed.

### 1.3. Organization of thesis

This dissertation is organized in the following format.

#### Chapter 1: Introduction

A brief introduction of renewable energy and grid-tied inverter has been provided in the first part. The latter part describes various current control methods for the three-phase grid-tied inverter system with LCL filter.

#### Chapter 2: Literature Review

This chapter compares the performance of filters like L and LCL to interconnect the PWM inverter and the utility grid. The stability analysis of current control methods like WACC, WACC with Passive Damping and WACC with Active Damping has been examined using pole-zero map and step response of the closed loop system.

#### Chapter 3: Weighted Average Current Control Method with Embedded Active Damping

A new current control method, WACC\_EAD for a three-phase LCL filtered grid-tied inverter has been proposed. The graph of inverter-side current gain and grid-side current gain has been presented to show the stability region of the system.

#### Chapter 4: Mathematical Analysis

The equation of inverter-side current gain and the grid side current gain has been derived. The stability analysis of a new current control methods, WACC\_EAD has been

examined using pole-zero map and step response of the closed loop system. The comparative evaluation of the transfer function of a system for WACC, WACC with Active Damping and WACC\_EAD method has been done by substituting the equations of inverter-side current gain and grid-side current gain. The relationship between the extra-feedback loop gain of WACC with Active Damping method and the damping factor of WACC\_EAD method has been derived.

#### Chapter 5: Modeling and Simulation Results

The three-phase grid-tied LCL filtered inverter system has been designed in Typhoon and MATLAB/Simulink for various current control methods. The total harmonic distortion of an injected grid current has been compared for various cases. The simulation waveforms have also been presented.

#### Chapter 6: Experimental Verifications

The experimental setup of Typhoon Hardware-in-loop (HIL) interfaced with PICCOLO F28035 controller has been shown. The hardware result of injected grid current and grid voltage of the three-phase grid-tied LCL filtered inverter system for various current control methods have been presented.

#### Chapter 7: Robustness of a System

The robustness of the system for WACC\_EAD method has been tested for various grid conditions and damping factor. The simulation waveforms of Typhoon have been presented. The graph of the gains of inverter-side current and that of grid-side current has been examined to analyze the stability of the system.

#### Chapter 8: Dynamic Stiffness

The dynamic stiffness characteristic of a three-phase grid-tied LCL filtered inverter system has been analyzed for various current control method.

#### Chapter 9: Conclusion and Future Work

This chapter concludes with a discussion on the various current control methods for a three-phase grid-tied LCL filtered inverter system. Future scope with regards to current estimation of the inverter-side current and stability of multiple inverters connected to grid has been discussed.

## CHAPTER 2: LITERATURE REVIEW

### 2.1. Introduction

The PWM inverters produces unwanted current harmonics, which flows into the grid section [37]. To reduce those harmonics, various filters like L, LCL etc. have been used in the past. Among them, LCL filter can attenuate 60 dB/decade for frequencies above resonant frequency [39] because of third order. On the other hand, first order filters like L may diminish only 20 dB/decade for all frequencies. Thus, converters with lower switching frequency and filters with lower inductance value may be used, in case of an LCL filter [40]-[42]. This makes the LCL filter a more desired filter for many applications [37], [38]. The transfer function of an L and LCL filter has been derived in this chapter to show the order of the filter.

The comparative assessment of various current control methods like Conventional Current Control (CCC), Weighted Average Current Control (WACC), WACC with passive damping, WACC with active damping of a three-phase LCL filtered grid-tied inverter system has been presented in this chapter. The transfer function of a closed-loop system for all the current control methods has been derived. The transfer function of the compensator is also derived for designing the controller. The pole-zero map and step response of a system has been plotted for all the current control methods, to analyze the stability of a system. The bode-plot of a closed-loop system is also examined to analyze the harmonics of an injected grid-current for various cases.

## 2.2. LCL filter

The schematic of an L filter is shown in figure 2.1. Here,  $V_{inv}$  represents the output voltage across the inverter,  $V_g$  denotes the grid voltage,  $L$  is an inductance and  $I_g$  indicate injected grid current.

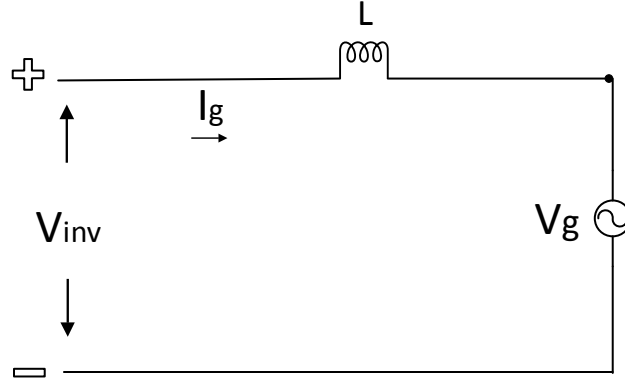


**Figure 2.1: Simplified circuit schematic of L filter**

The transfer function from  $V_{inv}$  to  $I_g$  has been derived in (2.11) using state space analysis.  $I_g$  is a state variable. Let  $x = I_g$ .

$$V_{inv} = L \frac{dI_g}{dt} + V_g \quad (2.1)$$

Since  $I_g$  is the controlled variable, let output,  $y = I_g$ .

$$[\dot{x}] = \begin{bmatrix} 1 & -1 \\ L & L \end{bmatrix} \begin{bmatrix} V_{inv} \\ V_g \end{bmatrix} \quad (2.2)$$

$$[y] = [1][x] \quad (2.3)$$

By comparing the above equations with  $\dot{x} = Ax + Bu$  and  $y = Cx + Du$ , the following things may be determined as:

$$A = [0] \quad (2.4)$$

$$B = \begin{bmatrix} 1 & -1 \\ L & L \end{bmatrix} \quad (2.5)$$

$$C = [1] \quad (2.6)$$

$$D = [0] \quad (2.7)$$

$$\text{Transfer function, } G(s) = C(sI - A)^{-1}B + D \quad (2.8)$$

$$G(s) = [1][s]^{-1} \begin{bmatrix} 1 & 1 \\ L & -L \end{bmatrix} + 0 \quad (2.9)$$

$$G(s) = \begin{bmatrix} 1 & 1 \\ sL & -sL \end{bmatrix} \quad (2.10)$$

$$\text{Transfer function, } \frac{I_g}{V_{inv}} = \frac{1}{sL} \quad (2.11)$$

The schematic of an LCL filter is shown in figure 2.2. Here,  $V_{inv}$  represents the output voltage across the inverter,  $V_g$  denotes the grid voltage,  $L_1$  is an inductance of inverter side,  $L_2$  is an inductance of grid side,  $C$  is the capacitance,  $V_c$  represents the voltage across the capacitor and  $I_{inv}$  and  $I_g$  indicates the inverter side current and the injected grid current respectively.

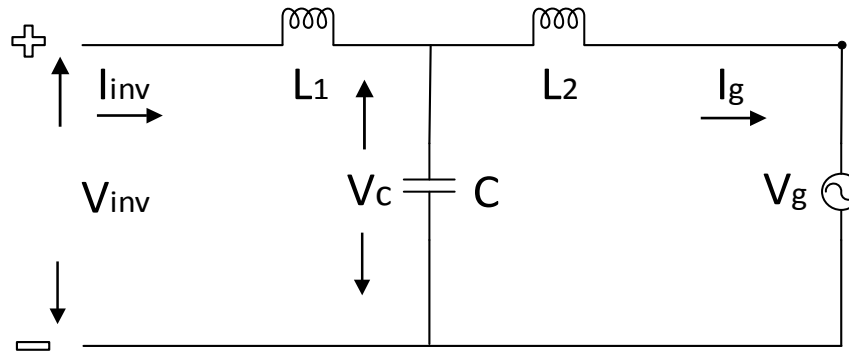


**Figure 2.2: Simplified circuit schematic of LCL filter**

The transfer function from  $V_{inv}$  to  $I_g$  has been derived in (2.26) using state space analysis.  $I_{inv}$ ,  $V_c$  and  $I_g$  are the state variables. Let  $x_1 = I_{inv}$ ,  $x_2 = V_c$  and  $x_3 = I_g$ .

$$V_{\text{inv}} = L \frac{dI_g}{dt} + V_g \quad (2.12)$$

$$V_c = L_2 \frac{dI_g}{dt} + V_g \quad (2.13)$$

$$\dot{x}_1 = -\frac{x_2}{L_1} + \frac{V_{\text{inv}}}{L_1} \quad (2.14)$$

$$\dot{x}_3 = \frac{x_2}{L_2} + \frac{V_g}{L_2} \quad (2.15)$$

$$\dot{x}_2 = \frac{x_1}{C} - \frac{x_3}{C} \quad (2.16)$$

Since  $I_g$  is the controlled variable, let output,  $y = I_g$ .

$$\begin{bmatrix} \dot{x}_1 \\ \dot{x}_2 \\ \dot{x}_3 \end{bmatrix} = \begin{bmatrix} 0 & -\frac{1}{L_1} & 0 \\ \frac{1}{C} & 0 & -\frac{1}{C} \\ 0 & \frac{1}{L_2} & 0 \end{bmatrix} \begin{bmatrix} x_1 \\ x_2 \\ x_3 \end{bmatrix} + \begin{bmatrix} \frac{1}{L_1} & 0 \\ 0 & 0 \\ 0 & -\frac{1}{L_2} \end{bmatrix} \begin{bmatrix} V_{\text{inv}} \\ V_g \end{bmatrix} \quad (2.17)$$

$$[y] = [0 \quad 0 \quad 1] \begin{bmatrix} x_1 \\ x_2 \\ x_3 \end{bmatrix} \quad (2.18)$$

By comparing the above equations with  $\dot{x} = Ax + Bu$  and  $y = Cx + Du$ , the following things may be determined as:

$$A = \begin{bmatrix} 0 & -\frac{1}{L_1} & 0 \\ \frac{1}{C} & 0 & -\frac{1}{C} \\ 0 & \frac{1}{L_2} & 0 \end{bmatrix} \quad (2.19)$$

$$B = \begin{bmatrix} \frac{1}{L_1} & 0 \\ 0 & 0 \\ 0 & -\frac{1}{L_2} \end{bmatrix} \quad (2.20)$$

$$C = [0 \quad 0 \quad 1] \quad (2.21)$$

$$D = [0] \quad (2.22)$$

$$\text{Transfer function, } G(s) = C(sI - A)^{-1}B + D \quad (2.23)$$

$$G(s) = [0 \quad 0 \quad 1] \left[ \begin{array}{ccc} s & 0 & 0 \\ 0 & s & 0 \\ 0 & 0 & s \end{array} \right] - \left[ \begin{array}{ccc} 0 & -\frac{1}{L_1} & 0 \\ \frac{1}{C} & 0 & -\frac{1}{C} \\ 0 & \frac{1}{L_2} & 0 \end{array} \right]^{-1} \left[ \begin{array}{c} \frac{1}{L_1} \\ 0 \\ 0 \end{array} \right] \left[ \begin{array}{c} 0 \\ 0 \\ -\frac{1}{L_2} \end{array} \right] \quad (2.24)$$

$$G(s) = \left[ \begin{array}{cc} \frac{1}{L_1 L_2 C} & -\frac{s^2}{L_2} - \frac{1}{L_1 L_2 C} \\ \frac{s}{s^3 + \frac{s}{L_2 C} + \frac{s}{L_1 C}} & \frac{s}{s^3 + \frac{s}{L_2 C} + \frac{s}{L_1 C}} \end{array} \right] \quad (2.25)$$

$$\text{Transfer function, } \frac{I_g}{V_{inv}} = \frac{\frac{1}{L_1 L_2 C}}{s^3 + \frac{s}{L_2 C} + \frac{s}{L_1 C}} = \frac{1}{L_1 L_2 C s^3 + (L_1 + L_2)s} \quad (2.26)$$

The transfer functions derived in (2.11) and (2.26) are the transfer functions from the output voltage across the inverter,  $V_{inv}$  to the injected grid current,  $I_g$  of L filter and LCL filter respectively. It has been observed that the transfer function of an L filter is of first order, whereas, the transfer function of an LCL filter is of third order [37]-[39]. Thus, the LCL filter is a more desired filter, as compared to an L filter, for the attenuation of high frequency current harmonics [40]-[42]. However, the use of LCL filter affects the stability of the system and makes the controller design complex [43].

### 2.3. Conventional Current Control Method

The current control method where the grid current is employed as a feedback signal is known as Conventional Current Control Method (CCC).

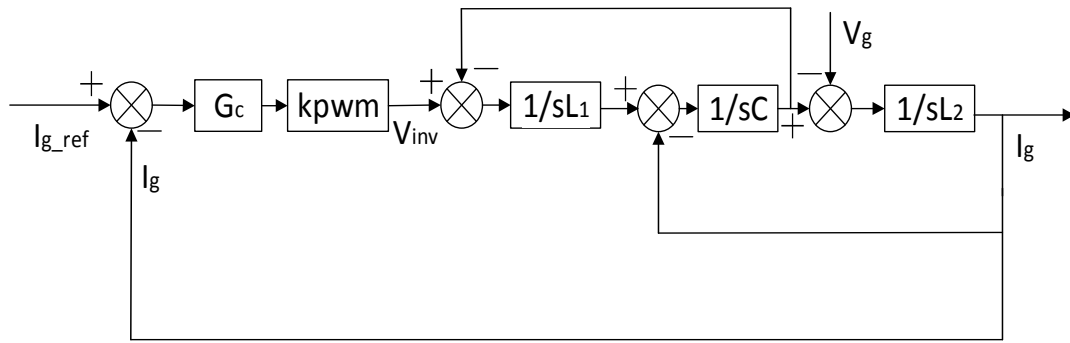


Figure 2.3: Control schematic of Conventional Current Control Method

Table 2.1: Parameters of the Three-Phase Grid-Tied Inverter

Parameter	Values
Inverter side inductance, $L_1$	0.6 mH
Grid side inductance, $L_2$	0.2 mH
Grid inductance, $L_g$	0.2 mH
Capacitance, $C$	30 $\mu$ F
Injected grid power, $P_g$	7 kW
Grid voltage, $V_g$	120 V rms
Injected grid current, $I_g$	27.5 A peak
DC link voltage, $V_{dc}$	400 V
Switching frequency, $f_{sw}$	10 kHz
Amplitude of the triangular carrier wave, $V_{tri}$	1 p.u.

Here,  $kpwm$  is the transfer function of the PWM inverter, which is defined as  $V_{dc}/V_{tri}$  [15].  $G_c$  is the transfer function of the compensator.

$$G_c = \frac{4s+3+0.0001s^2}{s} \quad (2.27)$$

From equation 2.27, it may be seen that the compensator used for controlling the injected grid current is a Proportional Integral Derivative (PID) compensator. This compensator will help in making the steady state error of the system zero because of an integrator. It also increases the phase margin of the system because of a differentiator. However, the gain value of a differentiator should be very small because the derivative controller increases the steady state error of the system.

The closed-loop transfer function of a three-phase grid-tied inverter with LCL filter for CCC method has been derived in (2.28) from the reference current,  $I_{g\_ref}$  to the injected grid current,  $I_g$  by using the control schematic shown in figure 2.3.

$$\frac{I_g}{I_{g\_ref}} = \frac{G_c k_{pwm}}{L_1 L_2 C s^3 + (L_1 + L_2) s + G_c k_{pwm}} \quad (2.28)$$

The pole-zero map and the step response of a system has been plotted for analyzing the stability of a system, by using the parameter values of table 2.1.

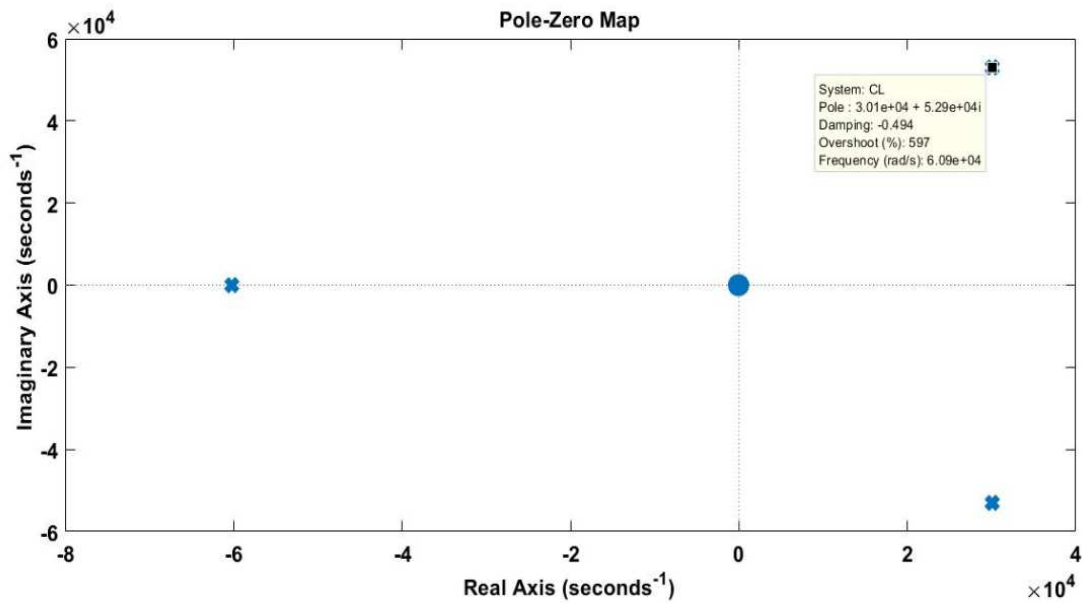
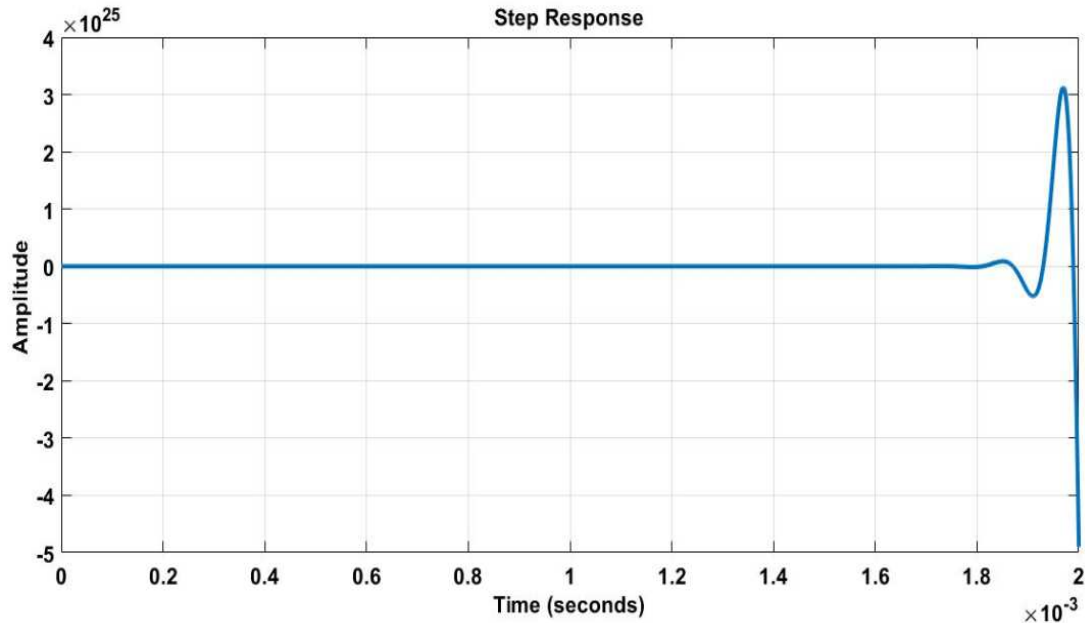


Figure 2.4: Pole-Zero map of a three-phase grid-tied LCL filtered inverter - CCC method

From figure 2.4, it may be seen that the system contains complex conjugate poles in the right half of s-plane. The closed-loop poles are located at  $3.01e4 + 5.29e4i$  and  $3.01e4 - 5.29e4i$ . Thus, the system is unstable. The step response of a system shown in figure 2.5 also shows the instability of a system.



**Figure 2.5: Step Response of a three-phase grid-tied LCL filtered inverter - CCC method**

From the stability analysis of a CCC method, it may be said that the controller of a three-phase grid-tied LCL-filtered inverter system is complex to design, if the injected grid current is used for the feedback control. Stability of a system gets affected by using an LCL filter [44].

#### 2.4. Weighted Average Current Control Method

It has been noticed in the previous section that it is not simple to design the controller of the system, if the injected grid current is used to perform the feedback control because the transfer function from the output voltage across the inverter,  $V_{inv}$  to the injected grid current,  $I_g$  of an LCL filter is of third order as shown in (2.26). Inverter-side current,  $I_{inv}$

has also been considered for the feedback control. The transfer function from  $V_{inv}$  to  $I_{inv}$  of an LCL filter has been derived in (2.38) using state space analysis.  $I_{inv}$ ,  $V_c$  and  $I_g$  are the state variables. Let  $x_1 = I_{inv}$ ,  $x_2 = V_c$  and  $x_3 = I_g$ .

Since  $I_{inv}$  is the controlled variable, let output,  $y = I_{inv}$ .

$$\begin{bmatrix} \dot{x}_1 \\ \dot{x}_2 \\ \dot{x}_3 \end{bmatrix} = \begin{bmatrix} 0 & -\frac{1}{L_1} & 0 \\ \frac{1}{C} & 0 & -\frac{1}{C} \\ 0 & \frac{1}{L_2} & 0 \end{bmatrix} \begin{bmatrix} x_1 \\ x_2 \\ x_3 \end{bmatrix} + \begin{bmatrix} \frac{1}{L_1} & 0 \\ 0 & 0 \\ 0 & -\frac{1}{L_2} \end{bmatrix} \begin{bmatrix} V_{inv} \\ V_g \end{bmatrix} \quad (2.29)$$

$$[y] = [1 \quad 0 \quad 0] \begin{bmatrix} x_1 \\ x_2 \\ x_3 \end{bmatrix} \quad (2.30)$$

By comparing the above equations with  $\dot{x} = Ax + Bu$  and  $y = Cx + Du$ , the following things may be determined as:

$$A = \begin{bmatrix} 0 & -\frac{1}{L_1} & 0 \\ \frac{1}{C} & 0 & -\frac{1}{C} \\ 0 & \frac{1}{L_2} & 0 \end{bmatrix} \quad (2.31)$$

$$B = \begin{bmatrix} \frac{1}{L_1} & 0 \\ 0 & 0 \\ 0 & -\frac{1}{L_2} \end{bmatrix} \quad (2.32)$$

$$C = [1 \quad 0 \quad 0] \quad (2.33)$$

$$D = [0] \quad (2.34)$$

$$\text{Transfer function, } G(s) = C(sI - A)^{-1}B + D \quad (2.35)$$

$$G(s) = [1 \quad 0 \quad 0] \left[ \begin{array}{ccc} s & 0 & 0 \\ 0 & s & 0 \\ 0 & 0 & s \end{array} \right] - \left[ \begin{array}{ccc} 0 & -\frac{1}{L_1} & 0 \\ \frac{1}{C} & 0 & -\frac{1}{C} \\ 0 & \frac{1}{L_2} & 0 \end{array} \right]^{-1} \left[ \begin{array}{cc} \frac{1}{L_1} & 0 \\ 0 & 0 \\ 0 & -\frac{1}{L_2} \end{array} \right] \quad (2.36)$$

$$G(s) = \left[ \begin{array}{cc} \frac{s^2 + \frac{1}{L_1 L_2 C}}{s^3 + \frac{s}{L_2 C} + \frac{s}{L_1 C}} & -\frac{1}{L_1 L_2 C} \\ \frac{1}{L_1 L_2 C} & \frac{s^2 + \frac{1}{L_1 L_2 C}}{s^3 + \frac{s}{L_2 C} + \frac{s}{L_1 C}} \end{array} \right] \quad (2.37)$$

$$\text{Transfer function, } \frac{I_g}{V_{inv}} = \frac{\frac{s^2 + \frac{1}{L_1 L_2 C}}{s^3 + \frac{s}{L_2 C} + \frac{s}{L_1 C}}}{\frac{s^2 + \frac{1}{L_1 L_2 C}}{s^3 + \frac{s}{L_2 C} + \frac{s}{L_1 C}}} = \frac{L_2 C s^2 + 1}{L_1 L_2 C s^3 + (L_1 + L_2) s} \quad (2.38)$$

From (2.38), it has been found that the transfer function from the output voltage across the inverter,  $V_{inv}$  to the inverter side current,  $I_{inv}$  of an LCL filter is also of third order. Thus, the complexity in the controller design of the system may not be reduced, if the inverter-side current is used as feedback signal. To overcome from this limitation, the transfer function from the output voltage across the inverter,  $V_{inv}$  to the weighted average current,  $I_{wac}$  has been derived (2.41). Weighted average current is the weighted average of the inverter-side current and the grid-side current [45]. Here,  $K_1 = \frac{L_1}{(L_1 + L_2)}$  and  $K_2 = \frac{L_2}{(L_1 + L_2)}$  are the gain of the inverter-side current and the grid-side current respectively [46].

$$\frac{I_{wac}}{V_{inv}} = K_1 \frac{I_{inv}}{V_{inv}} + K_2 \frac{I_g}{V_{inv}} \quad (2.39)$$

$$\frac{I_{wac}}{V_{inv}} = \frac{L_1}{(L_1 + L_2)} \frac{L_2 C s^2 + 1}{L_1 L_2 C s^3 + (L_1 + L_2) s} + \frac{L_2}{(L_1 + L_2)} \frac{1}{L_1 L_2 C s^3 + (L_1 + L_2) s} \quad (2.40)$$

$$\text{Transfer function, } \frac{I_{wac}}{V_{inv}} = \frac{1}{(L_1 + L_2) s} \quad (2.41)$$

From (2.41), it has been noticed that the transfer function from the output voltage across the inverter,  $V_{inv}$  to the weighted average current,  $I_{wac}$  is of first order instead of a third [46]. Thus, if the weighted average current is used to perform the feedback control then the controller design of the system will become relatively simpler [47]. This method is called as the Weighted Average Current Control Method (WACC) [45]-[47].

Along with the weighted average current, this method also controls the current flowing into the grid indirectly. The current which is flowing into the grid section is not the weighted average current [46]. Thus, the performance of the system is analyzed by using method.

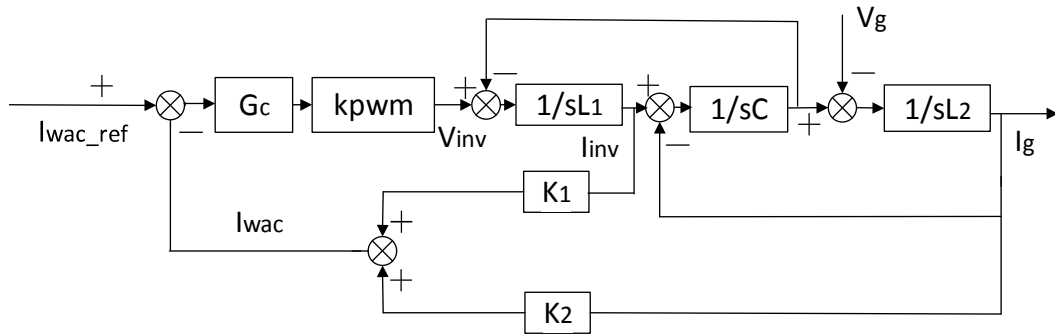


**Figure 2.6: Control schematic of Weighted Average Current Control Method - Undamped**

The closed-loop transfer function of a three-phase grid-tied inverter with LCL filter for WACC method has been derived in (2.42) from the reference current,  $I_{wac\_ref}$  to the injected grid current,  $I_g$  by using the control schematic shown in figure 2.6.

$$\frac{I_g}{I_{wac\_ref}} = \frac{G_c k_{pwm}}{L_1 L_2 C s^3 + (L_1 + L_2) s + G_c k_{pwm} (K_1 L_2 C s^2 + K_1 + K_2)} \quad (2.42)$$

By using the parameter values of table 2.1, it has been found that the  $K_1$  value is 0.6 and  $K_2$  value is 0.4. By using the compensator shown in (2.27), the closed-loop poles are found to be located at  $-4.55e-13 + 1.18e4i$  and  $-4.55e-13 - 1.18e4i$ . This is making the

system marginally stable as these two poles are located almost at the imaginary axis. The pole-zero map and the step response of a system has been examined for analyzing the stability of a system.

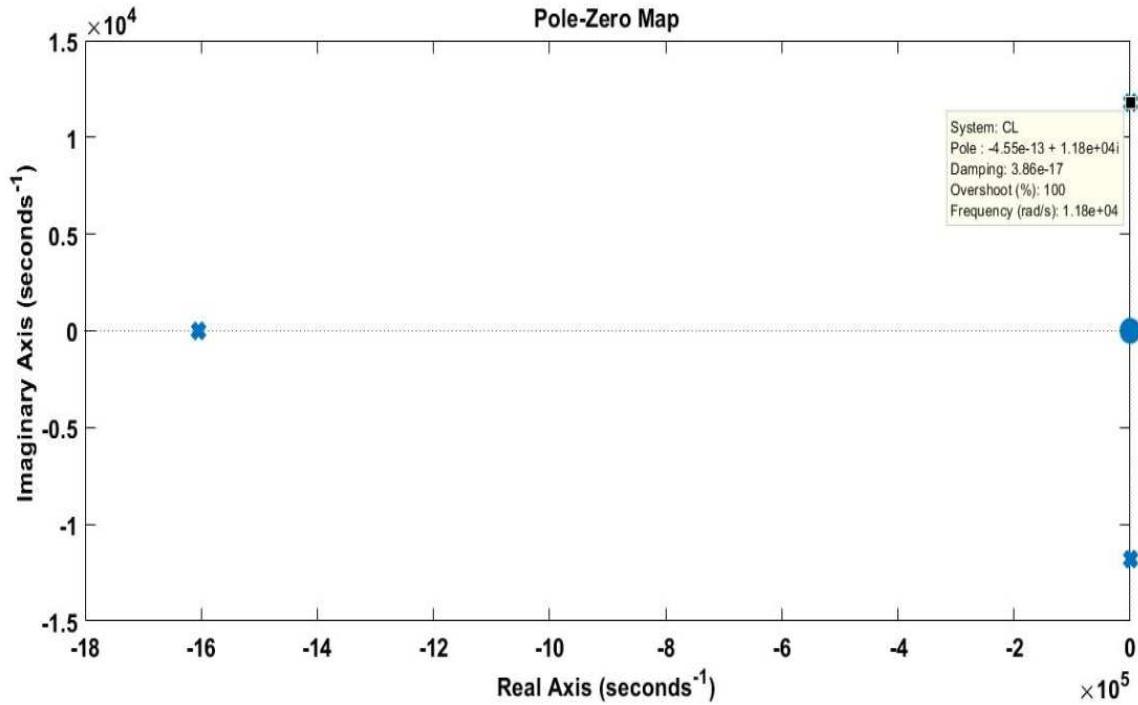


Figure 2.7: Pole-Zero map of a three-phase grid-tied LCL filtered inverter – WACC (Undamped) method

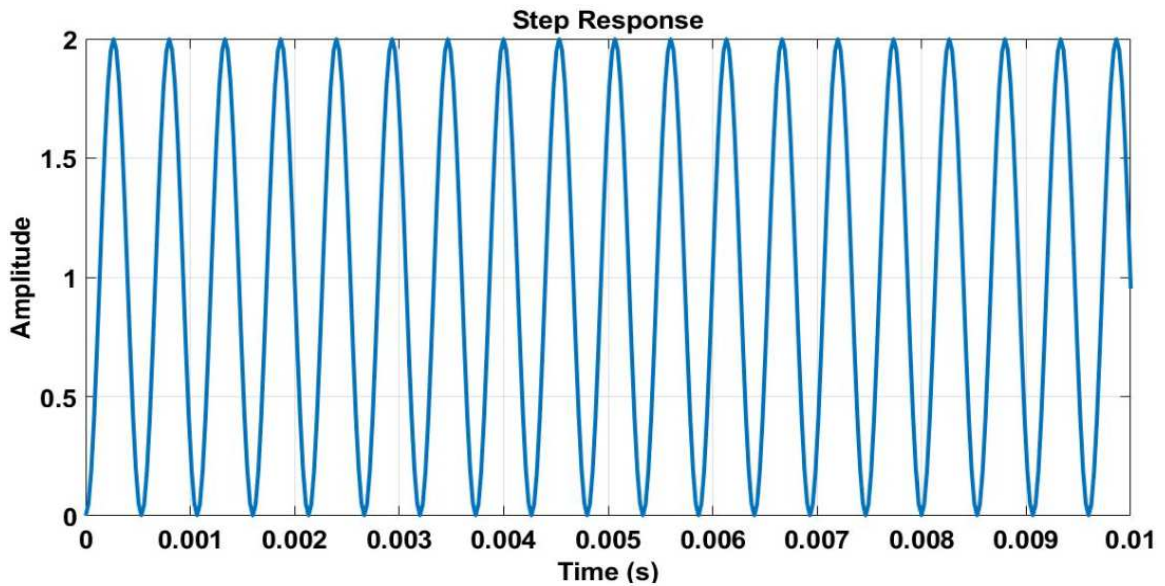
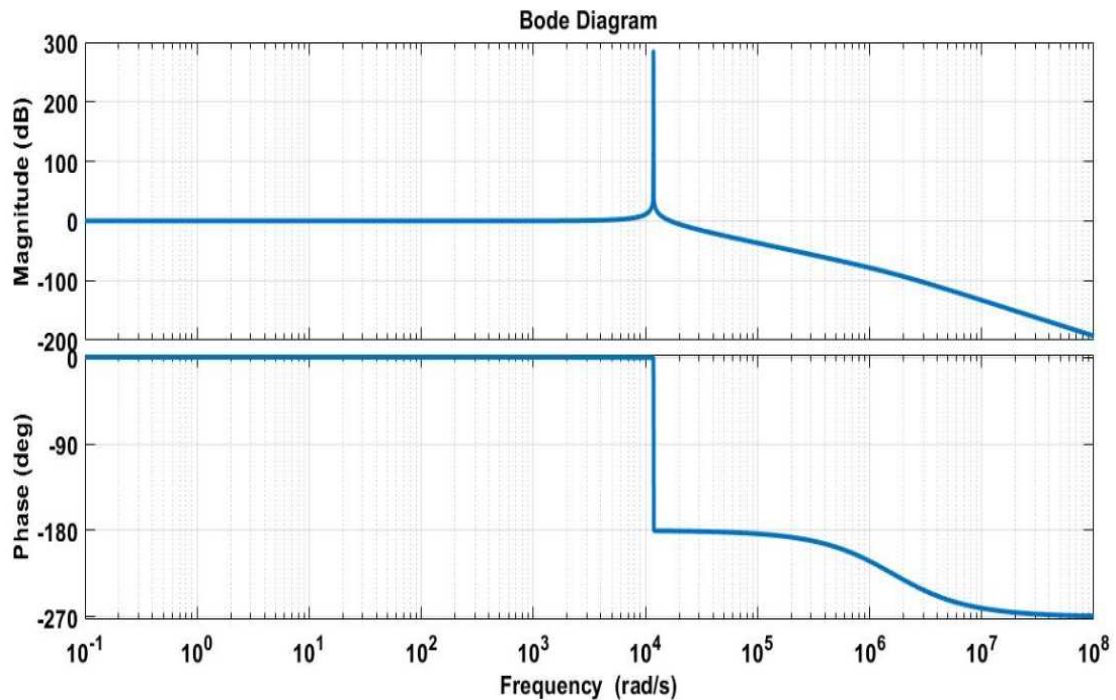


Figure 2.8: Step Response of a three-phase grid-tied LCL filtered inverter – WACC (Undamped) method

The pole-zero map shown in figure 2.7 confirms that the closed-loop poles are located at the imaginary axis, which is making the system marginally stable. Hence, the step response of this system is oscillating in nature, shown in figure 2.8. Therefore, the system is undamped. From the stability analysis of a WACC method, it has been inferred that the controller design of a three-phase grid-tied LCL-filtered inverter system is simplified but the system is not stable [15].



**Figure 2.9: Bode plot of a closed loop three-phase grid-tied LCL filtered inverter system - WACC (Undamped) method**

Due to the presence of the complex conjugate poles at the resonant frequency, there is a huge peak at that frequency, which can be observed in the bode plot of a closed loop system, shown in figure 2.9. Thus, the harmonics of an injected grid current will be higher.

## 2.5. Damping Methods

Since the WACC method doesn't make the system stable, damping methods like passive damping and active damping have been implemented. In passive damping, a resistor ( $R_d$ )

is connected in series with the capacitor of an LCL filter [48], as shown in figure 11. As this resistance value increases, the system becomes more stable and damped [49].

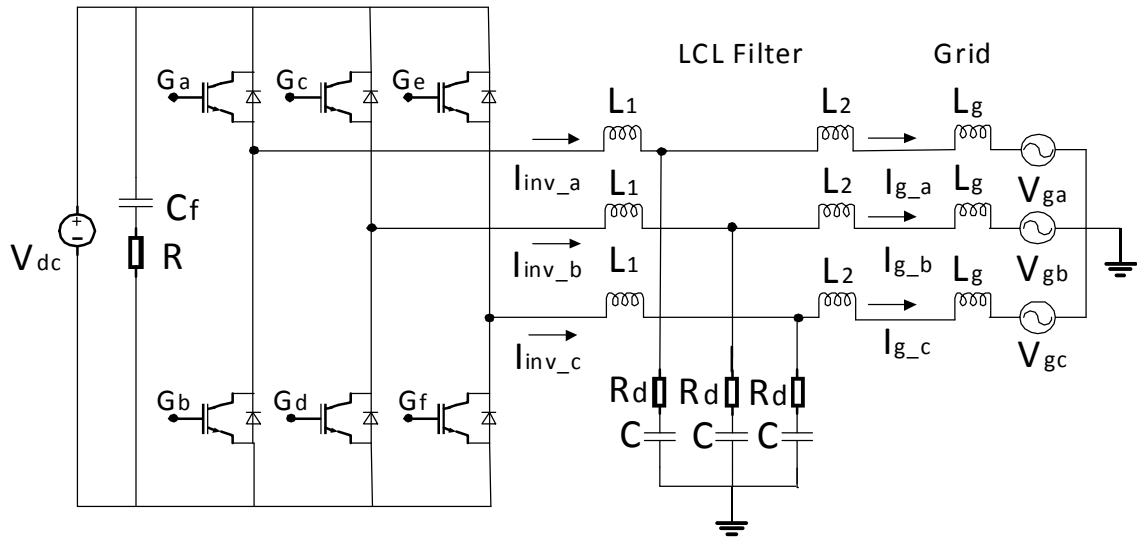


**Figure 2.10: Simplified schematic of a three-phase grid-tied inverter with LCL filter – Passive Damping**

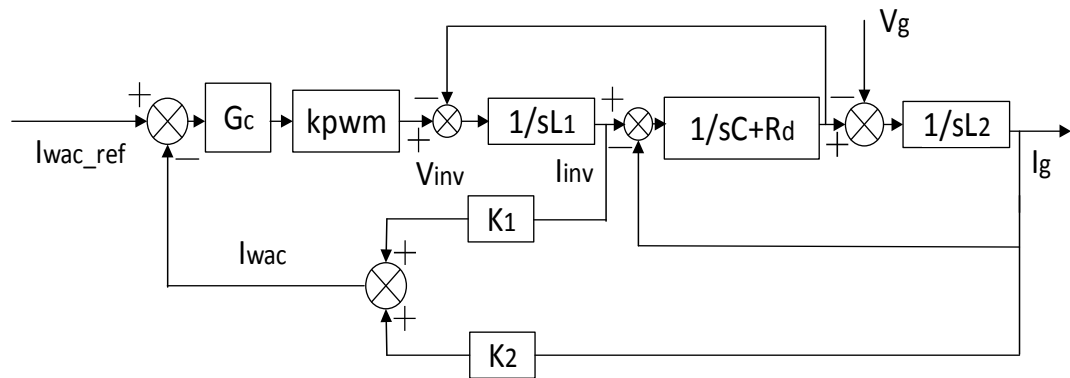


**Figure 2.11: Control schematic of Weighted Average Current Control Method – Passive Damping**

The closed-loop transfer function of a three-phase grid-tied inverter with LCL filter for WACC with Passive Damping method has been derived in (2.43) from the reference current,  $I_{wac\_ref}$  to the injected grid current,  $I_g$  by using the control schematic shown in figure 2.11.

$$\frac{I_g}{I_{wac\_ref}} = \frac{G_c k_{pwm}(1 + R_d Cs)}{L_1 L_2 Cs^3 + R_d C(L_1 + L_2)s^2 + (L_1 + L_2)s + G_c k_{pwm}(K_1 L_2 Cs^2 + (K_1 + K_2)(1 + R_d Cs))} \quad (2.43)$$

The parameter values shown in table 2.1 and compensator shown in (2.27) has been used for determining the location of the closed loop poles. The value of resistance  $R_d$  is considered as  $1 \Omega$ . The closed-loop poles are now located at  $-3.750e3 + 1.54e4i$  and  $-3.750e3 - 1.54e4i$ . They are shifted more towards the left half of s-plane, which makes the system stable [50]. The pole-zero map and the step response of a system has been examined for analyzing the stability of a system.

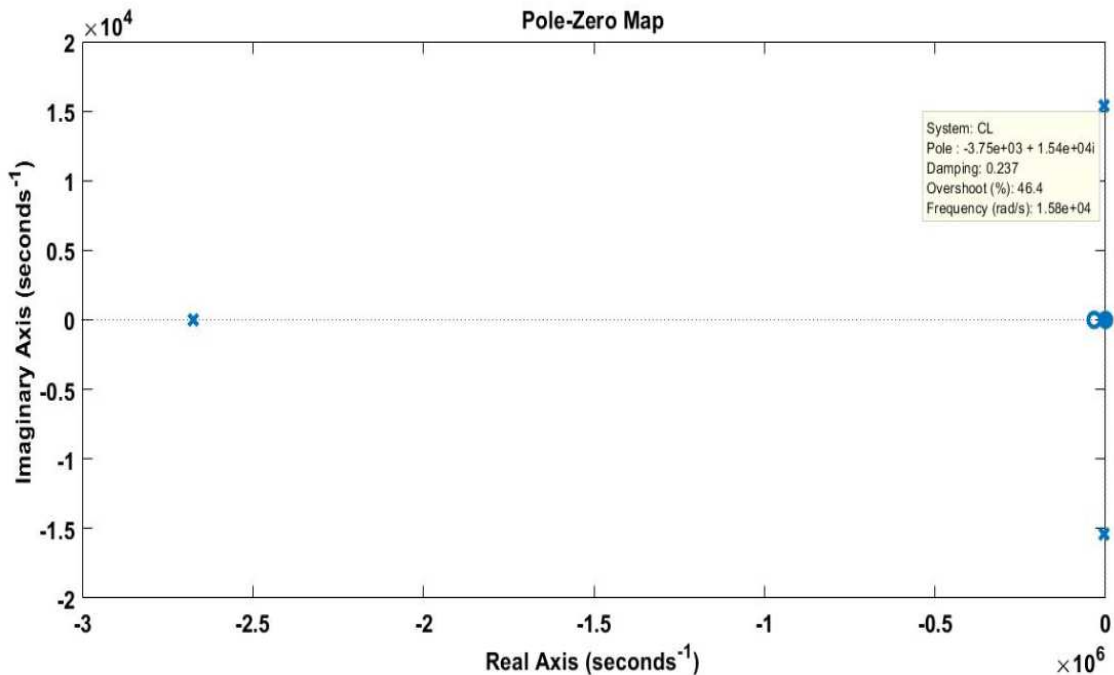


Figure 2.12: Pole-Zero map of a three-phase grid-tied LCL filtered inverter – WACC (Passive Damping) method

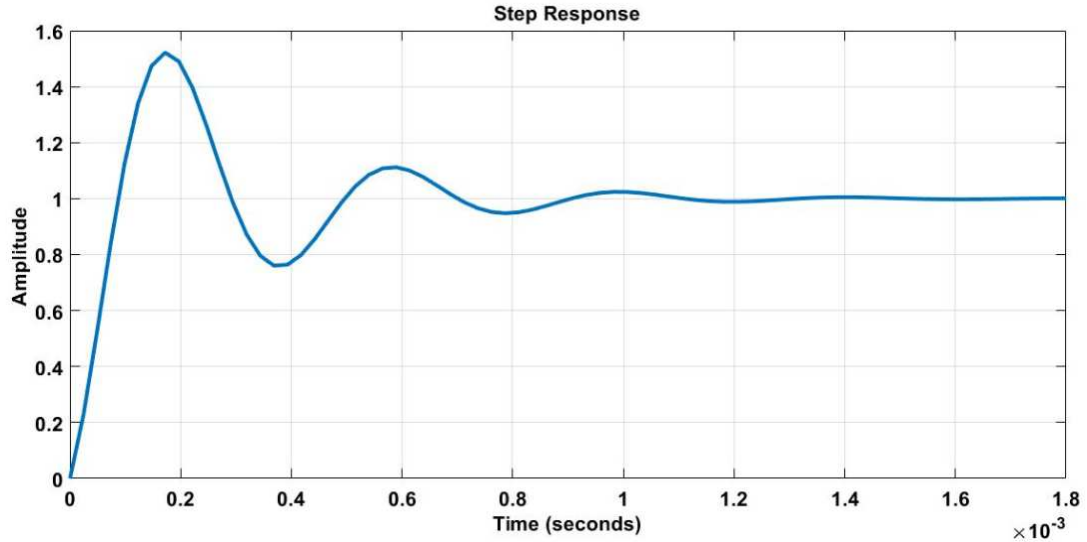


Figure 2.13: Step Response of a three-phase grid-tied LCL filtered inverter – WACC (Passive Damping) method

The pole-zero map shown in figure 2.12 confirms that the closed-loop poles are located at the left-half of s-plane, which is making the system stable. The system is now being called as an underdamped system instead of an undamped system. This underdamped behavior of the system can be observed in the step response of the system, shown in figure 2.13.

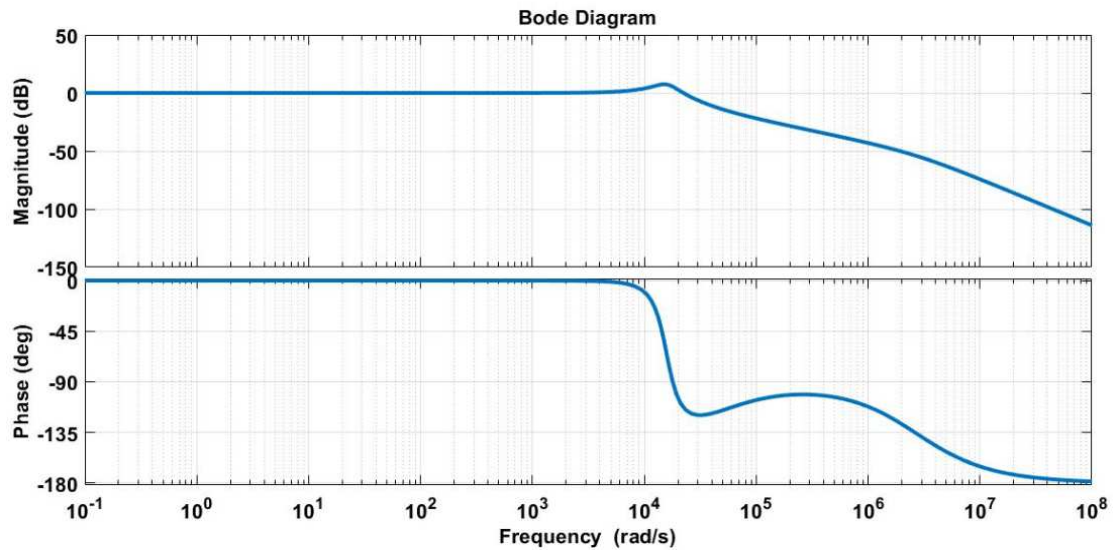
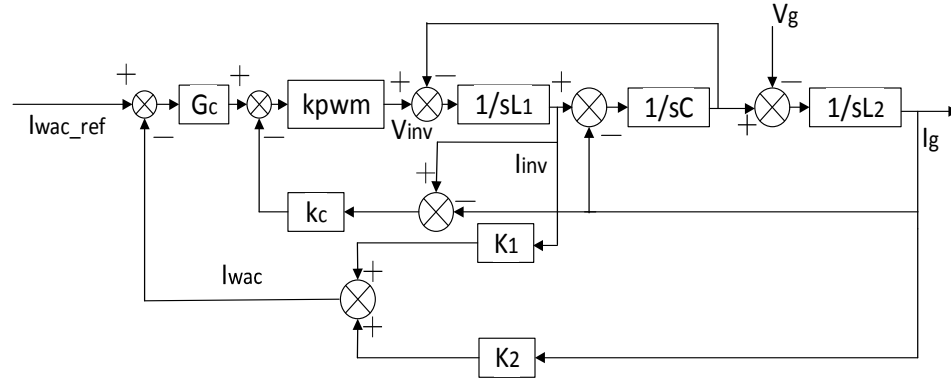


Figure 2.14: Bode plot of a closed loop three-phase grid-tied LCL filtered inverter system - WACC (Passive Damping) method

It may be deduced from the bode plot of the closed loop system, shown in figure 2.14 that with the implementation of the resistor  $R_d$ , the peak at the resonant frequency gets suppressed [24], [25]. Thus, the harmonics injected into the grid will also get reduced. As this resistance value of an LCL filter increases, the system will have less oscillations [26]. The system stability will also improve as the closed-loop poles of the system tends to shift more towards the left-half of s-plan. However, the effectiveness of an LCL filter gets reduced and this increases the power loss in the system, which further affects the efficiency of the entire system [27]. Thus, the passive damping method is very simple to implement [51] as there is only an inclusion of a resistor in an LCL filter and there is no modification required in the controller design of the system, but this method reduces systems efficiency. Therefore, it is not advisable to use a passive damping method for making the system stable.

In order to overcome the disadvantage of a passive damping method, another damping method called active damping have also been implemented [28], [29]. In this method, modification is done only in the controller design of the system instead of a power circuit [33]. Here, an extra-feedback of current or voltage state is employed to damp LCL resonance [30]-[32]. In this dissertation, the current flowing through the capacitor of an LCL is used for the extra-feedback [31]. This capacitor current is connected to a gain called extra-feedback gain,  $k_c$  [31]. As this  $k_c$  value increases, the system becomes more damped and stable [32].



**Figure 2.15: Control schematic of Weighted Average Current Control Method – Active Damping**

The closed-loop transfer function of a three-phase grid-tied inverter with LCL filter for WACC with Active Damping method has been derived in (2.44) from the reference current,  $I_{wac\_ref}$  to the injected grid current,  $I_g$  by using the control schematic shown in figure 2.15.

$$\frac{I_g}{I_{wac\_ref}} = \frac{G_c k_{pwm}}{L_1 L_2 C s^3 + k_{pwm} k_c L_2 C s^2 + (L_1 + L_2) s + G_c k_{pwm} (K_1 L_2 C s^2 + (K_1 + K_2))} \quad (2.44)$$

The parameter values shown in table 2.1 and compensator shown in (2.27) has been used for determining the location of the closed loop poles. The value of an extra-feedback gain (virtual resistance)  $k_c$  is considered as 1. From the calculations, it has been found that the complex-conjugate poles of a closed-loop system are now located at  $-10.6+8.71e3i$  and  $-10.6-8.71e3i$ . They are shifted towards the left half of s-plane, which makes the system stable. The pole-zero map and the step response of a system has been examined for analyzing the stability of a system.

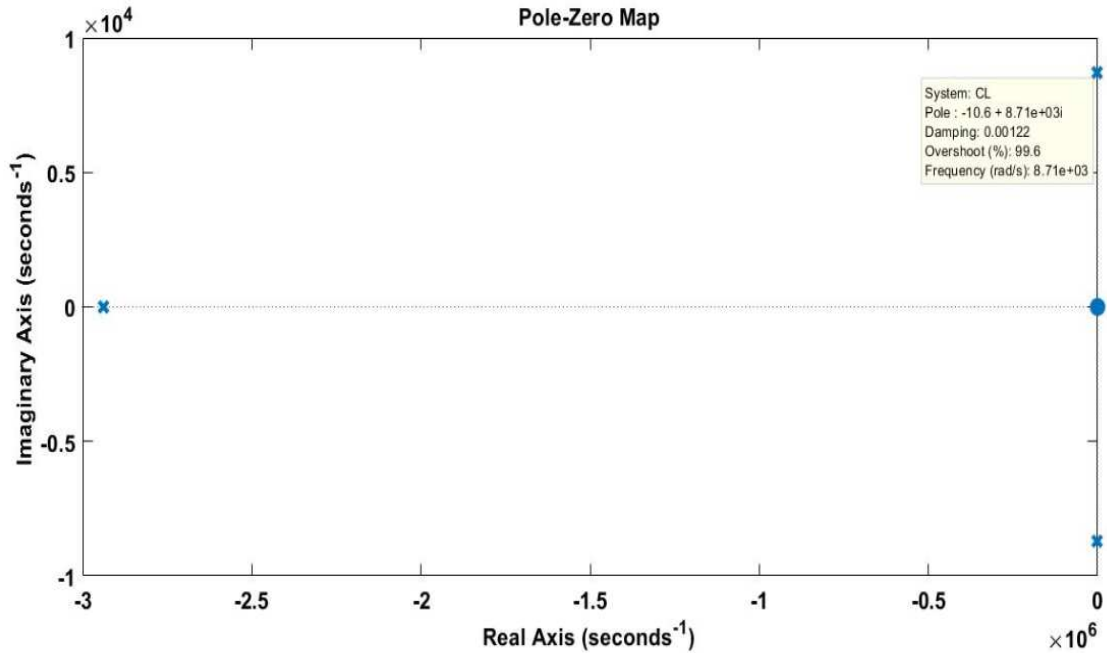


Figure 2.16: Pole-Zero map of a three-phase grid-tied LCL filtered inverter – WACC (Active Damping) method

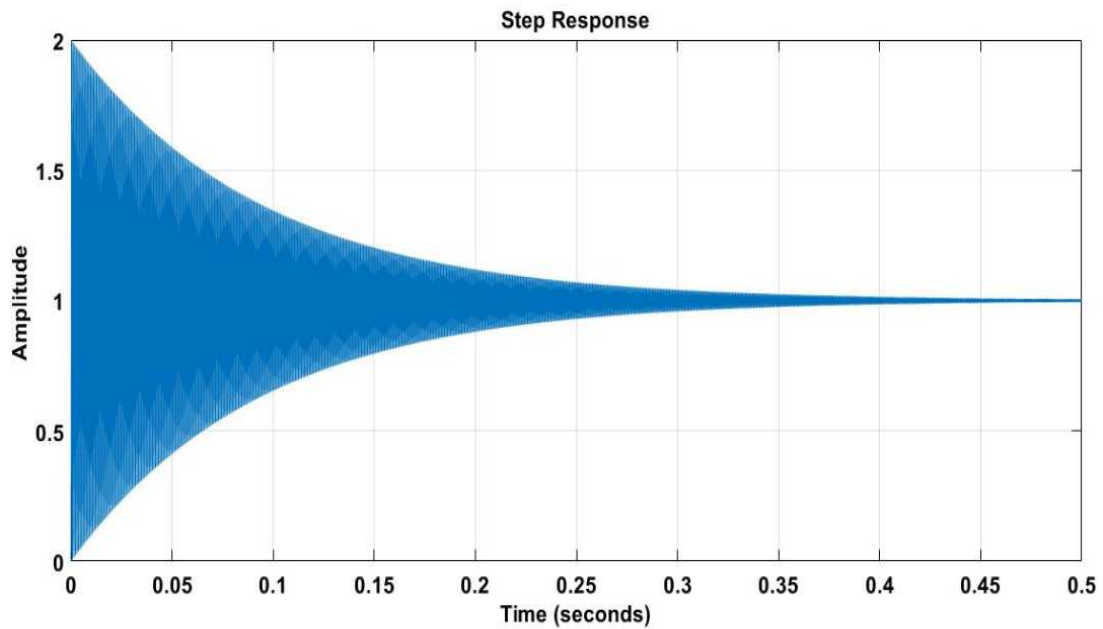
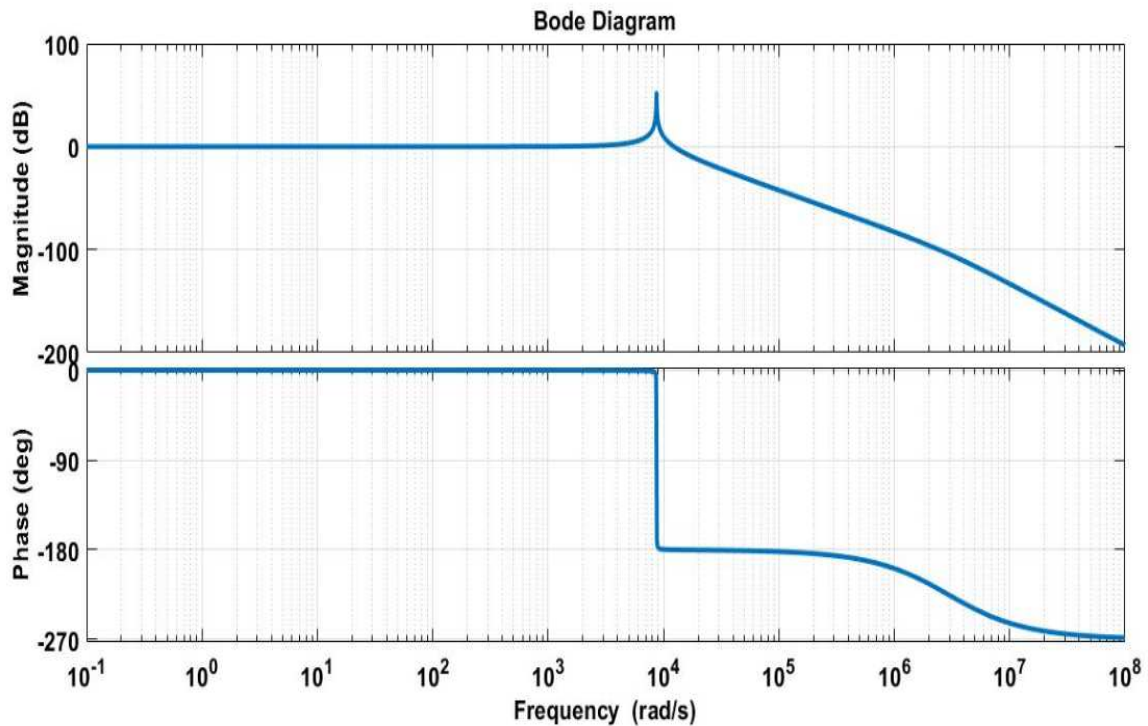


Figure 2.17: Step Response of a three-phase grid-tied LCL filtered inverter – WACC (Active Damping) method

The pole-zero map, shown in figure 2.16 confirms that the closed-loop poles are located at the left-half of the s-plane, which is making the system stable. This also makes the system

underdamped, which may be observed in the step response of the system, shown in figure 2.17.



**Figure 2.18: Bode plot of a closed loop three-phase grid-tied LCL filtered inverter system - WACC (Active Damping) method**

From the step response of both passive damping and active damping method, it has been noticed that the system is more damped in case of a passive damping method because the closed-loop poles are located more towards the left half of s-plane as compared to that of an active damping method. However, passive damping method has a drawback of less efficiency, which is not the case with the active damping. Thus, an active damping method is more efficient and desirable to use [52]. From the bode plot of the closed-loop system of an active damping method shown in figure 2.18, it has been observed that the peak at the resonant frequency is very less as compared to that of an undamped system. Thus, the harmonics of an injected grid current will also get reduced. Hence, with the inclusion of the extra-feedback with its gain  $k_c$ , the system becomes stable and damped [53], [54]. As

this  $k_c$  value increases, the system will have less oscillations. This will not reduce the effectiveness of an LCL filter unlike passive damping method [55], [56]. However, this method increases the complexity in the controller design of the system because of the extra-feedback loop.

## CHAPTER 3: WEIGHTED AVERAGE CURRENT CONTROL METHOD WITH EMBEDDED ACTIVE DAMPING

### 3.1. Introduction

In passive damping method, it has been found that the method is simple to implement but it leads to power losses in the system. This affects the efficiency of the entire system. Whereas in active damping method, the controller design is altered by adding an extra-feedback loop for the damping purpose. This method does not affect the efficiency of the system, but it does make the controller design of the system complex. Thus, a passive damping method has a drawback of less efficiency and an active damping method has a limitation of complex controller design. To overcome both these disadvantages, a new method has been proposed, which is known as the Weighted Average Current Controller with Embedded Active Damping (WACC\_EAD) method. In this new method, no resistor is connected in series with an LCL capacitor unlike passive damping and no extra-feedback loop is included in the controller design of the system unlike active damping.

As discussed, in a WACC method, the expressions of the gain of inverter side current,  $K_1$  and that of the grid side current,  $K_2$  was helping to make the controller design of the system simpler, but the system was not stable and damped. Thus, the damping methods, like passive damping and active damping have been implemented for the stability purpose. However, in the new method, the weighted average current controller is applied but the expressions of  $K_1$  and  $K_2$  is made in such a way that the system will be in a stable state, without using any external damping methods.  $K_1$  value will always be higher than  $K_2$ .

Here, with the help of  $K_1$  and  $K_2$  values, the system becomes actively damped. Therefore, in this method, the active damping is embedded into the weighted average current controller.

### 3.2. Graphical analysis of $K_1$ and $K_2$

In a WACC\_EAD method, the gain of the inverter side current is shown to be higher than that of the grid side current. Thus,  $K_1$  is always be greater than  $K_2$ . The system stability will get improved as the gain,  $K_1$  increases or the gain,  $K_2$  decreases. Whereas, if the gain  $K_2$  becomes larger than  $K_1$ , then the system will be unstable. Here, both  $K_1$  and  $K_2$  varies from 0 to 1 and the sum of  $K_1$  and  $K_2$  is always 1. Based on this relation, the graph of  $K_1$  vs  $K_2$  has been drawn in figure 3.1.

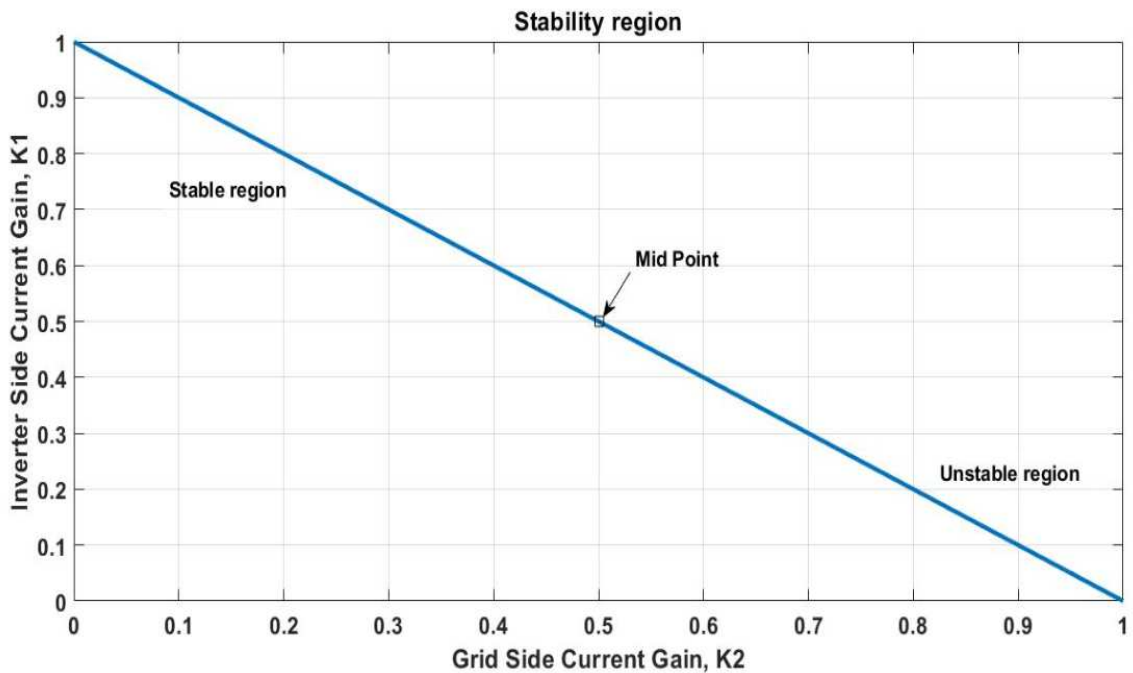


Figure 3.1: Graph of Current Gains

From figure 3.1, it has been observed that if the co-ordination point of  $K_1$  and  $K_2$  is in the left side of the mid-point, then the system is stable and if it is in the right side of the mid-point, then the system is unstable. This is because if the co-ordination point of  $K_1$  and

$K_2$  is in the left side of the mid-point, then the gain of the inverter side current will be higher than that of the grid side current. Whereas, if the co-ordination point of  $K_1$  and  $K_2$  is in the right side of the mid-point, then the gain of the inverter side current will be lesser than that of the grid side current.

## CHAPTER 4: MATHEMATICAL ANALYSIS OF A WACC\_EAD METHOD

### 4.1. Introduction

In WACC method, the equations of the inverter side current gain,  $K_1$  and the grid side current gain,  $K_2$  simplifies the controller design of the system. However, the system is only marginally stable. To make the system stable, damping methods like passive damping and active damping have been implemented. However, the passive damping method is less efficient, and the active damping method is more complex. Due to the shortcomings in both the damping methods, the equation of the inverter side current gain,  $K_1$  and the grid side current gain,  $K_2$  has been modified in this chapter. With the new equation,  $K_1$  value is shown to be higher than  $K_2$ . The system will remain stable as  $K_1$  is greater than  $K_2$ . Here, the system stability will depend on the values of  $K_1$  and  $K_2$ . Therefore, these new equations will provide active damping to the system without adding any extra-feedback loop in the controller design of the system. This new current control method is called as WACC\_EAD method.

The transfer function of a three-phase grid-tied LCL-filtered inverter system for WACC\_EAD method has been derived in this chapter. The pole-zero map and step response of a system has been plotted for WACC\_EAD method, to analyze the stability of a system. The bode-plot of a closed-loop system is also examined to analyze the harmonics of an injected grid-current. In addition to this, the comparative assessment of the transfer functions of WACC, WACC with Active Damping and WACC\_EAD method has been

done after substituting the equations of inverter-side current gain and the grid-side current gain.

#### 4.2. New expressions of $K_1$ and $K_2$ and its stability analysis

In a conventional WACC method,

$$K_1 = \frac{L_1}{(L_1+L_2)} \quad (4.1)$$

$$K_2 = \frac{L_2}{(L_1+L_2)} \quad (4.2)$$

In the proposed WACC\_EAD method,

$$K_1 = \frac{L_1 + \alpha K_d}{(L_1+L_2)} \quad (4.3)$$

$$K_2 = \frac{L_2 - \alpha K_d}{(L_1+L_2)} \quad (4.4)$$

Here,  $\alpha = L_1 L_2$  and  $K_d$  is a damping factor which may be varied from 1 to 1200. It is now being considered as 1000. From the above expression in (11), it may be inferred that in a WACC\_EAD method,  $K_1$  will always have higher value than  $K_2$ . Thus, the gain of inverter side current will always be higher than that of the grid side current. The control schematic of both WACC and WACC\_EAD method will look same but  $K_1$  and  $K_2$  values may vary.

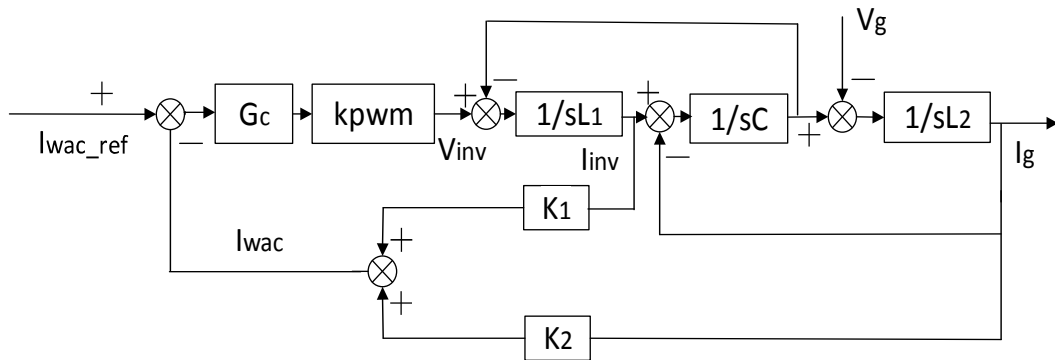


**Figure 4.1: Control schematic of Weighted Average Current Controller with Embedded Active Damping Method**

The closed-loop transfer function of a three-phase grid-tied inverter with LCL filter for WACC\_EAD method has been derived in (4.5) from the reference current,  $I_{WACC\_EAD\_ref}$  to the injected grid current,  $I_g$  by using the control schematic shown in figure 4.1.

$$\frac{I_g}{I_{WACC\_EAD\_ref}} = \frac{G_c k_{pwm}}{L_1 L_2 C s^3 + (L_1 + L_2) s + G_c k_{pwm} (K_1 L_2 C s^2 + (K_1 + K_2))} \quad (4.5)$$

The parameter values shown in table 2.1 and compensator shown in (2.27) has been used for determining the location of the closed loop poles. After doing the calculations, it has been found that the complex-conjugate poles of a closed-loop system are now located at  $-8.84 + 9.96e3i$  and  $-8.84 - 9.96e3i$ . They are shifted towards the left half of s-plane, which makes the system stable. The pole-zero map and the step response of a system has been examined for analyzing the stability of a system.

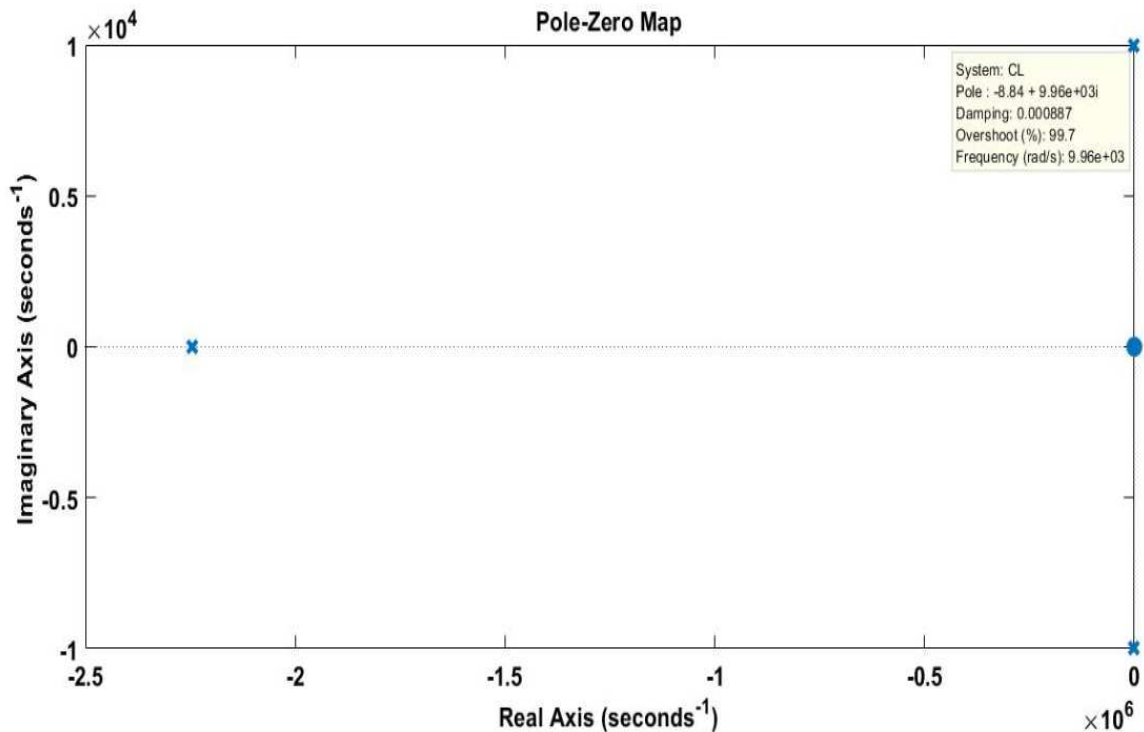


Figure 4.2: Pole-Zero map of a three-phase grid-tied LCL filtered inverter – WACC\_EAD method

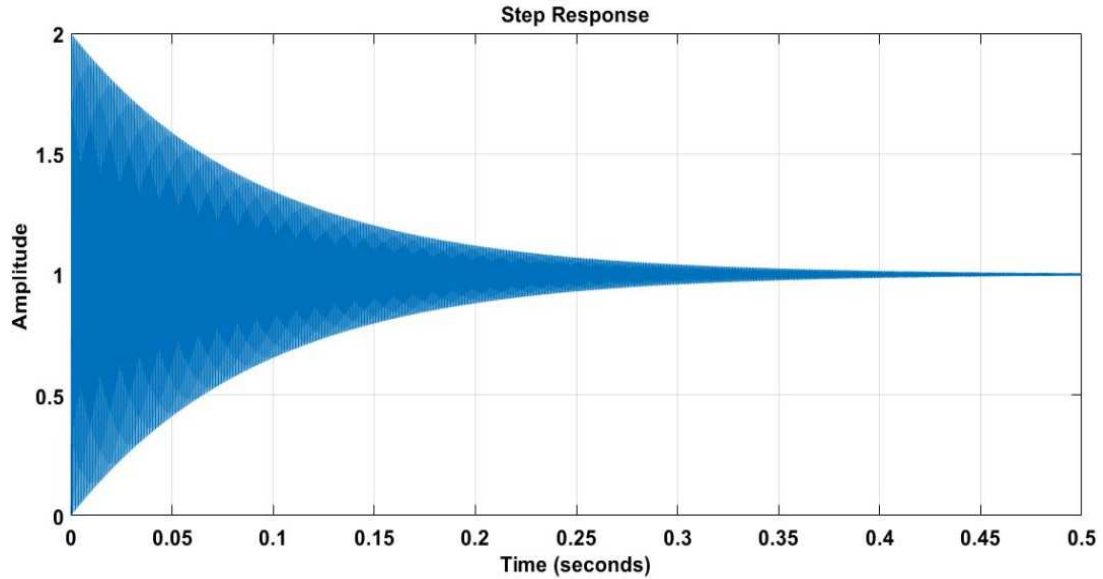


Figure 4.3: Step Response of a three-phase grid-tied LCL filtered inverter – WACC\_EAD method

The pole-zero map, shown in figure 4.2 confirms that the closed-loop poles are located at the left-half of the s-plane, which is making the system stable. This also makes the system underdamped, which may be observed in the step response of the system, shown in figure 4.3. Therefore, the system is stable and damped without applying any external damping methods.

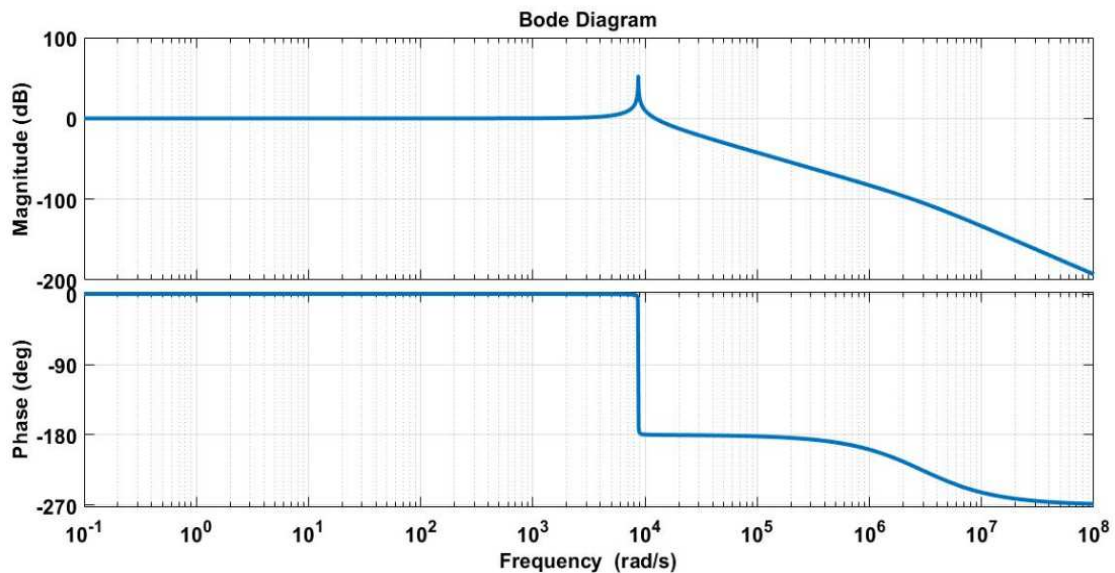


Figure 4.4: Bode plot of a closed loop three-phase grid-tied LCL filtered inverter system – WACC\_EAD method

From the bode plot of the closed-loop system shown in figure 4.4, it may be noticed that the peak at the resonant frequency is very less as compared to that of an undamped system. Thus, the harmonics of an injected grid current will get reduced. In (4.3) and (4.4), it may be noticed that the expressions of  $K_1$  and  $K_2$  of a WACC\_EAD method contains a damping factor,  $K_d$ . As the value of this damping factor increases, the damping in the system will also increase because the gain of inverter-side current will increase, and the gain of the grid-side current will decrease.

It has also been found that the plots of WACC with active damping method and WACC\_EAD method looks very similar to each other. The values of  $K_1$  and  $K_2$  has been found by using the parameter values of table 2.1.

$$\text{Here, } K_1 = \frac{L_1 + \alpha K_d}{(L_1 + L_2)} = \frac{0.6e-3 + 0.6 * 0.4e-6 * 1000}{(0.6 + 0.4)e-3} = 0.84 \text{ and } K_2 = \frac{L_2 - \alpha K_d}{(L_1 + L_2)} = \frac{0.4e-3 - 0.6 * 0.4e-6 * 1000}{(0.6 + 0.4)e-3} =$$

0.16. Therefore, the gain of the inverter-side current is higher than that of the grid-side current. This proves the stability of the system, which has also been demonstrated earlier from the plots in figure (4.2) and (4.3).

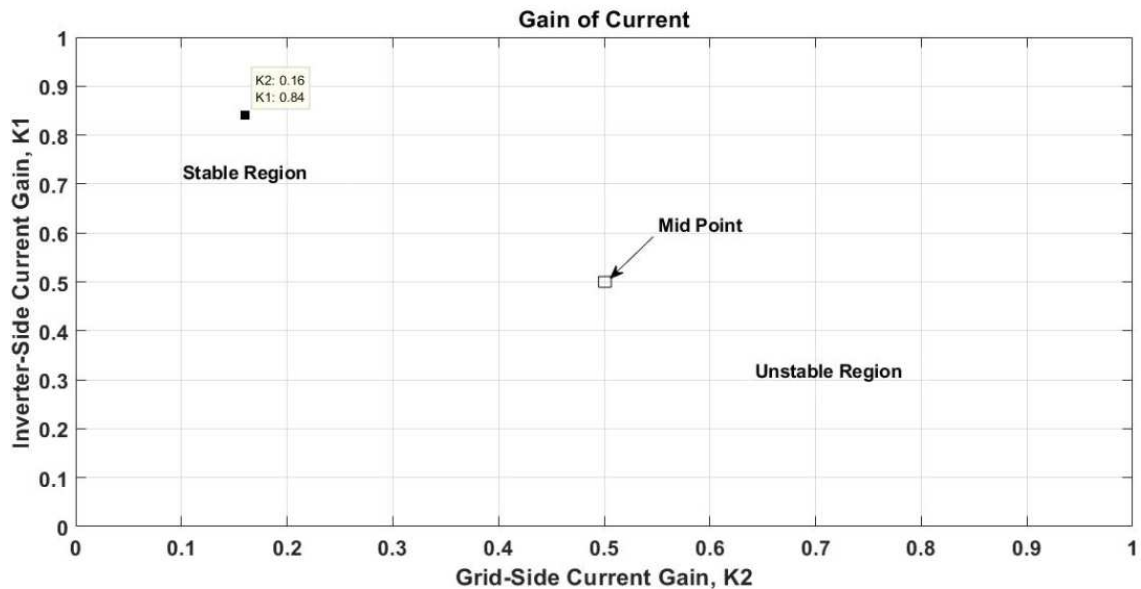


Figure 4.5: Graph of current gains for the parameter values of table 2.1

From the figure 4.5, it has been inferred that the coordinating point of  $K_1$  and  $K_2$  is in the left side of the mid-point, which is a stable region.

#### 4.3. Comparative evaluation of the transfer functions of WACC, WACC with Active Damping and WACC\_EAD methods

The objective of this section is to derive the transfer function of the system for all the current control methods, discussed so far by substituting the equation of inverter-side current gain,  $K_1$  and the grid-side current gain,  $K_2$  and to do the comparative analysis of all the cases.

For the WACC method, the transfer function of the system, shown in (2.42) is:

$$\frac{I_g}{I_{wac\_ref}} = \frac{G_c k_{pwm}}{L_1 L_2 C s^3 + (L_1 + L_2) s + G_c k_{pwm} (K_1 L_2 C s^2 + K_1 + K_2)} \quad (4.6)$$

In this current control method,  $K_1$  is  $\frac{L_1}{(L_1 + L_2)}$  and  $K_2$  is  $\frac{L_2}{(L_1 + L_2)}$ . The equation of  $K_1$  and  $K_2$  has been substituted in the above transfer function.

$$\frac{I_g}{I_{wac\_ref}} = \frac{G_c k_{pwm}}{L_1 L_2 C s^3 + (L_1 + L_2) s + G_c k_{pwm} \left( \frac{L_1}{(L_1 + L_2)} L_2 C s^2 + \frac{L_1}{(L_1 + L_2)} + \frac{L_2}{(L_1 + L_2)} \right)} \quad (4.7)$$

$$\frac{I_g}{I_{wac\_ref}} = \frac{G_c k_{pwm} (L_1 + L_2)}{L_1 L_2 C s^3 (L_1 + L_2) + (L_1 + L_2)^2 s + G_c k_{pwm} (L_1 L_2 C s^2 + L_1 + L_2)} \quad (4.8)$$

$$\frac{I_g}{I_{wac\_ref}} = \frac{G_c k_{pwm} (L_1 + L_2)}{L_1 L_2 C s^3 (L_1 + L_2) + (L_1 + L_2)^2 s + G_c k_{pwm} L_1 L_2 C s^2 + G_c k_{pwm} (L_1 + L_2)} \quad (4.9)$$

$$\frac{I_g}{I_{wac\_ref}} = \frac{G_c k_{pwm} (L_1 + L_2)}{s^3 L_1 L_2 C (L_1 + L_2) + s^2 G_c k_{pwm} L_1 L_2 C + s (L_1 + L_2)^2 + G_c k_{pwm} (L_1 + L_2)} \quad (4.10)$$

The final transfer function of the system for the WACC method has been derived in (4.10).

For the WACC with Active Damping method, the transfer function of the system, shown in (2.44) is:

$$\frac{I_g}{I_{wac\_ref}} = \frac{G_c k_{pwm}}{L_1 L_2 C s^3 + k_{pwm} k_c L_2 C s^2 + (L_1 + L_2) s + G_c k_{pwm} (K_1 L_2 C s^2 + K_1 + K_2)} \quad (4.11)$$

In this current control method,  $K_1$  is  $\frac{L_1}{(L_1 + L_2)}$  and  $K_2$  is  $\frac{L_2}{(L_1 + L_2)}$ . The equation of  $K_1$  and  $K_2$

has been substituted in the above transfer function.

$$\frac{I_g}{I_{wac\_ref}} = \frac{G_c k_{pwm}}{L_1 L_2 C s^3 + k_{pwm} k_c L_2 C s^2 + (L_1 + L_2) s + G_c k_{pwm} \left( \frac{L_1}{(L_1 + L_2)} L_2 C s^2 + \frac{L_1}{(L_1 + L_2)} + \frac{L_2}{(L_1 + L_2)} \right)} \quad (4.12)$$

$$\frac{I_g}{I_{wac\_ref}} = \frac{G_c k_{pwm} (L_1 + L_2)}{L_1 L_2 C s^3 (L_1 + L_2) + k_{pwm} k_c L_2 C (L_1 + L_2) s^2 + (L_1 + L_2)^2 s + G_c k_{pwm} (L_1 L_2 C s^2 + L_1 + L_2)} \quad (4.13)$$

$$\frac{I_g}{I_{wac\_ref}} = \frac{G_c k_{pwm} (L_1 + L_2)}{L_1 L_2 C s^3 (L_1 + L_2) + k_{pwm} k_c L_2 C (L_1 + L_2) s^2 + (L_1 + L_2)^2 s + G_c k_{pwm} L_1 L_2 C s^2 + G_c k_{pwm} (L_1 + L_2)} \quad (4.14)$$

$$\frac{I_g}{I_{wac\_ref}} = \frac{G_c k_{pwm} (L_1 + L_2)}{s^3 L_1 L_2 C (L_1 + L_2) + s^2 k_{pwm} k_c L_2 C (L_1 + L_2) + s^2 G_c k_{pwm} L_1 L_2 C + s (L_1 + L_2)^2 + G_c k_{pwm} (L_1 + L_2)} \quad (4.15)$$

The final transfer function of the system for WACC with Active Damping method has been derived in (4.15). It may be inferred from this transfer function that the term  $s^2 k_{pwm} k_c L_2 C (L_1 + L_2)$  has been added to the denominator, which was not there in the transfer function of a system for WACC method, shown in (4.10). This extra term provides damping to the system. It contains an extra-feedback gain,  $k_c$ . As the value of  $k_c$  increases, the system becomes stable.

For WACC\_EAD method, the transfer function of the system, shown in (4.5) is:

$$\frac{I_g}{I_{WACC\_EAD\_ref}} = \frac{G_c k_{pwm}}{L_1 L_2 C s^3 + (L_1 + L_2) s + G_c k_{pwm} (K_1 L_2 C s^2 + K_1 + K_2)} \quad (4.16)$$

In this current control method,  $K_1 = \frac{L_1 + \alpha K_d}{(L_1 + L_2)}$  and  $K_2 = \frac{L_2 - \alpha K_d}{(L_1 + L_2)}$ ,  $\alpha = L_1 L_2$ . This new equation of  $K_1$  and  $K_2$  has been substituted in the above transfer function.

$$\frac{I_g}{I_{WACC\_EAD\_ref}} = \frac{G_c k_{pwm}}{L_1 L_2 C s^3 + (L_1 + L_2) s + G_c k_{pwm} \left( \frac{L_1 + \alpha K_d}{(L_1 + L_2)} L_2 C s^2 + \frac{L_1 + \alpha K_d}{(L_1 + L_2)} + \frac{L_2 - \alpha K_d}{(L_1 + L_2)} \right)} \quad (4.17)$$

$$\frac{I_g}{I_{WACC\_EAD\_ref}} = \frac{G_c k_{pwm}}{L_1 L_2 C s^3 + (L_1 + L_2) s + G_c k_{pwm} \left( \frac{L_1 + L_1 L_2 K_d}{(L_1 + L_2)} L_2 C s^2 + \frac{L_1 + L_1 L_2 K_d}{(L_1 + L_2)} + \frac{L_2 - L_1 L_2 K_d}{(L_1 + L_2)} \right)} \quad (4.18)$$

$$\frac{I_g}{I_{WACC\_EAD\_ref}} = \frac{G_c k_{pwm} (L_1 + L_2)}{L_1 L_2 C s^3 (L_1 + L_2) + (L_1 + L_2)^2 s + G_c k_{pwm} ((L_1 + L_1 L_2 K_d) L_2 C s^2 + L_1 + L_2)} \quad (4.19)$$

$$\frac{I_g}{I_{WACC\_EAD\_ref}} = \frac{G_c k_{pwm} (L_1 + L_2)}{L_1 L_2 C s^3 (L_1 + L_2) + (L_1 + L_2)^2 s + G_c k_{pwm} L_1 L_2 C s^2 + G_c k_{pwm} L_1 L_2 K_d L_2 C s^2 + G_c k_{pwm} (L_1 + L_2)} \quad (4.20)$$

$$\frac{I_g}{I_{WACC\_EAD\_ref}} = \frac{G_c k_{pwm} (L_1 + L_2)}{s^3 L_1 L_2 C (L_1 + L_2) + s^2 G_c k_{pwm} L_1 L_2 K_d L_2 C + s^2 G_c k_{pwm} L_1 L_2 C + s (L_1 + L_2)^2 + G_c k_{pwm} (L_1 + L_2)} \quad (4.21)$$

The final transfer function of the system for WACC\_EAD method has been derived in (4.21). It can be inferred from this transfer function that the term  $s^2 G_c k_{pwm} L_1 L_2 K_d L_2 C$  has been added to the denominator, which was not there in the transfer function of a system for WACC method, shown in (4.10). This extra term provides damping to the system. It

contains a damping factor,  $K_d$ . As the value of  $K_d$  increases, the system becomes stable. From the transfer of a system for WACC method and for WACC with Active Damping method shown in (4.10) and (4.15) respectively, it has been found that if the extra-feedback gain ( $k_c$ ) in (4.15) becomes zero, then the transfer function of the system for WACC with Active Damping method will be same as the transfer function of the system for WACC method. Thus, there will be no extra-feedback loop present in the system, which can provide damping. The system will transform to an undamped system.

Similarly, from the transfer of a system for WACC method and for WACC\_EAD method shown in (4.10) and (4.21) respectively, it has been found that if the damping factor ( $K_d$ ) in (4.21) becomes zero, then the transfer function of the system for WACC\_EAD will be same as the transfer function of the system for WACC method. Thus, there will be no damping factor term in the equation of the inverter-side current gain and the grid-side current gain. This system will also transform an undamped system.

From the transfer of a system for WACC with Active Damping method and for WACC\_EAD method shown in (4.15) and (4.21) respectively, it may be inferred that both the transfer functions look same except one term which provides damping to the system. In WACC with Active Damping method, that damping term is  $s^2 k_{pwm} k_c L_2 C (L_1 + L_2)$  and in WACC\_EAD method, that damping term is  $s^2 G_c k_{pwm} L_1 L_2 K_d L_2 C$ . Thus, both the current control methods provide active damping to the system. The relationship between the extra-feedback gain ( $k_c$ ) and the damping factor ( $K_d$ ) can be found by comparing the transfer functions in (4.15) and (4.21).

$$s^2 G_c k_{pwm} L_1 L_2 K_d L_2 C = s^2 k_{pwm} k_c L_2 C (L_1 + L_2) \quad (4.22)$$

$$G_c L_1 L_2 K_d = k_c (L_1 + L_2) \quad (4.23)$$

$$K_d = \frac{k_c(L_1+L_2)}{G_c L_1 L_2} \quad (4.24)$$

Thus, the damping factor ( $K_d$ ) of WACC\_EAD method is directly proportional to the extra-feedback gain ( $k_c$ ) of WACC method.

## CHAPTER 5: MODELING AND SIMULATION RESULTS

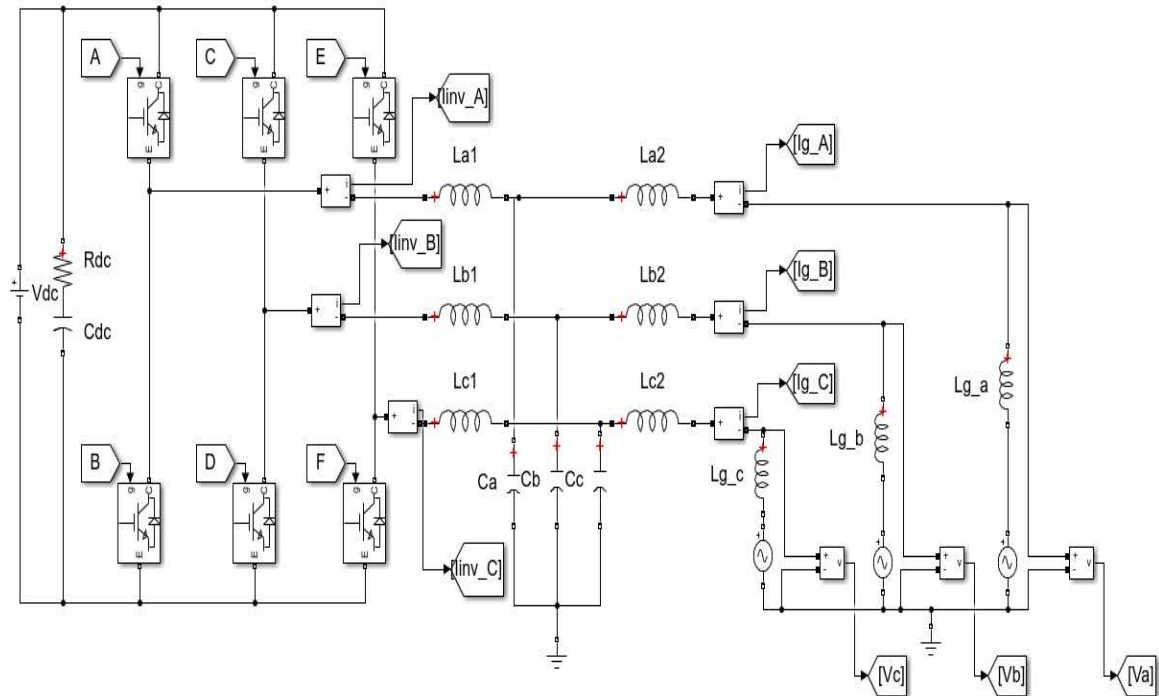
### 5.1. Introduction

The three-phase grid-tied LCL filtered inverter system has been designed in MATLAB Simulink and Typhoon for various current control methods like WACC, WACC with Passive Damping, WACC with Active Damping and WACC\_EAD. In the model shown in figure 5.1 and 5.6, a DC link voltage,  $V_{dc}$  of 400 V is connected in parallel to a capacitor,  $C_{dc}$  of 10  $\mu$ F, which is in series with a resistor,  $R_{dc}$  of 1 mH. The DC link is then connected to a two-level inverter parallelly to converter DC power to AC [4]. The PWM inverter helps interconnecting DC link and utility grid [7]. The LCL filter interconnects the grid of 120 V rms to the inverter to reduce the current harmonics generated by PWM inverter [9], [10]. In the figure 5.1 and 5.6,  $L_{a1}$ ,  $L_{b1}$  and  $L_{c1}$  are inductance at the inverter side for phase a, b and c respectively.  $L_{a2}$ ,  $L_{b2}$  and  $L_{c2}$  are inductance at the grid side for phase a, b and c respectively.  $L_{g_a}$ ,  $L_{g_b}$  and  $L_{g_c}$  are the grid inductance of each phase.  $C_a$ ,  $C_b$  and  $C_c$  are capacitance of each phase. The inverter-side inductance, grid-side inductance and capacitance of an LCL filter are considered as 0.6 mH, 0.2 mH and 30  $\mu$ F respectively. The grid inductance is 0.2 mH. In WACC, WACC with Active Damping and WACC\_EAD method, the power circuit is same, whereas, in WACC with Passive Damping method, resistor  $R_{d_a}$ ,  $R_{d_b}$  and  $R_{d_c}$  are connected in series with the capacitor of an LCL filter in phase a, b and c respectively.

In the controller design, the grid voltage of each phase has been connected to a phase-locked loop (PLL) block to generate  $\omega t$ . The inverter-side current and the grid-side current of each phase has been connected to the inverter-side current gain and the grid-side current gain respectively to produce the weighted average current of each phase. This weighted average current of each phase is connected to abc-dq0 block to generate  $I_d$  and  $I_q$ . The  $\omega t$  generated from the PLL block is also connected to abc-dq0 block to lock the phases of grid voltage and current. To inject an active power of 7 kW, the required current is 27.5 A peak. Thus,  $I_{d\_ref}$  is considered as 27.5 A and  $I_{q\_ref}$  as 0 A. The  $I_d$  is compared with  $I_{d\_ref}$  and  $I_q$  is compared with  $I_{q\_ref}$ . This will produce an error, which has been reduced or made zero by using a PID compensator. In WACC, WACC with Passive Damping and WACC\_EAD method, the output of the compensator is connected to dq0-abc block to transform the signal back to abc form. Whereas in WACC with Active Damping, an extra-feedback loop of capacitor current connected to a gain  $k_c$  has been compared with the output of the compensator and then, the output of that comparator is connected to dq0-abc block to transform the signal back to abc form. After that, the signal has been compared with the carrier signal of 10 kHz (switching frequency), which generates Pulse Width Modulated (PWM) signal. These digital signals are connected to the gates of the inverter. The simulation results for all the current control methods has been shown. The harmonics of an injected grid current for various cases has been examined in both MATLAB Simulink and Typhoon.

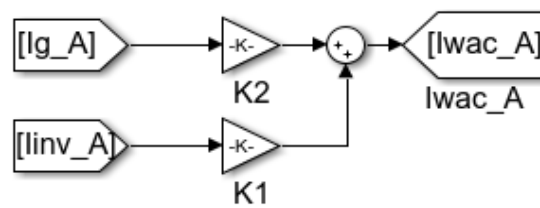
## 5.2. Typhoon and MATLAB Simulink model of an undamped WACC method and their simulation results

The model of a three-phase grid-tied inverter with LCL filter for various current control methods has been first designed in MATLAB Simulink. The controller design and the harmonics of an injected grid current have also been examined for all the cases.



**Figure 5.1: MATLAB Simulink model of a three-phase LCL filtered grid-tied inverter – WACC**

In WACC method, the inverter side current and the grid side current are connected to inverter side current gain and the grid side current gain to form the weighted average current, shown in figure 5.2. The inverter side current gain is the ratio of inverter side inductance to the sum of inductances of inverter side and grid side and the grid side current gain is the ratio of the of grid side inductance to the sum of inductances of inverter side and grid side.





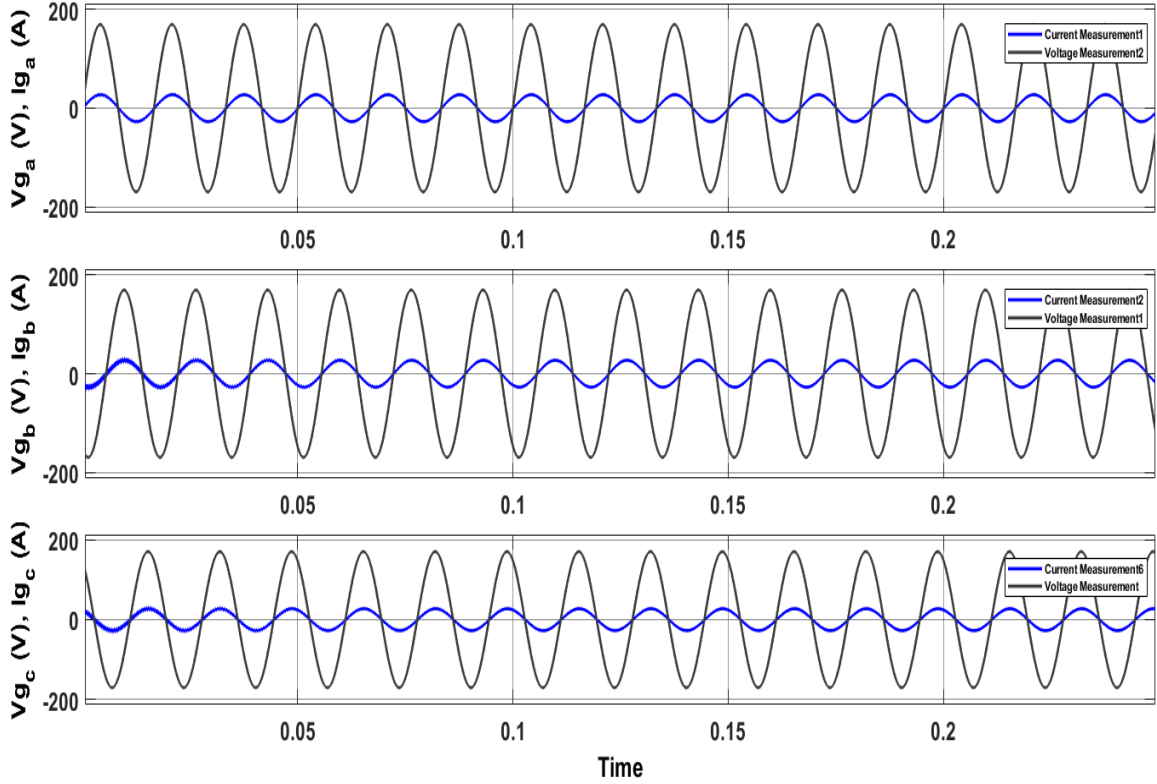


Figure 5.4: Grid Voltage and Grid Current – WACC (Undamped)

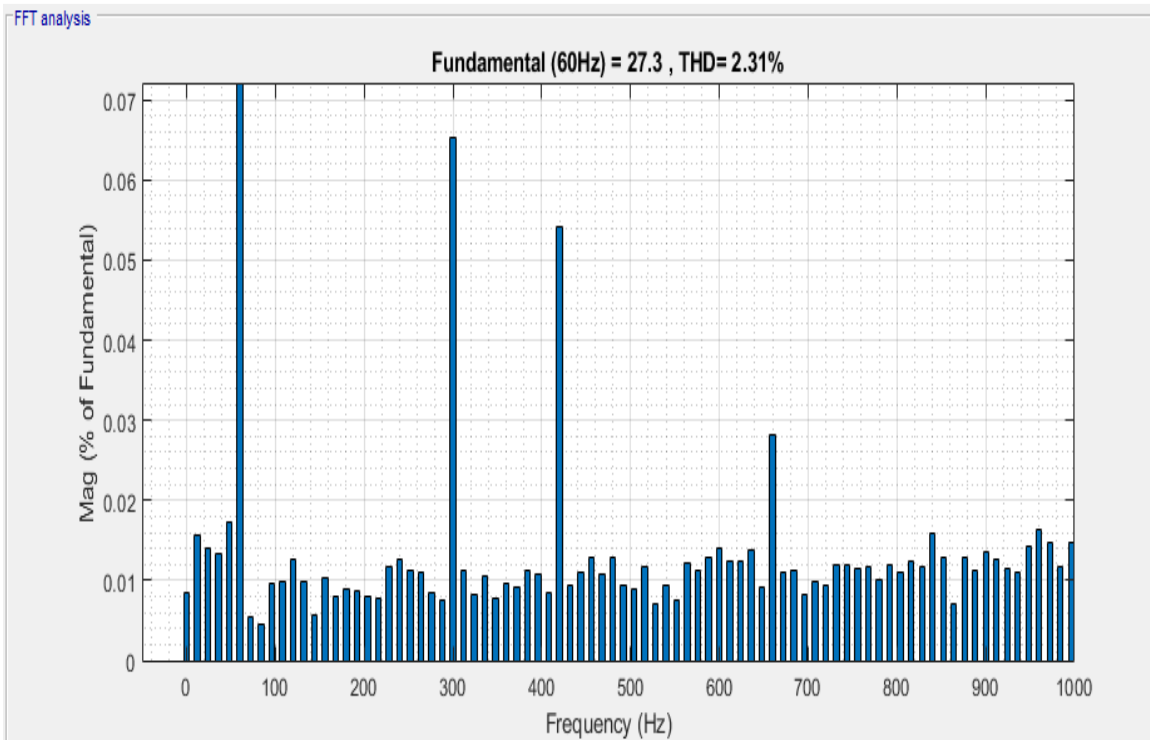


Figure 5.5: THD of a Grid Current - WACC



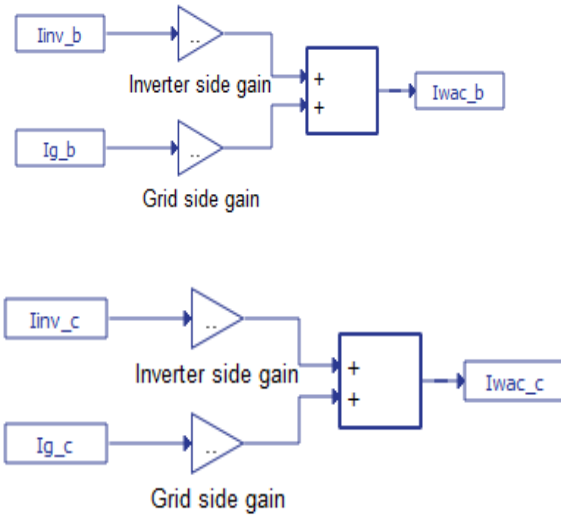


Figure 5.7: Weighted Average Current of each phase in Typhoon

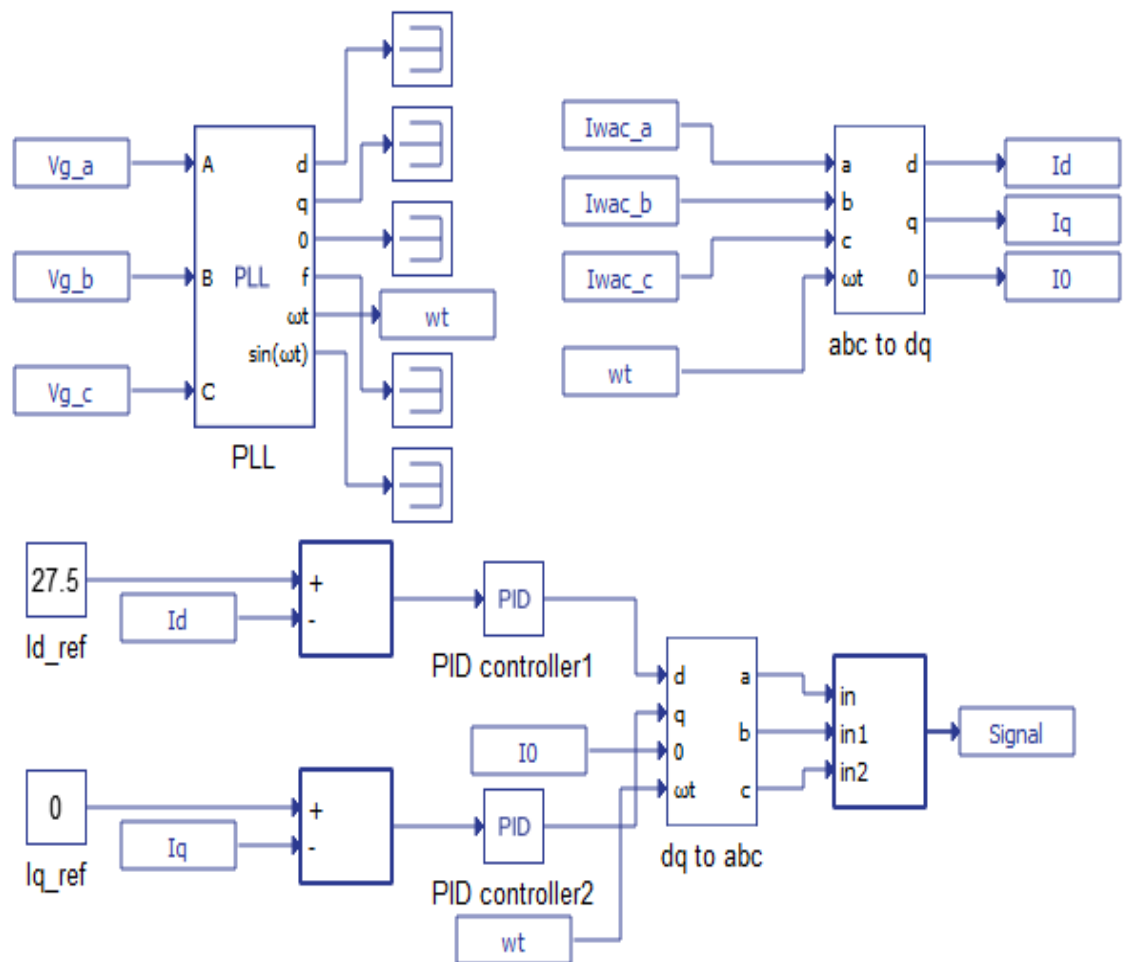


Figure 5.8: Controller design of a WACC method (Undamped) in Typhoon

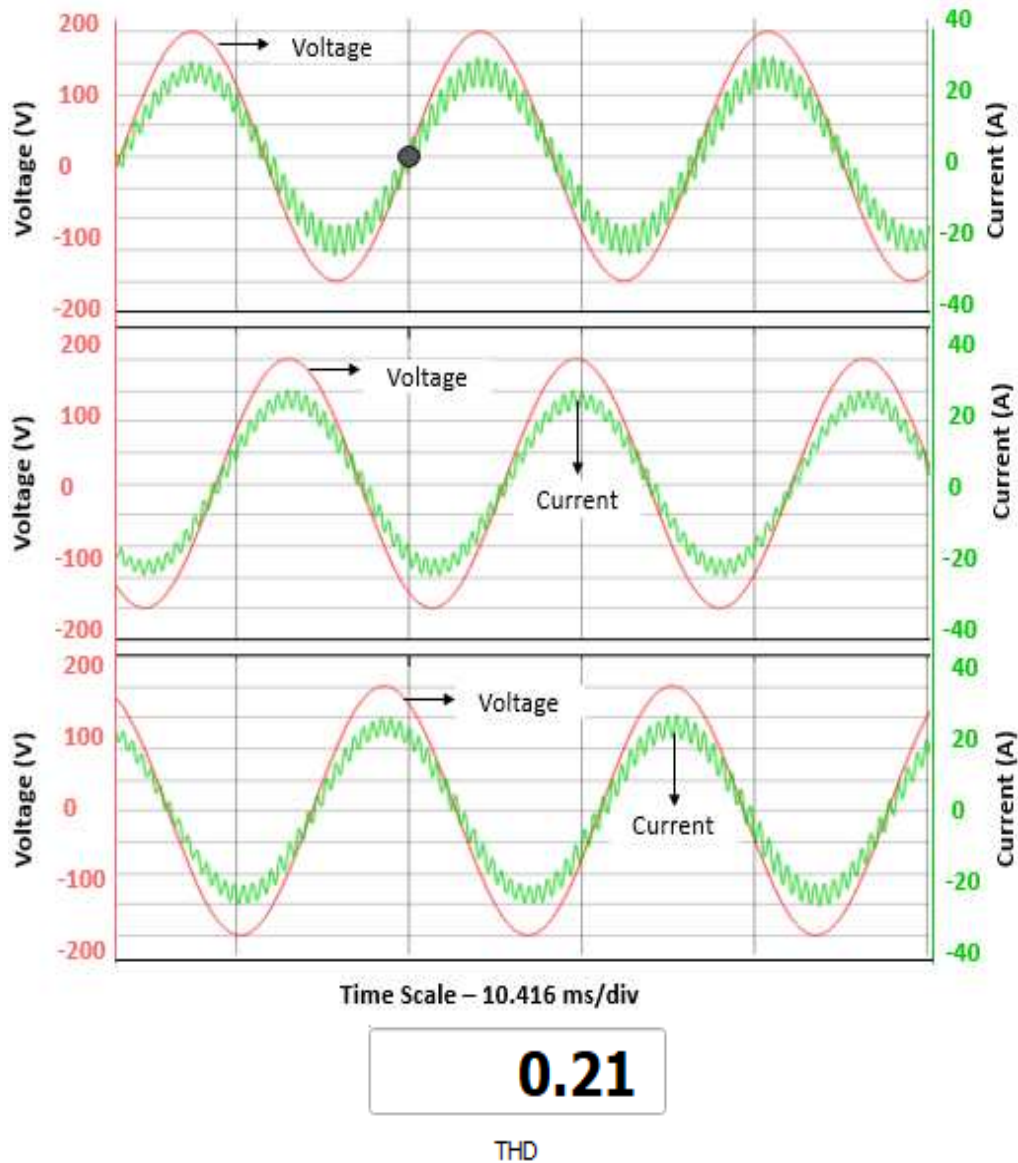
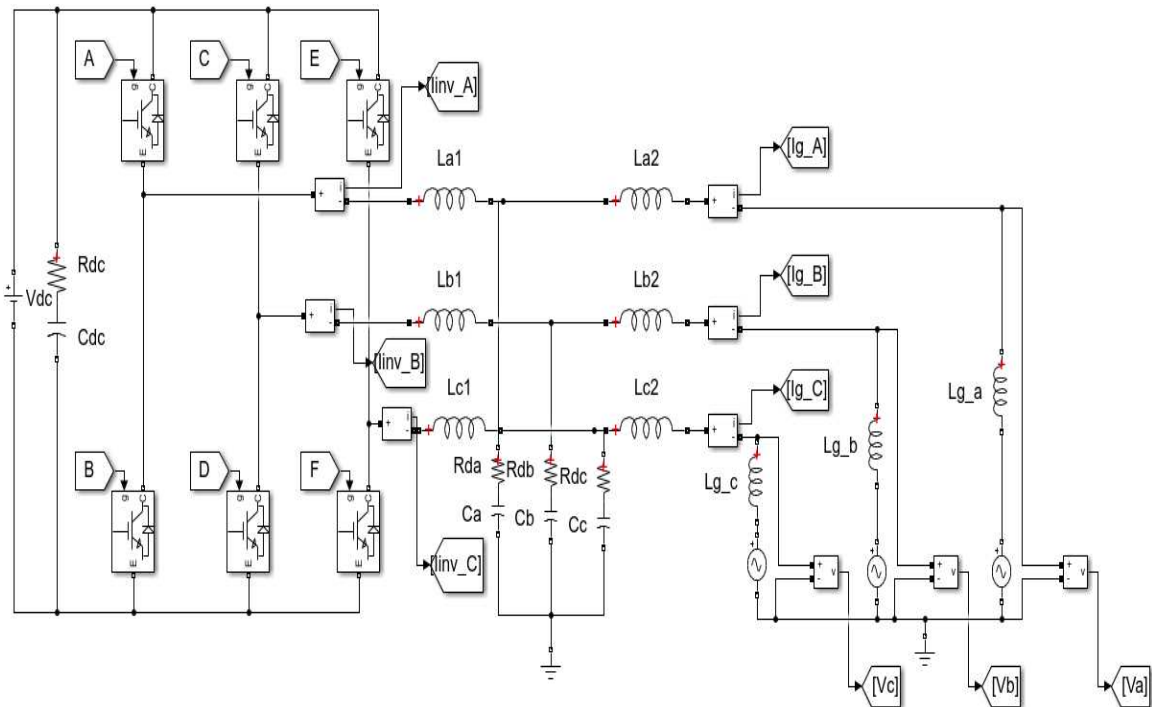


Figure 5.9: Grid Voltage and Grid Current – WACC (Undamped)

From the simulation waveforms of a system for WACC (undamped) method shown in figure 5.9, it may be observed that the injected grid current has a very high harmonic. The total harmonic distortion is around 21%. The system is not damped. Thus, damping methods like passive damping and active damping have been implemented.

### 5.3. Typhoon and MATLAB Simulink model of a WACC with Passive Damping method and their simulation result

In passive damping method, a resistor  $R_d$  is connected in series with the LCL capacitor as shown in figure 5.10 and 5.12. In this method, the power circuit has been modified. However, the controller design of the system is not required to alter. Thus, the same controller design, shown in figure 5.3 may be followed in this case. This method is very simple to implement. The model has been first designed in MATLAB Simulink. The controller design and the harmonics of an injected grid current have also been examined.



**Figure 5.10: MATLAB Simulink model of a three-phase LCL filtered grid-tied inverter – WACC (Passive Damping)**

There is no alteration required in the controller design of the system for WACC with Passive Damping method.

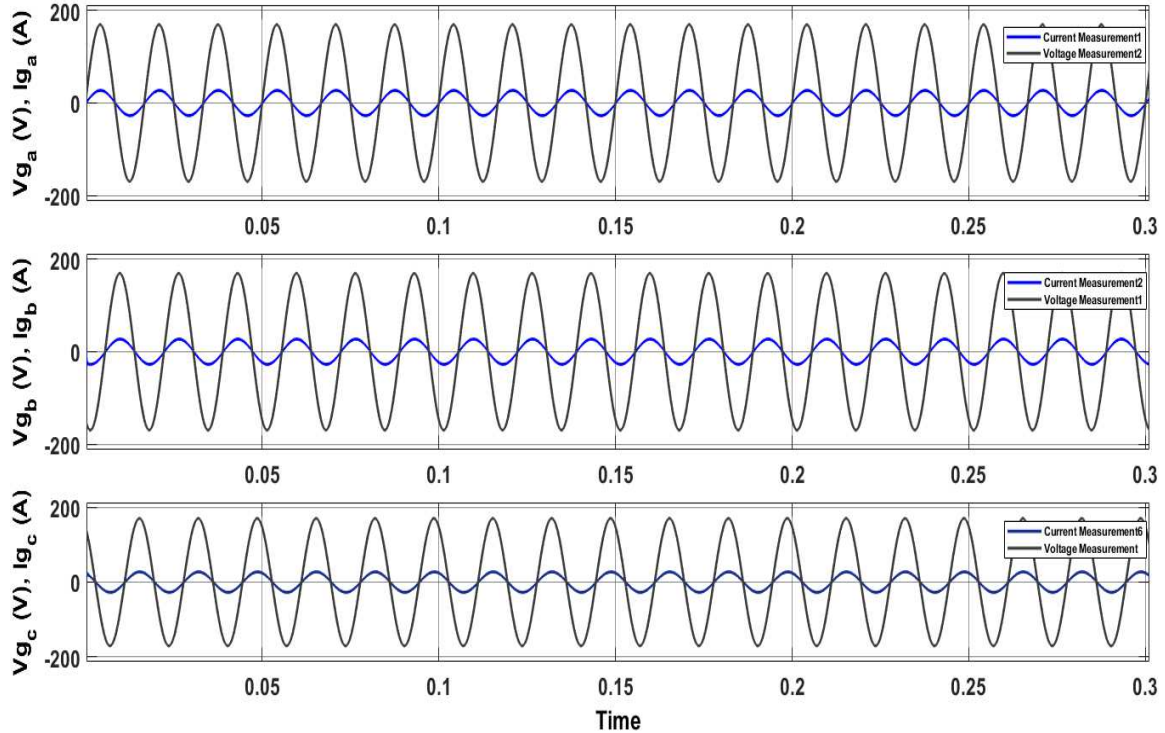


Figure 5.11: Grid Voltage and Grid Current – WACC with Passive Damping

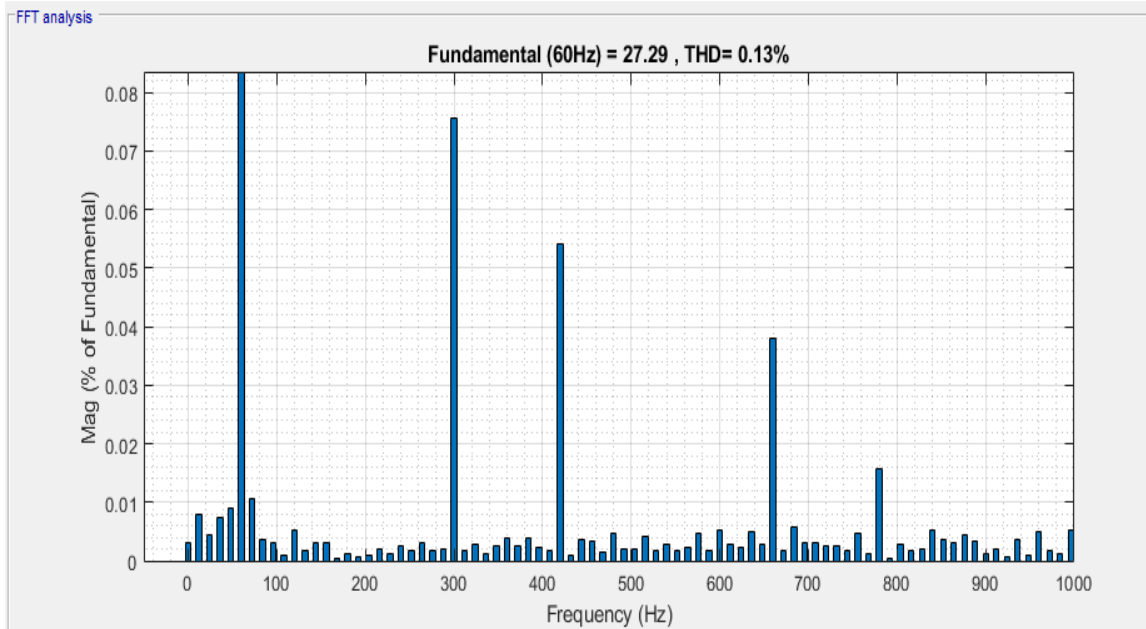


Figure 5.12: THD of a Grid Current – WACC (Passive Damping)

The harmonics of injected grid current is reduced to 0.13%, shown in figure 5.12. Thus, the system is stable and damped in passive damping method. However, it is less efficient.

The model has also been designed in Typhoon, shown in figure 5.13.

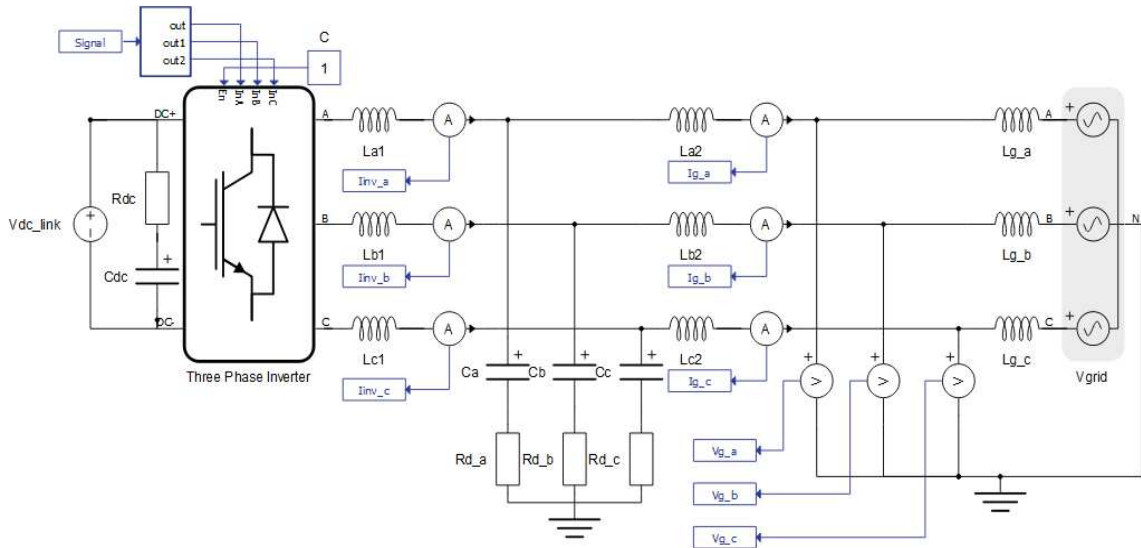


Figure 5.13: Typhoon model of a three-phase LCL filtered grid-tied inverter – WACC (Passive Damping)

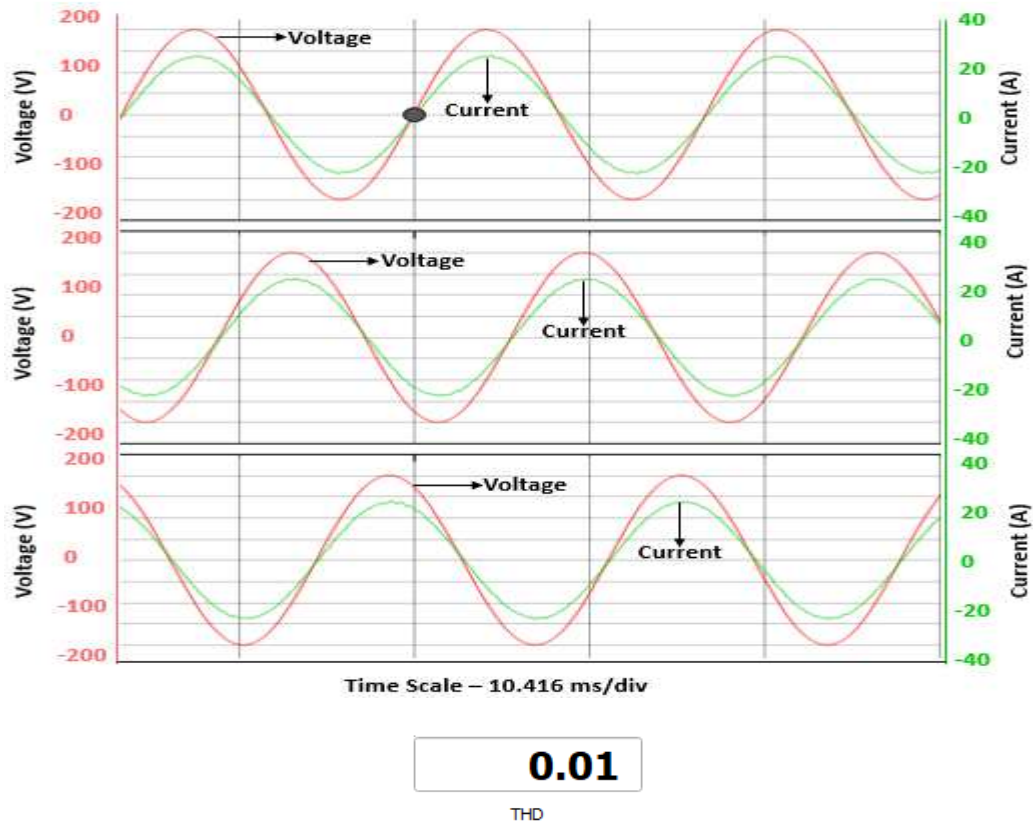


Figure 5.14: Grid Voltage and Grid Current – WACC with Passive Damping

From figure 5.14, it may be observed that the grid current has less harmonics as compared to an undamped system. The total harmonic distortion (THD) is only 1 %. The system is stable and damped. The damping behavior of the system increases with the increase of the damping resistor  $R_d$ . However, this resistor increases the losses in the system. This will affect the efficiency of the entire system.

#### 5.4. Typhoon and MATLAB Simulink model of a WACC with Active Damping method and their simulation result

In this method, there is no modification required in the power circuit. Hence, the model shown in figure 5.1 may be used. Here, the controller design is altered for providing damping to the system. The model has been first designed in MATLAB Simulink. As there is no modification in the power circuit of the system, only controller design of the system has been shown in figure 5.15.

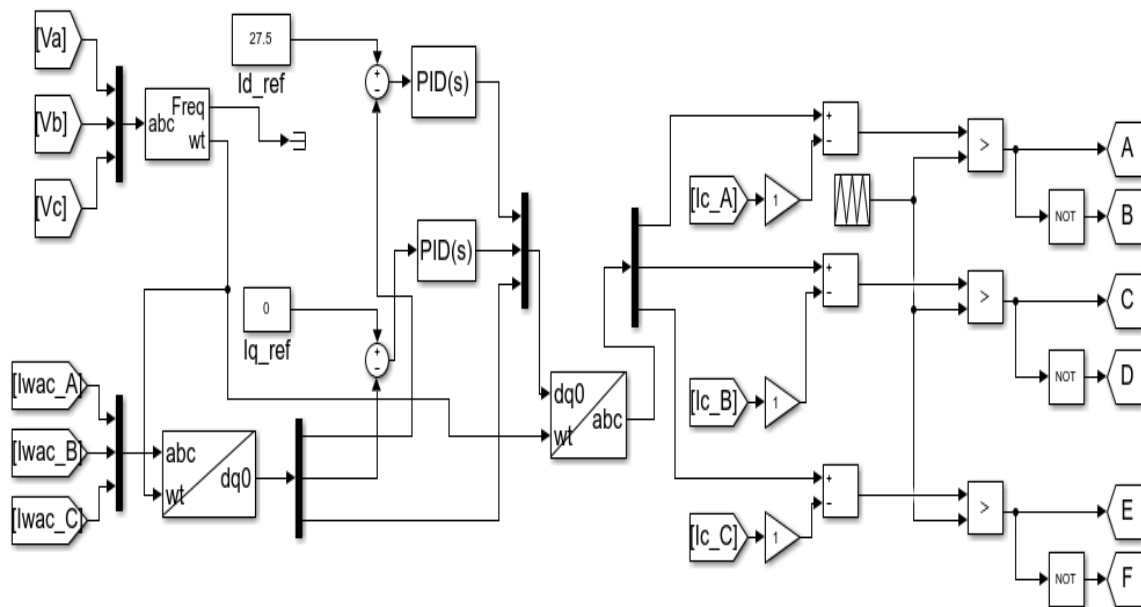
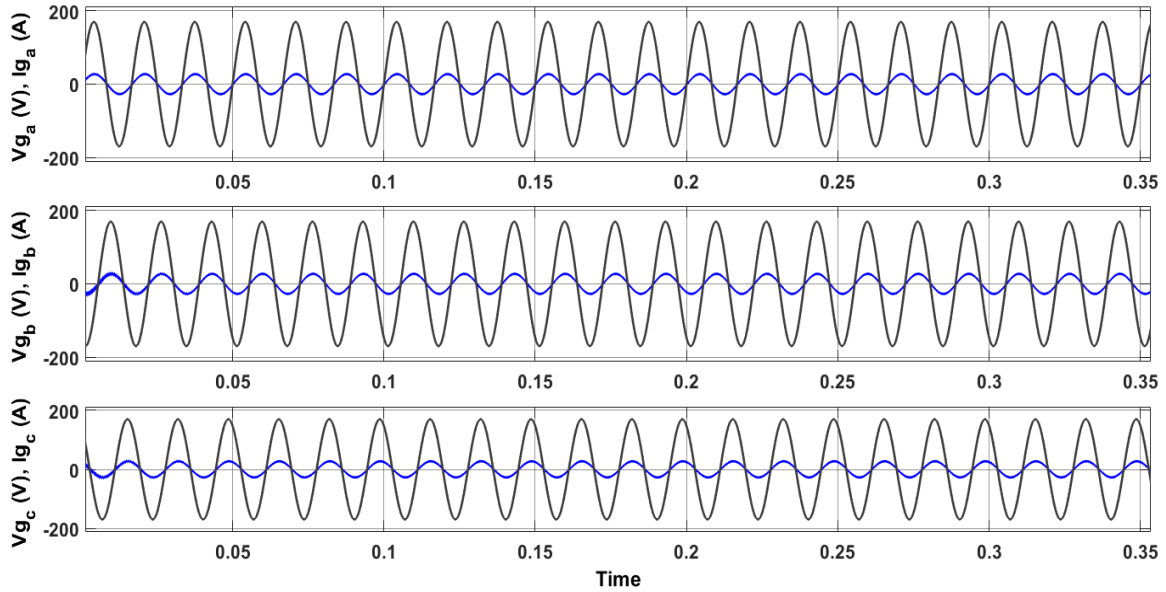
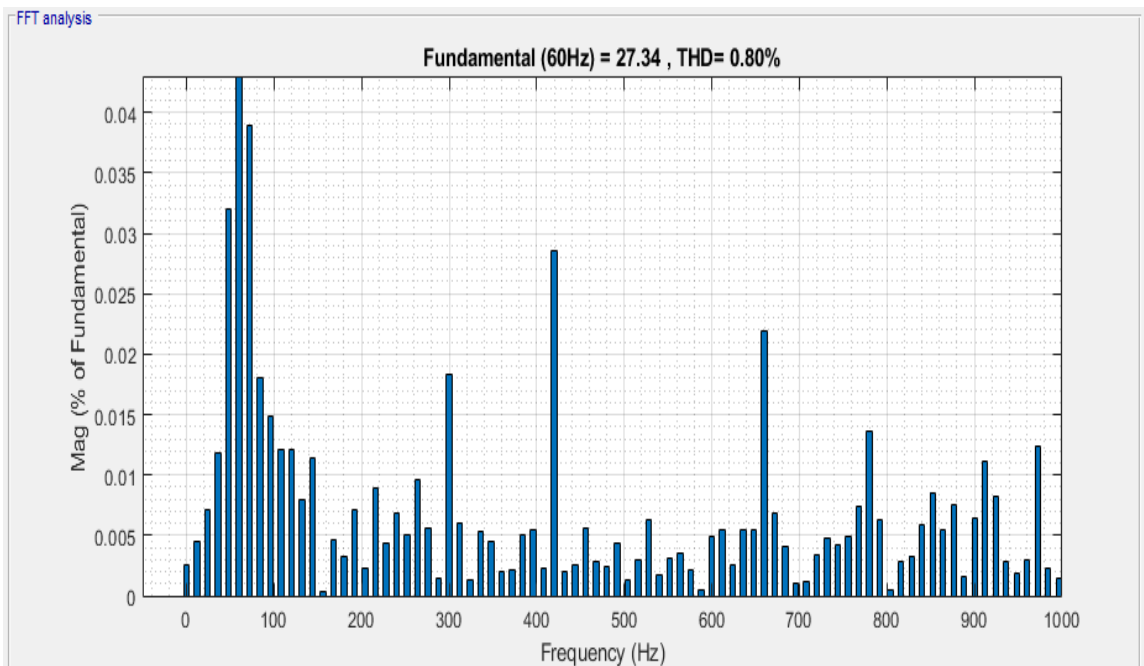


Figure 5.15: Controller design of a WACC with Active Damping method in MATLAB Simulink



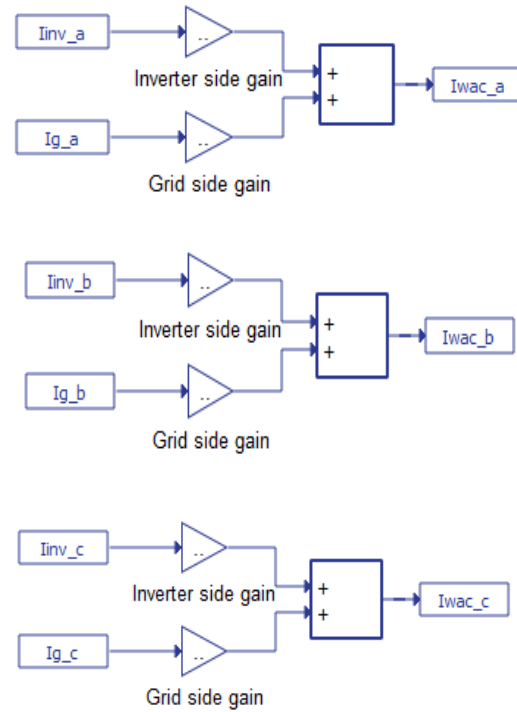
**Figure 5.16: Grid Voltage and Grid Current – WACC with Active Damping**



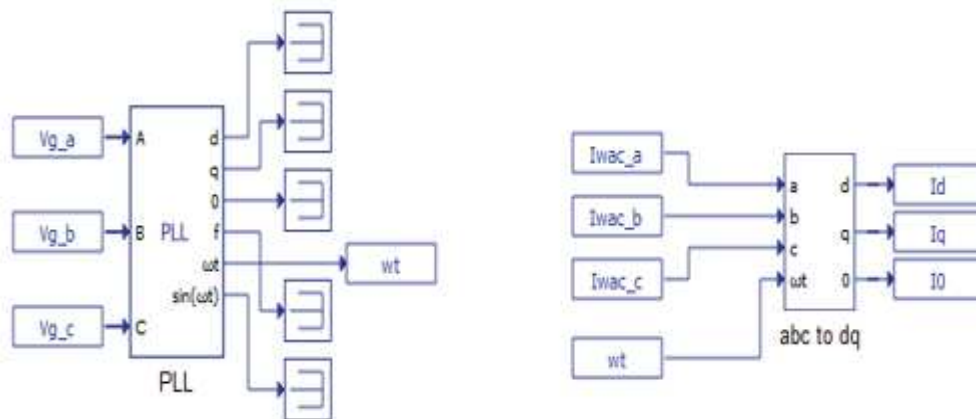
**Figure 5.17: THD of a Grid Current – WACC (Active Damping)**

The harmonics of an injected grid current has been reduced to 0.8%, shown in figure 5.17. It is less than the harmonics of grid current of an undamped system. Thus, the system is damped and stable in active damping method. It is also more efficient than passive damping method, but the controller design of the system is complex.

The controller design of the system for WACC with Active Damping method has also been designed in Typhoon, shown in figure 5.19.



**Figure 5.18: Weighted Average Current of each phase**



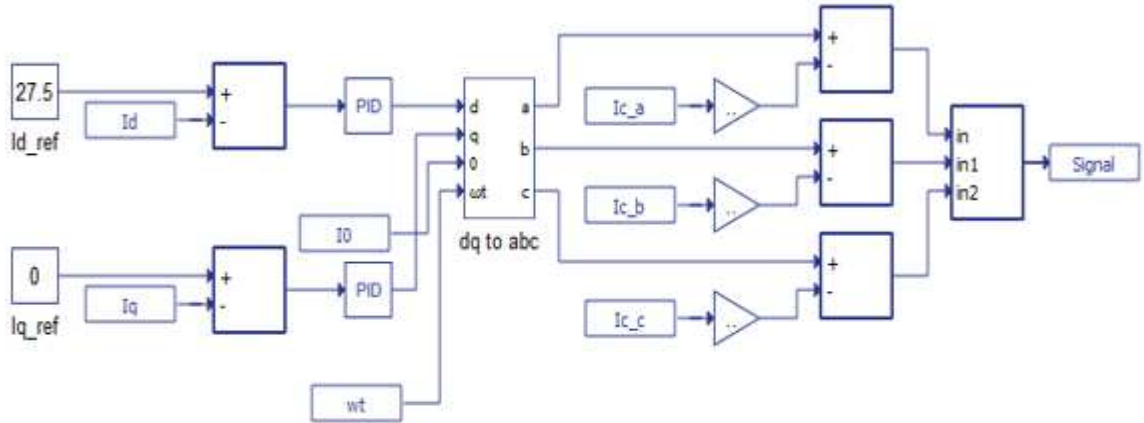


Figure 5.19: Controller design of a WACC with Active Damping method

An extra-feedback loop of capacitor currents,  $I_c$  with its gain,  $k_c$  is used for damping LCL resonance, as shown in figure 5.19.

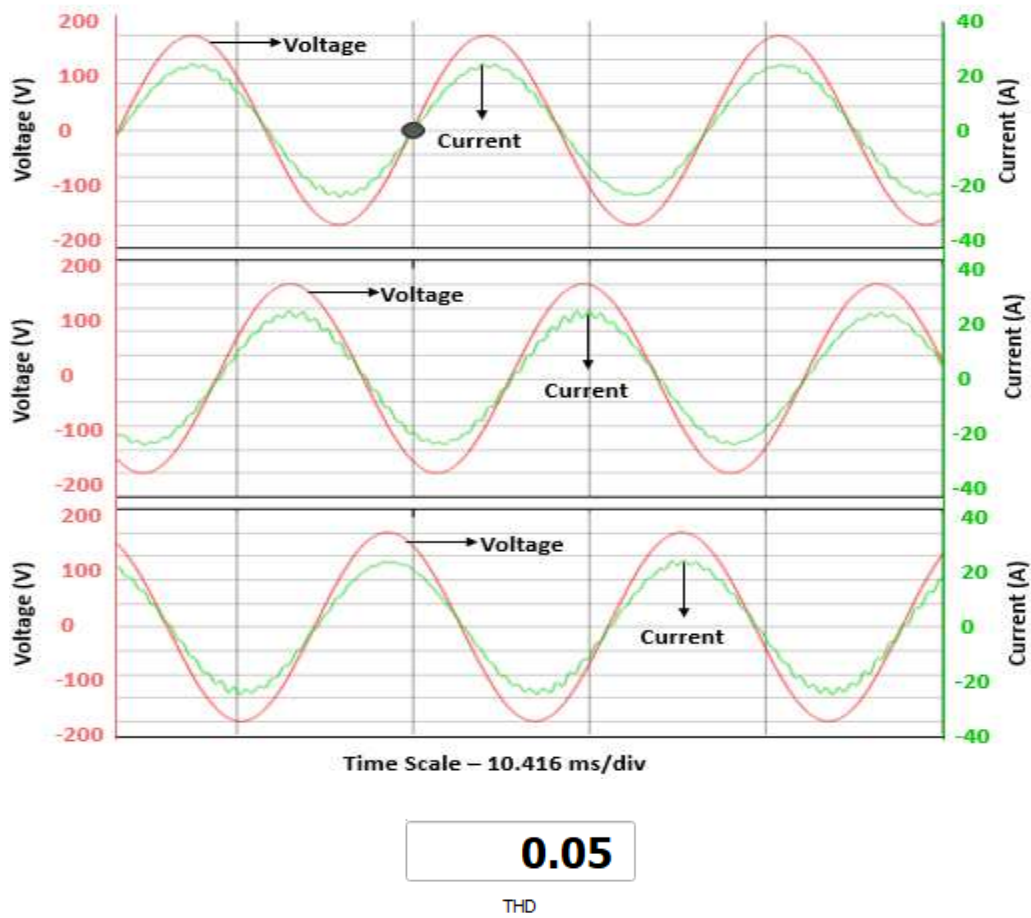
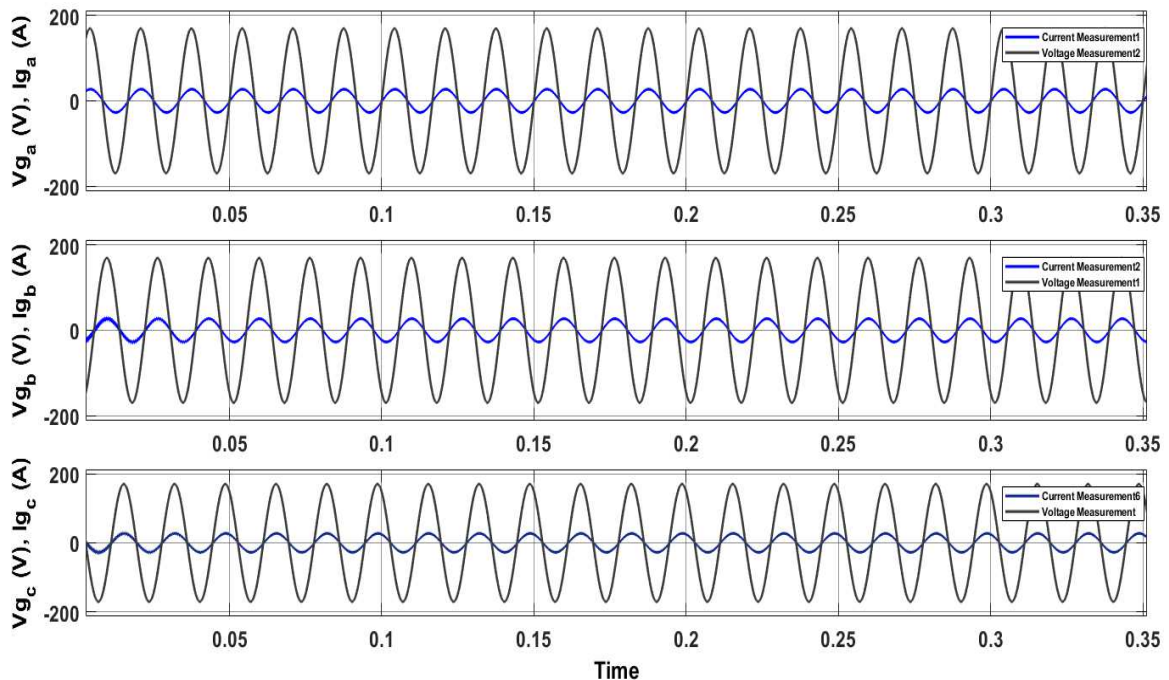


Figure 5.20: Grid Voltage and Grid Current – WACC with Active Damping

From figure 5.20, it may be observed that the grid current has less harmonics as compared to an undamped system. The total harmonic distortion (THD) is only 5 %. The system is stable and damped.

#### 5.5. Typhoon and MATLAB Simulink model of a WACC\_EAD method and their simulation result

As there is a drawback of less efficiency in passive damping method and an issue of complex controller design in active damping method, a new current control method has been proposed, known as WACC\_EAD method. In this method, same power circuit shown in figure 5.1 is used. Thus, there is no change in the power circuit. The controller design looks similar to that of an undamped system, except the values of  $K_1$  and  $K_2$ . The new equations of  $K_1$  and  $K_2$  provides damping to the system. The value of  $K_1$  is shown to be higher than  $K_2$ . The system has been first modelled in MATLAB Simulink.



**Figure 5.21: Grid Voltage and Grid Current – WACC\_EAD**

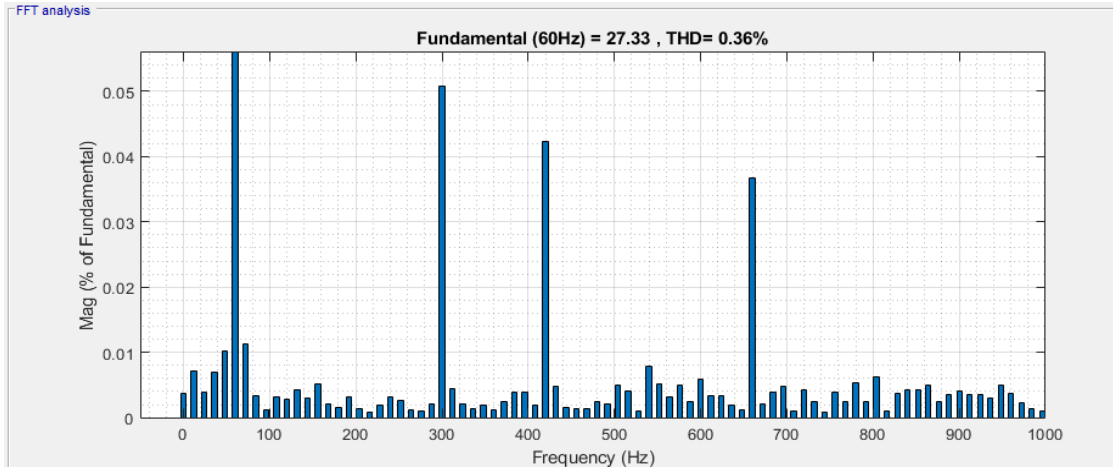


Figure 5.22: THD of a Grid Current – WACC\_EAD

From figure 5.21 and 5.22, it has been observed that the harmonics of an injected grid is reduced to 0.36%. Thus, the system is damped and stable. This has been achieved without adding any extra-feedback loop in the controller. Thus, this method is more efficient and less complex. After MATLAB Simulink, the model has also been designed in Typhoon.

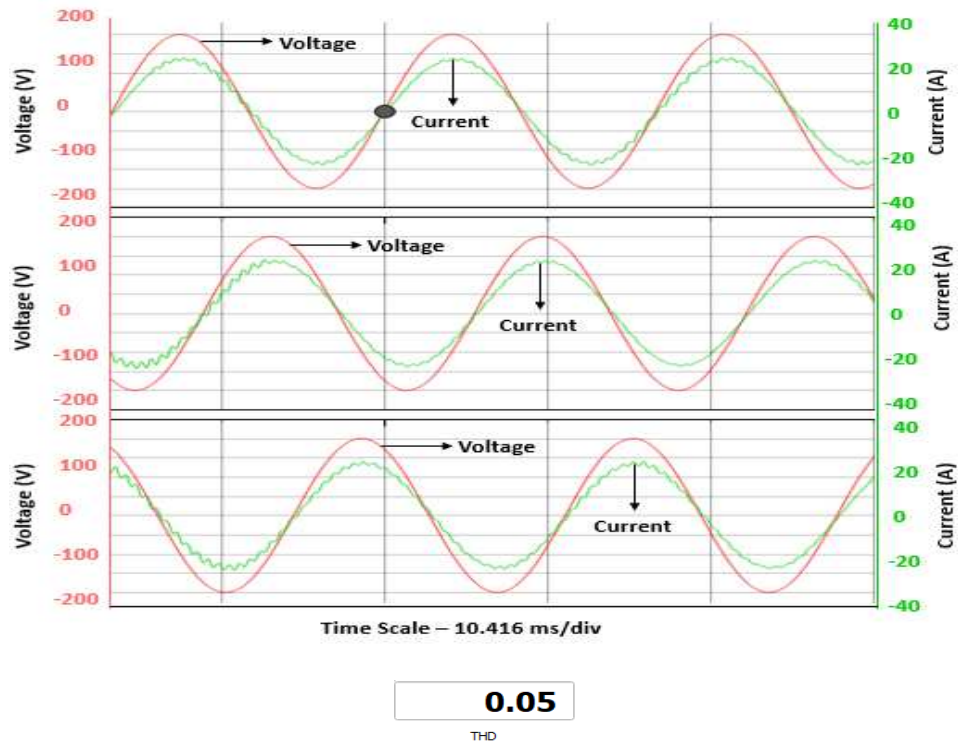


Figure 5.23: Grid Voltage and Grid Current – WACC\_EAD

From figure 5.23, it may be observed that the grid current has less harmonic as compared to an undamped system. The total harmonic distortion (THD) is only 5 %. Thus, the system is stable and damped.

**Table 5.1: Harmonics (THD) of injected grid current for various current control method from simulations**

Type of System	Harmonics of an injected grid (THD) from MATLAB Simulink	Harmonics of an injected grid (THD) from Typhoon Simulation
WACC - Undamped	2.31%	21%
WACC - Passive Damping	0.13%	1%
WACC - Active Damping	0.8%	5%
WACC_EAD	0.36%	5%

## CHAPTER 6: EXPERIMENTAL VERIFICATION

### 6.1. Introduction

After demonstrating all the current control methods using Typhoon and MATLAB Simulink, hardware experimental results using Typhoon Hardware-in-loop (HIL) and PICCOLO-F28035 controller has been presented in this chapter. The version of the Typhoon HIL is HIL-603. In the Typhoon, the three-phase grid-tied inverter with LCL filter has been designed. The topology of the inverter used is 2-level. The analog signals like the inverter-side current and the grid-side current of each phase has been measured by using current sensors and the grid voltage of each phase has been measured by using voltage sensor. After measuring the signals, all the analog signals have been scaled down in the typhoon, before sending them to the PICCOLO controller. The coding for the controller design of the system for various current control methods has been done in Code Composer Studio (CCS).

The code has been successfully debugged and has been transferred to the PICCOLO controller by using an USB cable. The controller works according to the code written in CCS for various current control methods and generates PWM signals, which will trigger the gates of the inverter.

The experimental set up of Typhoon HIL interfaced with the PICCOLO-F28035 controller has been shown. The hardware results of all the current control methods have been presented and the total harmonic distortion of an injected grid current has also been examined in this chapter.

## 6.2. Experimental Setup

From figure 6.1, it may be observed that the Typhoon HIL 603 has been interfaced with the PICCOLO-F28035 controller. In this setup, nine wires have been connected from the analog output port of the Typhoon to the analog pins of the PICCOLO controller. In this way, the analog signals (like the grid voltage, inverter-side current and the grid-side current of all phases) are flowing from the Typhoon to the PICCOLO controller. Whereas, six wires have been connected from the digital pins of the PICCOLO controller to the digital input port of the Typhoon. In this way, the digital signals (PWM signals) are flowing from the PICCOLO controller to the Typhoon HIL.

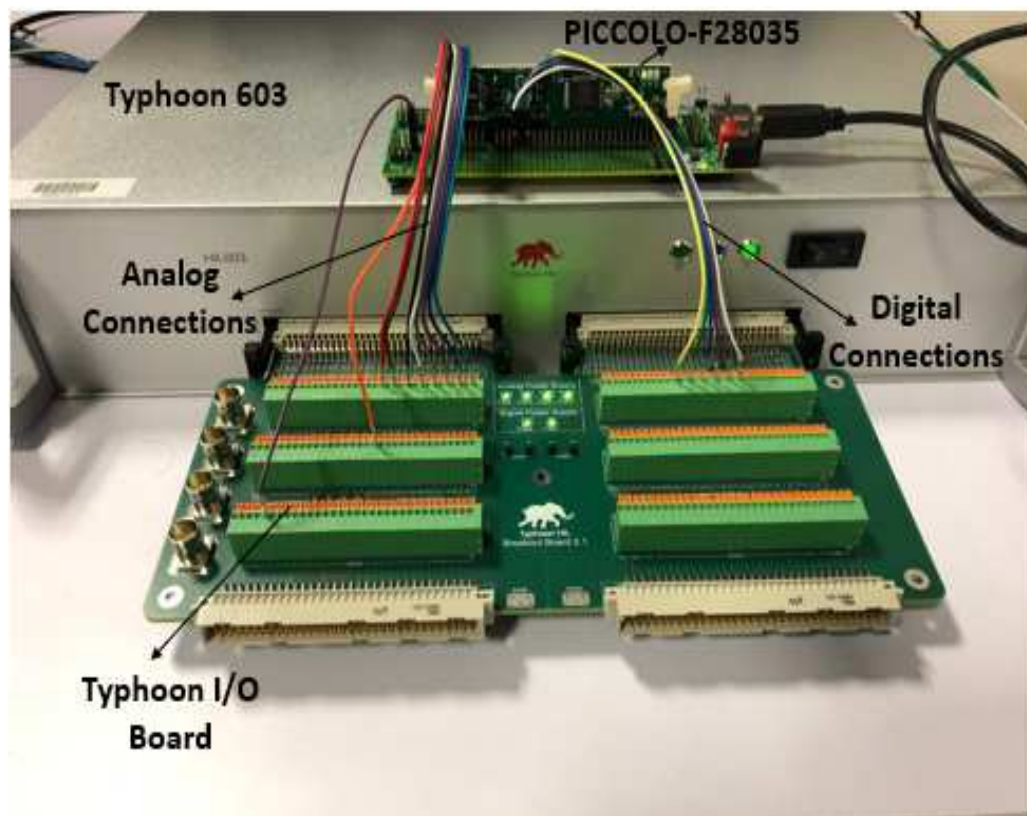
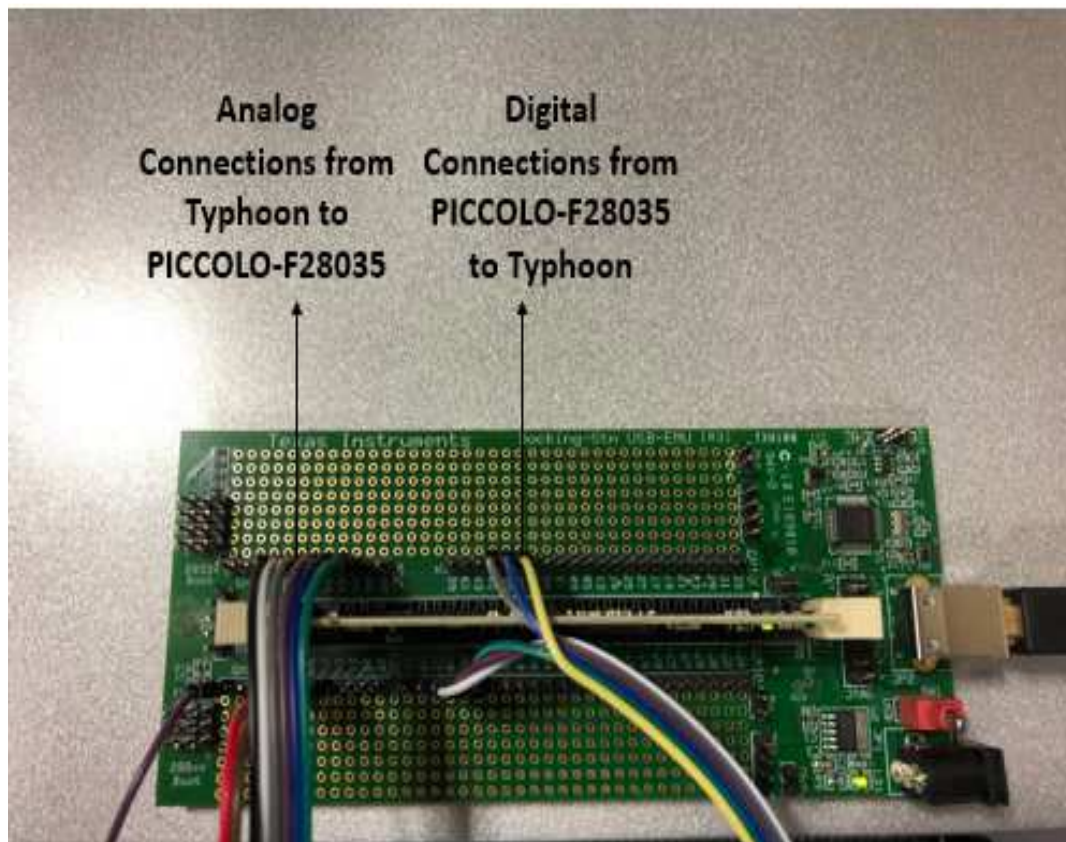


Figure 6.1: Experimental setup of Typhoon HIL 603 interfaced with the PICCOLO-F28035 controller

Before sending the analog signals from the Typhoon to the PICCOLO controller, the ratings of the input voltage of the controller must be checked from its manual. From the manual, it has been found that the ratings are 0-3.3 V. Therefore, all the analog signals in the Typhoon are scaled down to an acceptable range. However, the negative values are also not acceptable according to the ratings of the controller. Hence, a DC offset is also added after scaling down the signal.



**Figure 6.2: PICCOLO-F28035 Controller**

When the analog signals are being sent to the PICCOLO-F28035 controller from the Typhoon, the controller works according to a code written in C language. This code is transferred to the controller using CCS. In CCS, the code is written by following the controller design made in the Simulation part in chapter 5. When the code is triggered and

the model in Typhoon is executed, the digital signals are generated from the PICCOLO controller which are passed to the Typhoon. After a successful completion of this loop, the waveforms may be seen by the scope in the HIL Scada.

### 6.3. Hardware Results

In the PICCOLO controller, the codes of all the current control methods like WACC, WACC with Passive Damping, WACC with Active Damping, WACC\_EAD have been transferred one by one by using CCS and the waveforms of grid voltage and grid current of all the methods have been shown.

For WACC method, the grid voltage and the grid current has been shown in figure 6.3.

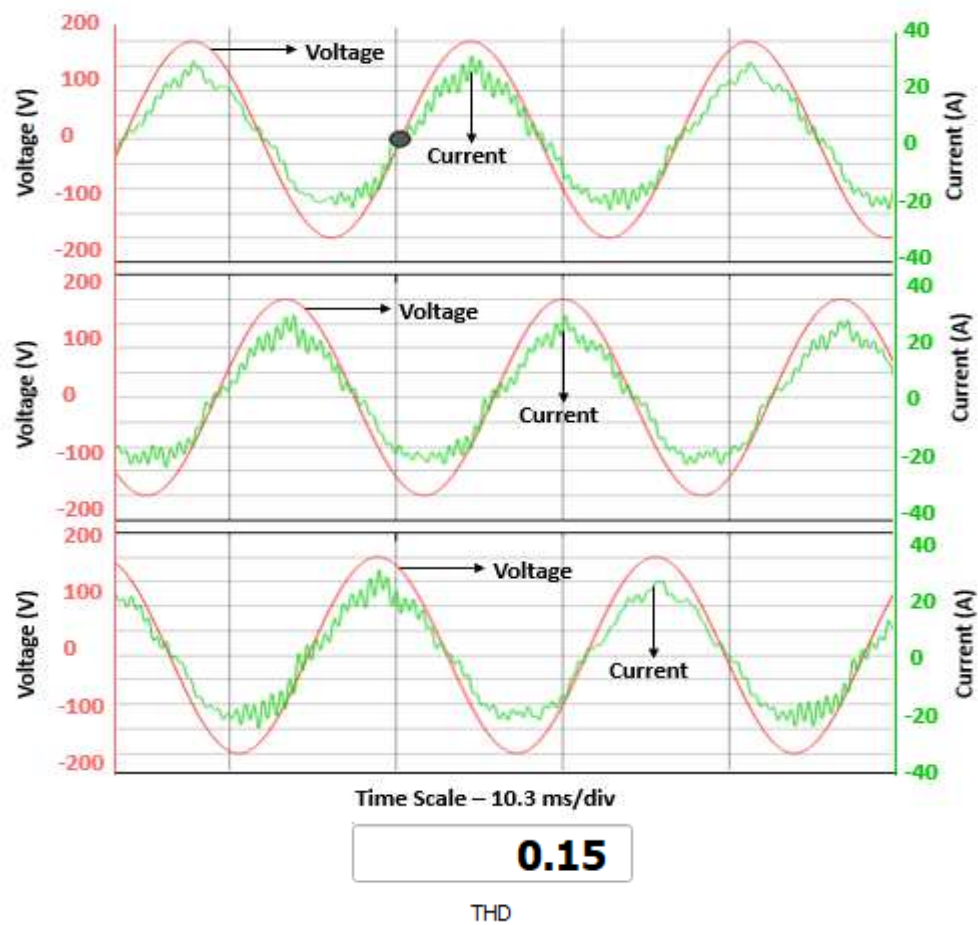


Figure 6.3: Grid Voltage and Grid Current – WACC

From figure 6.3, it has been inferred that the total harmonic distortion (THD) of a grid current is 15%. Thus, the injected grid current has a very high harmonics because the system with only WACC method is undamped in nature. Hence, the system is critically stable.

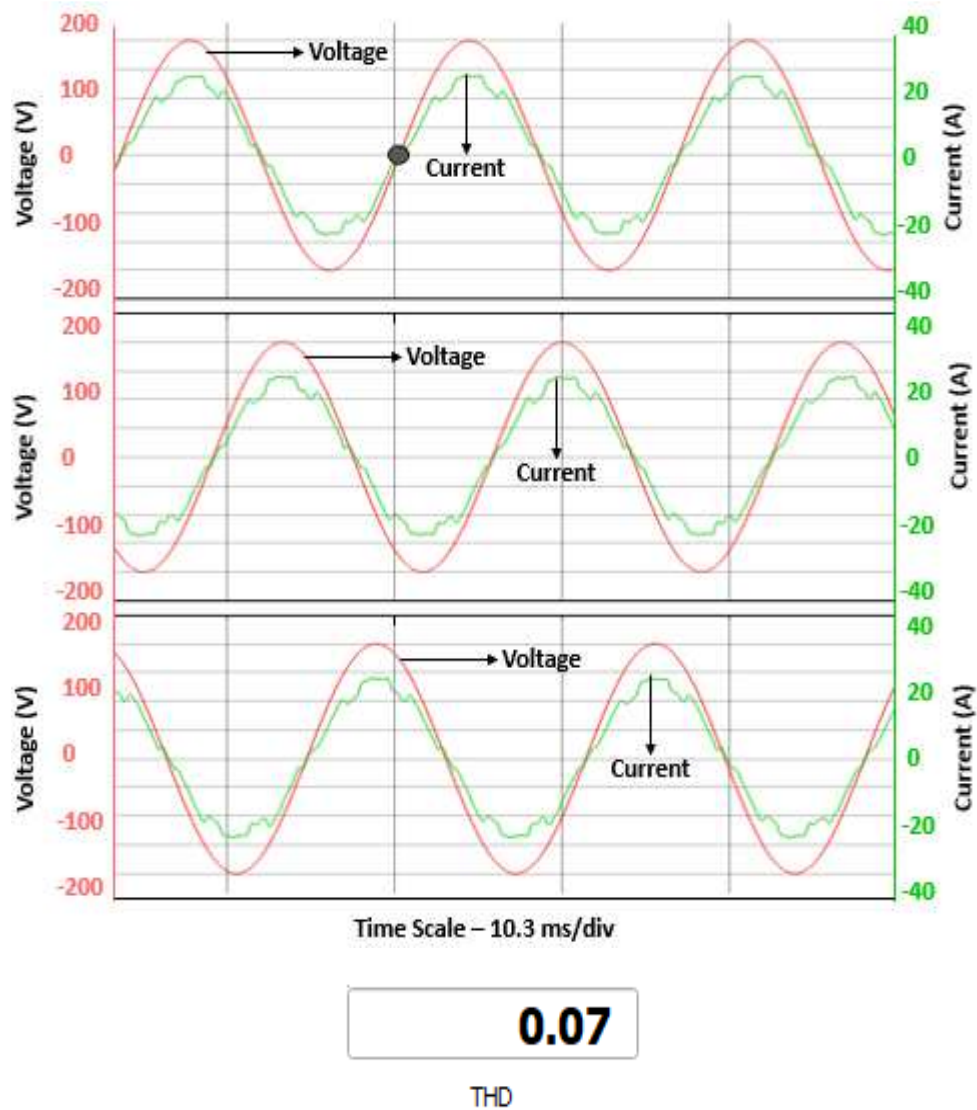


Figure 6.4: Grid Voltage and Grid Current – WACC with Passive Damping

The grid voltage and the grid current waveforms of a system for WACC with Passive Damping method has been shown in figure 6.4. From this figure, it has been noticed that the total harmonic distortion (THD) of an injected grid current is 7%. Thus, the harmonics

of an injected grid current is reduced. The resistor connected in series with LCL capacitor is making the system more damped. Hence, the system becomes stable and damped by using this method.

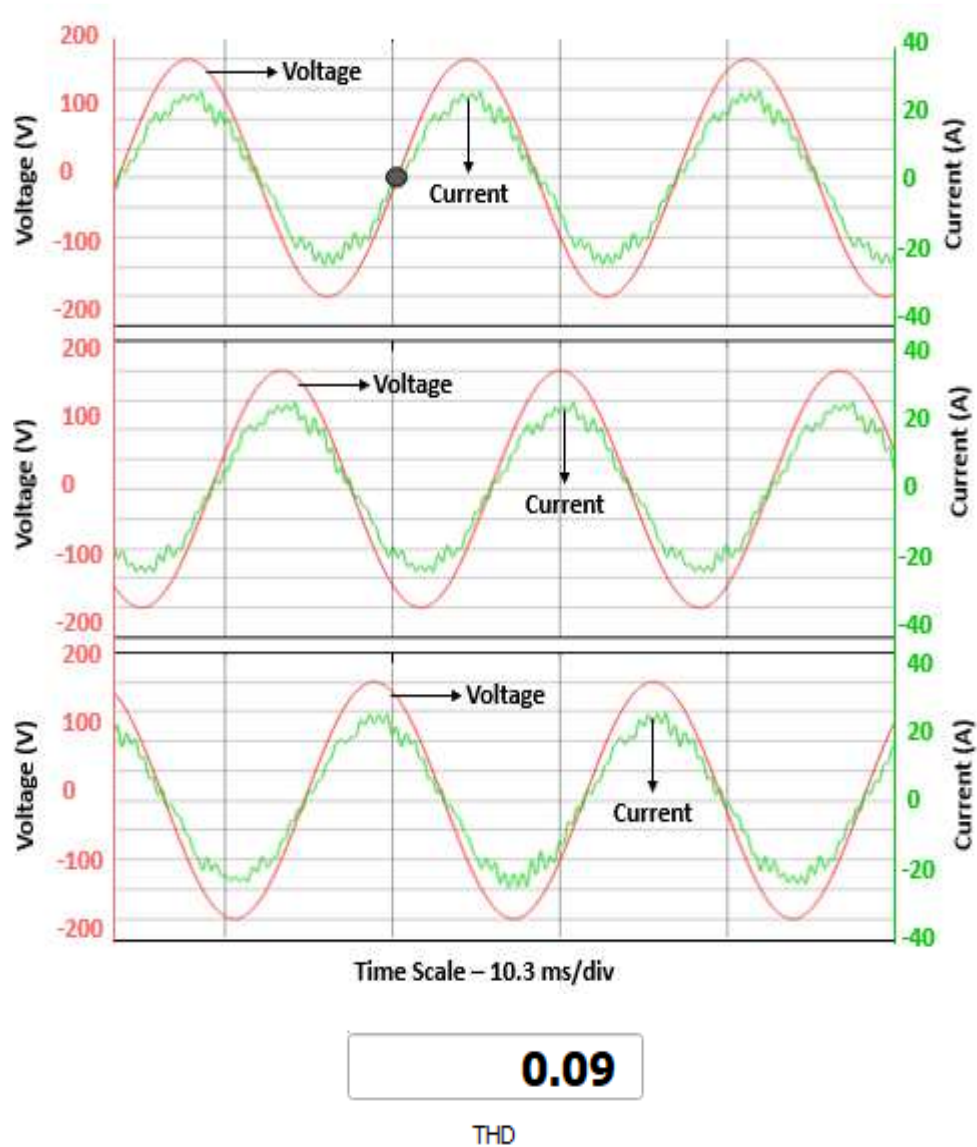


Figure 6.5: Grid Voltage and Grid Current – WACC with Active Damping

The grid voltage and the grid current waveforms of a system for WACC with Active Damping method has been shown in figure 6.5. From this figure, it has been observed that the total harmonic distortion (THD) of a grid current is 9%. Thus, the harmonics of an injected grid current is less than that of a system for WACC method. Here, the extra-

feedback loop gain is providing damping to the system. Thus, the system is becoming stable and damped by using this method.

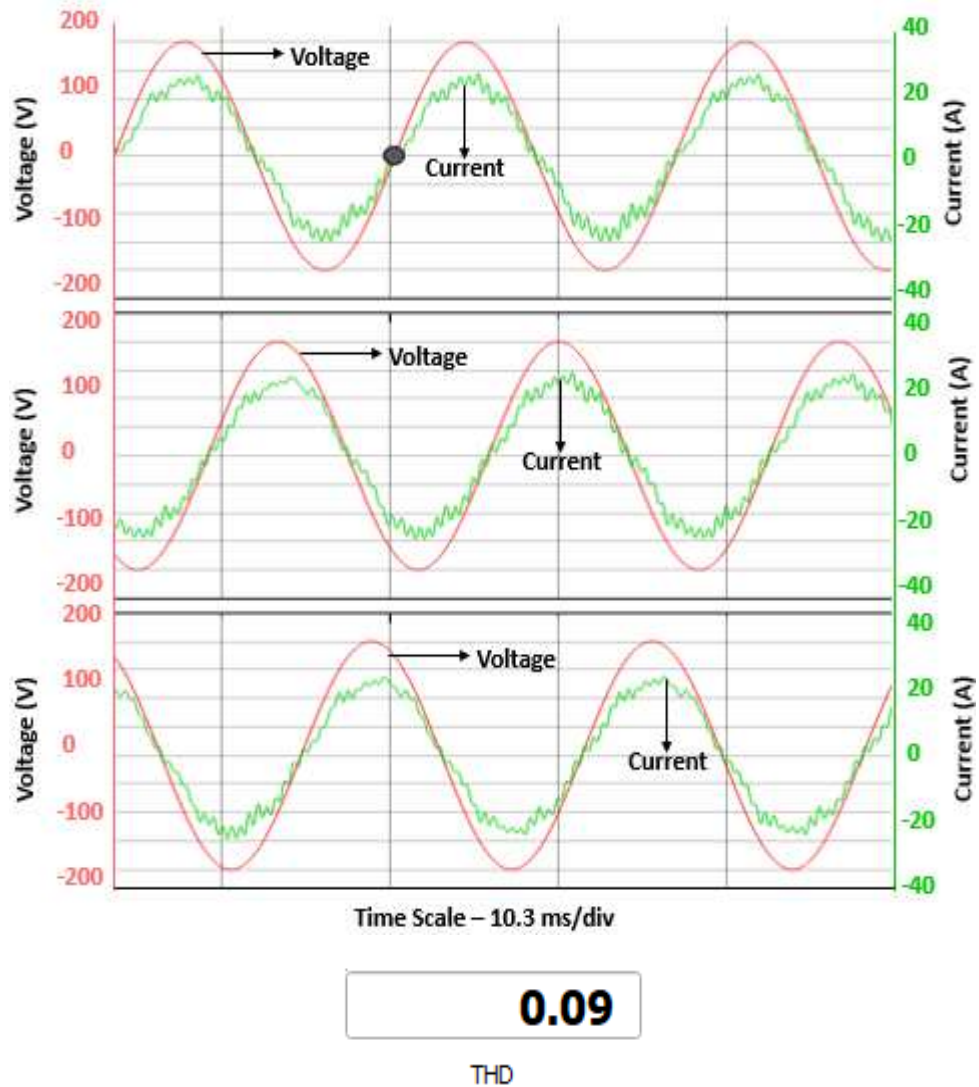


Figure 6.6: Grid Voltage and Grid Current – WACC\_EAD

The grid voltage and the grid current waveforms of a system for WACC\_EAD method has been shown in figure 6.6. From this figure, it has been inferred that the total harmonic distortion (THD) of an injected grid current is 9%. Thus, the harmonics of an injected grid current is less than that of a system for WACC method. Here, the gain of an inverter-side

current and that of a grid-side current is providing damping to the system. Thus, the system is becoming stable and damped by using this method.

**Table 6.1: Harmonics (THD) of injected grid current for various types of current control methods from hardware experiments**

Current control methods	Harmonics (THD) of an injected grid current from Hardware Experimental results
WACC - Undamped	15%
WACC - Passive Damping	7%
WACC - Active Damping	9%
WACC_EAD	9%

## CHAPTER 7: ROBUSTNESS OF A SYSTEM

### 7.1. Introduction

After designing the three-phase grid-tied LCL-filtered inverter system in Typhoon and MATLAB Simulink for various current control methods, the robustness of the system has been tested for WACC\_EAD method in Typhoon. The robustness has been first tested for strong and weak grid conditions. In this test, the ratio of the sum of the grid-side inductance and grid inductance to the inverter-side inductance has been found for various grid conditions. If this ratio is higher, the system stability will decrease and if the ratio is lesser, then the system stability will improve. The simulation waveforms have been presented for various grid conditions and the total harmonic distortions (THD) of an injected grid current has been examined.

The inverter-side current gain and the grid-side current gain of the system for WACC\_EAD method contains damping factor ( $K_d$ ). If this damping factor value is higher, then the system stability will improve and if the damping factor value is lower, then the system stability will get worse. For damping factor,  $K_d = 0$ , the system is critically stable. In such case, the current controller behaves as WACC method. Therefore, along with various grid conditions, the robustness of the system have also been tested for various damping factor values. The graph of inverter-side current gain and the grid-side current gain of WACC\_EAD method has been plotted for various damping factor values. In that graph, if the operating point or the coordination point is the left side of the mid-point, then the system is found to be stable because the inverter-side current gain will be more than

the grid-side current gain. However, if the coordination point is the right side of the mid-point, then the system is found to be unstable because the inverter-side current gain will be lesser than the grid-side current gain.

## 7.2. Test of robustness of a system for various grid conditions

In chapter 4, a mathematical analysis has been done for the WACC\_EAD method. Here, for the parameter  $L_1 = 0.6$  mH,  $L_2 = 0.2$  mH,  $L_g = 0.2$  mH and  $C = 30$  uF, the value of inverter-side current gain,  $K_1$  is 0.84 and the value of grid-side current gain,  $K_2$  is 0.16. The system is stable as the closed-loop poles are located at  $-8.84+9.96e3i$  and  $-8.84-9.96e3i$  i.e. in the left-half of s-plane, shown in figure 4.2. The stability of the system may also be verified from the figure 25, where the coordinate point of  $K_1$  and  $K_2$  is in the left side of the mid-point i.e. the stable region.

In this chapter, the stability of the system has been analyzed for various grid conditions. The stability of a system may be determined from the ratio of the sum of the grid side inductance ( $L_2$ ) and grid inductance ( $L_g$ ) to the inverter side inductance ( $L_1$ ). If this ratio increases, then the system will move towards instability and if the ratio decreases, then the system stability will improve. This ratio is 0.6667:1 for the parameter values mentioned in table 2.1.

For strong grid conditions, the grid inductance value has been reduced. The new parameter values are  $L_1=0.9$  mH,  $L_2=0.45$  mH,  $L_g=0.05$  mH. The ratio of the sum of the grid-side inductance and grid inductance ( $L_2+L_g$ ) to the inverter-side inductance ( $L_1$ ) is 0.5555. This ratio is found to be less, as compared to its previous case. Thus, the system stability will get improved.

The values of the gain of the inverter side current and that of the grid side current is also found to analyze the stability of a system for a strong grid condition.

$$K_1 = \frac{L_1 + \alpha K_d}{(L_1 + L_2)} = \frac{0.9e-3 + 0.9 * 0.5e-6 * 1000}{(0.9 + 0.5)e-3} = 0.9643 \text{ and } K_2 = \frac{L_2 - \alpha K_d}{(L_1 + L_2)} = \frac{0.9e-3 - 0.9 * 0.5e-6 * 1000}{(0.9 + 0.5)e-3} = 0.0357$$

As the system becomes more stable, the gain of inverter side current increases and the gain of the grid side current decreases, which may be seen in figure 7.1.

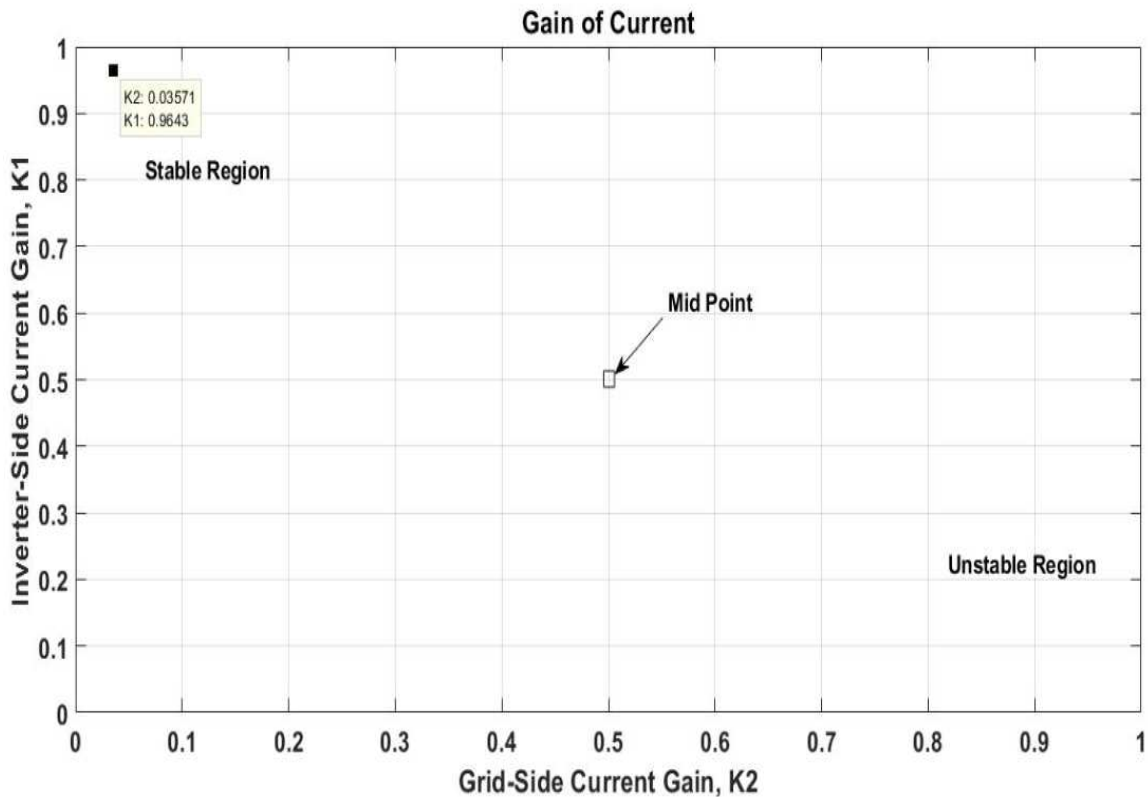


Figure 7.1: Graph of current gains for strong grid

From figure 7.1, it may be observed that the coordinate point of  $K_1$  and  $K_2$  is shifted more towards the left side of the mid-point i.e. the stable region. The closed loop poles are now located at  $-10.1 + 8.31e3i$  and  $-10.1 - 8.31e3i$ , which may be seen in the figure 7.2. Thus, the closed loop poles for strong grid condition are shifted more towards the left half of s-plane. This improves the stability of the entire system.

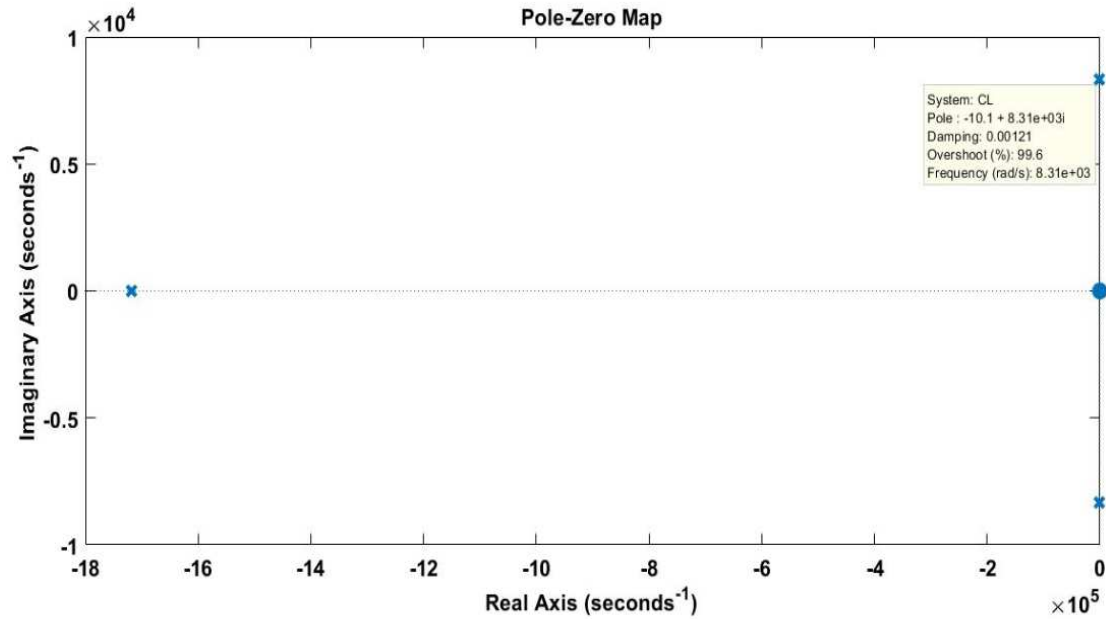


Figure 7.2: Pole-Zero plot - Strong Grid

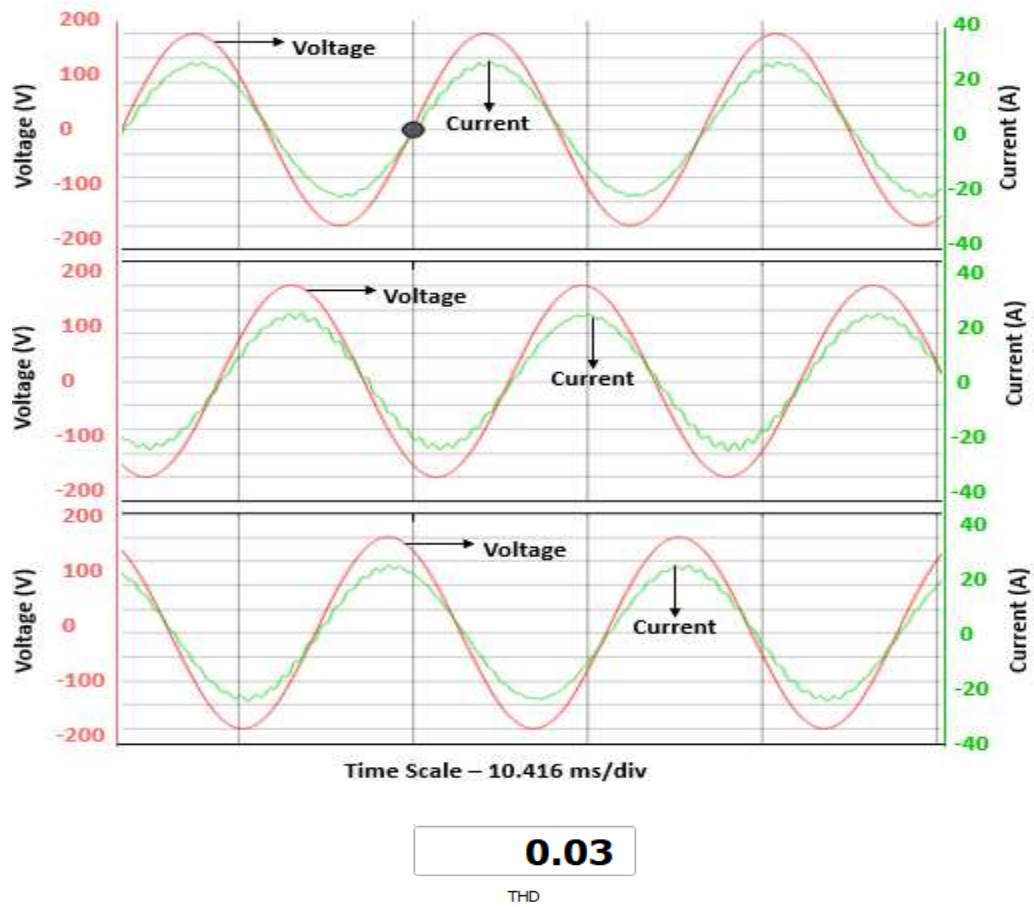


Figure 7.3: Grid Voltage and Grid Current- Strong Grid

From figure 7.3, it may be inferred that the THD of a grid current for a strong grid condition is reduced to 3% from 5%. For weak grid conditions, the grid inductance value has been increased. The new parameter values are  $L_1=0.2$  mH,  $L_2=0.02$  mH and  $L_g=0.28$  mH. The ratio of the sum of the grid-side inductance and grid inductance ( $L_2+L_g$ ) to the inverter-side inductance ( $L_1$ ) is 1.5. This ratio is found to be more, as compared to its previous cases. Thus, the system stability will get worse. The values of the gain of the inverter side current and that of the grid side current is also found to analyze the stability of a system for a weak grid condition.

$$K_1 = \frac{L_1 + \alpha K_d}{(L_1 + L_2)} = \frac{0.2e-3 + 0.2 * 0.3e-6 * 1000}{(0.2 + 0.3)e-3} = 0.52 \text{ and } K_2 = \frac{L_2 - \alpha K_d}{(L_1 + L_2)} = \frac{0.2e-3 - 0.2 * 0.3e-6 * 1000}{(0.2 + 0.3)e-3} = 0.48$$

As the system stability decreases, the gain of the inverter side current decreases and the gain of the grid side current increases, which may be seen in figure 7.4.

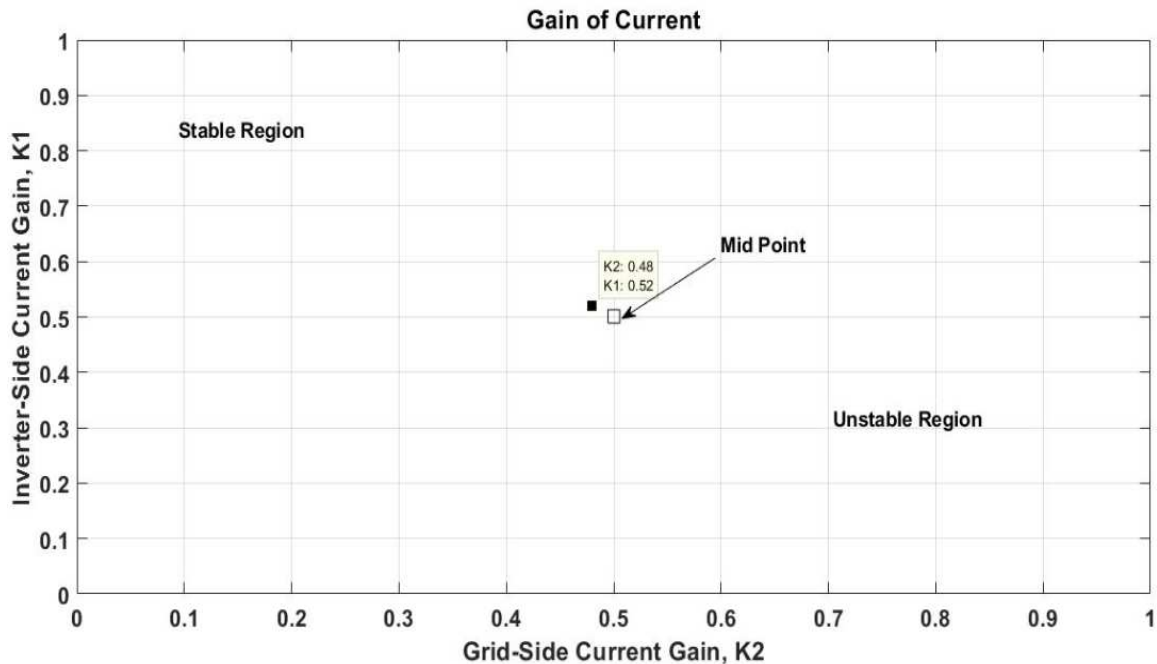


Figure 7.4: Graph of current gains for a weak grid

From figure 7.4, it may also be observed that the coordinate point of  $K_1$  and  $K_2$  is just at the left side of the mid-point. Hence, the stability of the system is poor in a weak grid

condition. The closed loop poles are now located at  $-7.69+1.46e4i$  and  $-7.69-1.46e4i$ , which may be seen in figure 7.5. Hence, the closed loop poles for a weak grid are shifted more towards the mid-point.

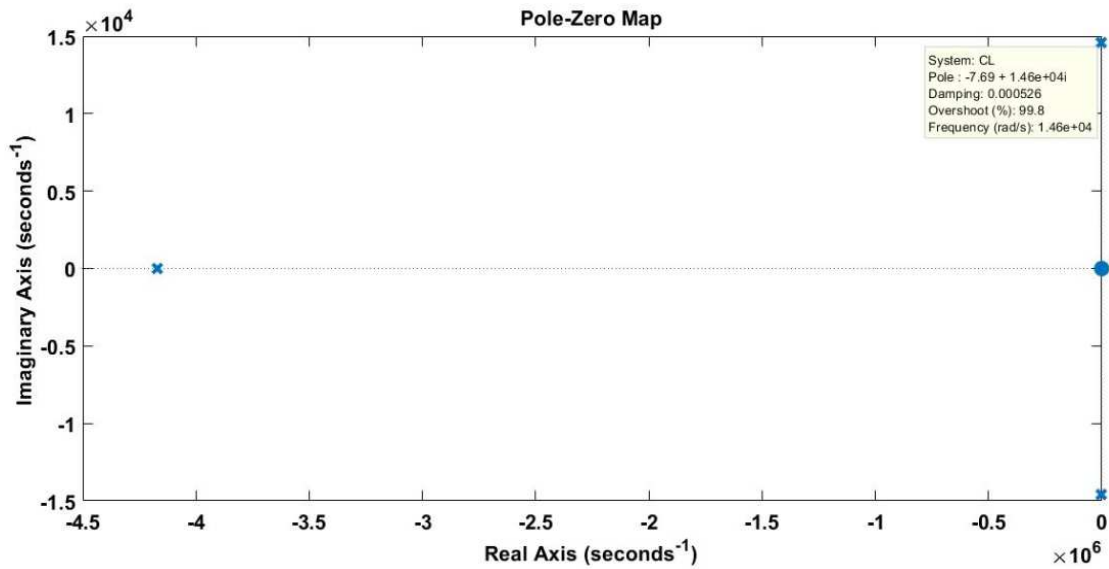
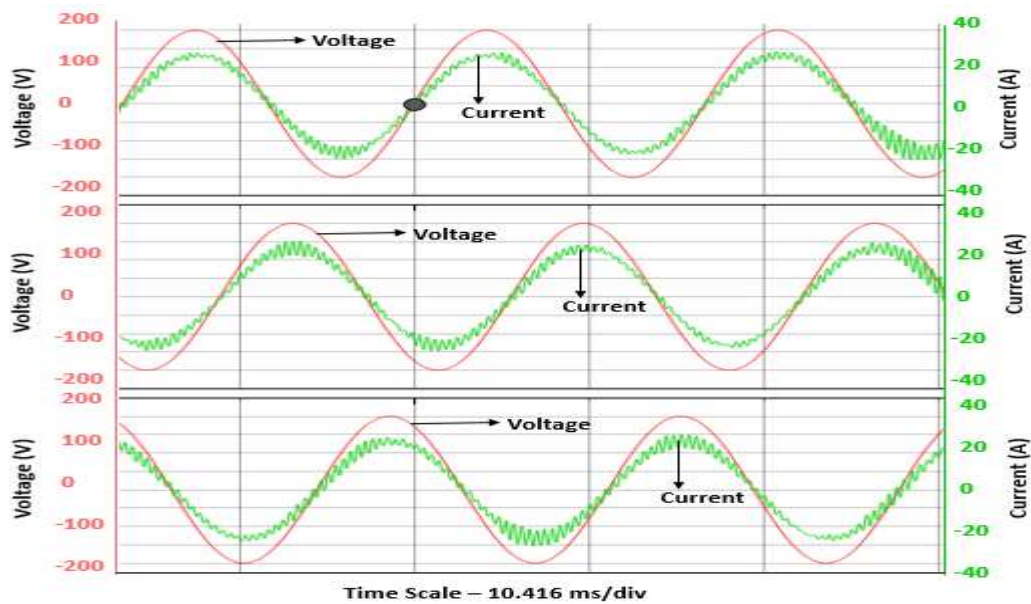


Figure 7.5: Pole-Zero plot - Weak Grid



**0.11**

THD

Figure 7.6: Grid Voltage and Grid Current – Weak Grid

From figure 7.6, it may be inferred that the THD of a grid current increases to 11% from 5% for a weak grid condition.

**Table 7.1: Performance of a system under strong and weak grid conditions**

Parameter Values	Inverter Side Current Gain, $K_1$	Grid Side Current Gain, $K_2$	Stability of a system	Harmonics of an injected grid current (THD)
$L_1=0.6$ mH, $L_2=0.2$ mH and $L_g=0.2$ mH	0.84	0.16	System is stable	5%
Strong Grid- $L_1=0.9$ mH, $L_2=0.45$ mH and $L_g=0.05$ mH	0.9643	0.0357	System stability increases	3%
Weak Grid- $L_1=0.2$ mH, $L_2=0.02$ mH and $L_g=0.28$ mH	0.52	0.48	System stability decreases	11%

### 7.3. Test of robustness of a system for various damping factor, $K_d$

It has been noticed from the Mathematical Analysis in Chapter 4 that the inverter side current gain,  $K_1$  and the grid side current gain,  $K_2$  in a WACC\_EAD method depends on a damping factor,  $K_d$ . If the value of  $K_d$  is higher, then the system stability is improved and

if it lower, then the system stability decreases. Thus,  $K_d$  also affects the stability of the system.

In chapter 4 and 5,  $K_d$  has been considered as 1000. For testing the robustness of the system, the  $K_d$  value has been increased to 1200 and the parameter values of table 2.1 has been used for finding the values of inverter-side current gain and the grid-side current gain.

With  $K_d=1200$ ,

$$K_1 = \frac{L_1 + \alpha K_d}{(L_1 + L_2)} = \frac{0.6e-3 + 0.6 * 0.4e-6 * 1200}{(0.6 + 0.4)e-3} = 0.888 \text{ and } K_2 = \frac{L_2 - \alpha K_d}{(L_1 + L_2)} = \frac{0.6e-3 - 0.6 * 0.4e-6 * 1200}{(0.6 + 0.4)e-3} = 0.112$$

With the increase of the damping factor,  $K_d$  value, the inverter side current gain increases to 0.888 from 0.84 and the grid side current gain decreases to 0.112 from 0.16. Thus, the system should move more towards stability.

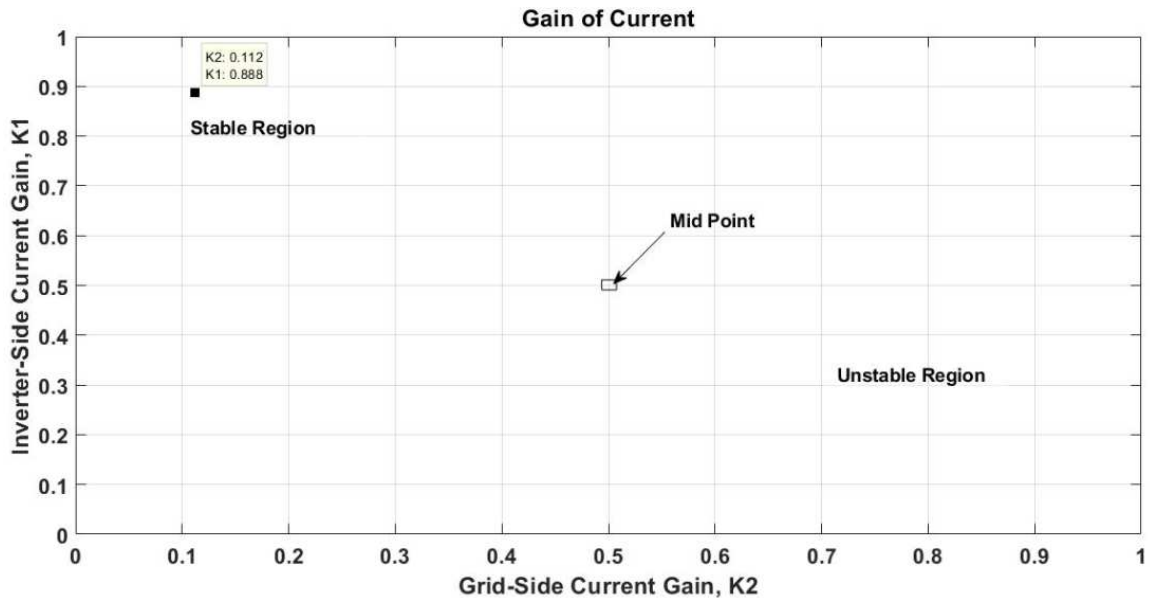


Figure 7.7: Graph of current gains for higher  $K_d$

From figure 7.7, it may be noticed that with the increase of  $K_d$  value, the coordinate point of  $K_1$  and  $K_2$  has been shifted more towards the left side of the mid-point, which means a more stable region. The closed loop poles of the system for  $K_d = 1200$  are found to be located at  $-9.49 + 9.69e3i$  and  $-9.49 - 9.69e3i$ , as shown in figure 6.8. Thus, the closed

loop poles are shifted more towards the left half of s-plane, which improves the system stability.

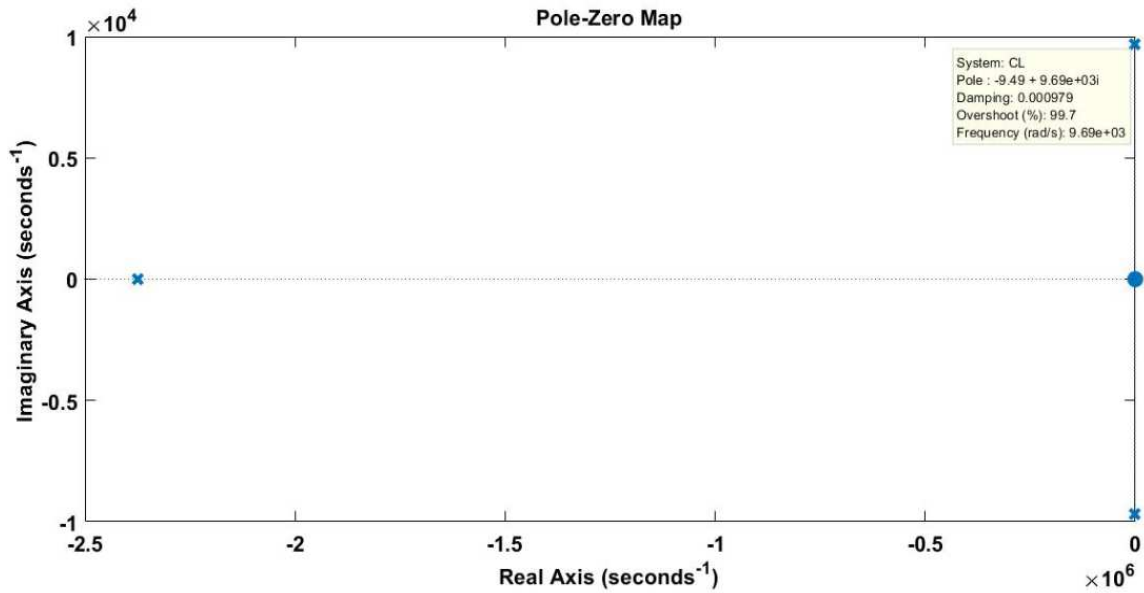


Figure 7.8: Pole-Zero plot for higher  $K_d$

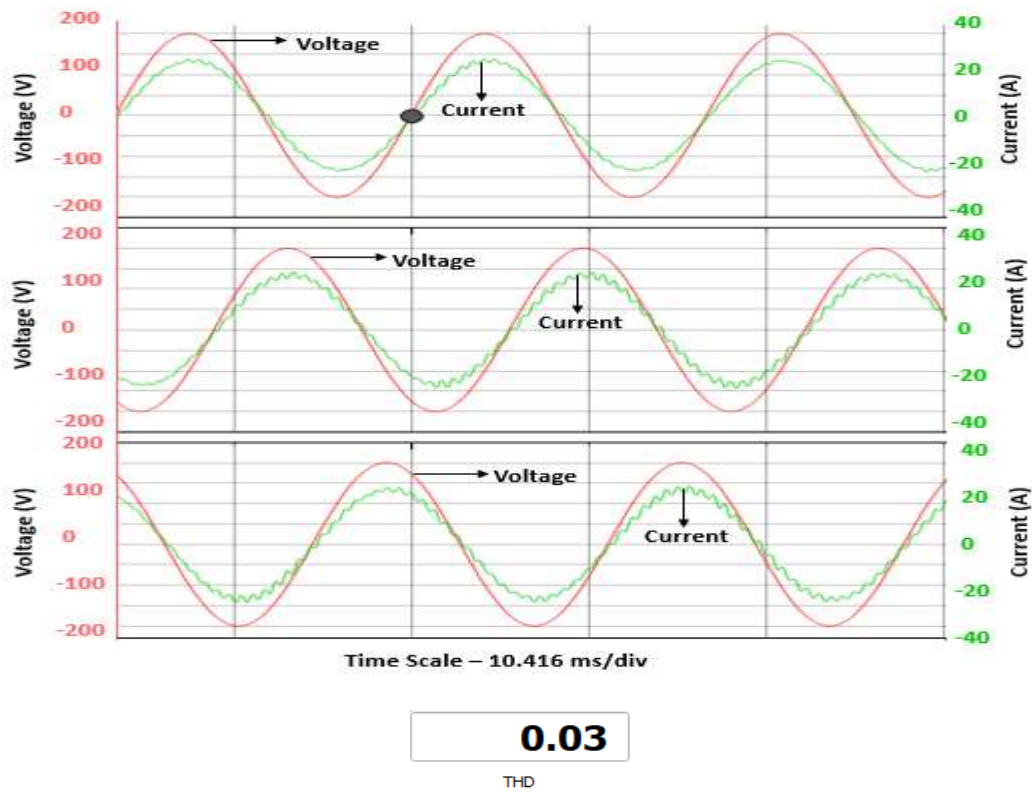


Figure 7.9: Grid Voltage and Grid Current - Higher  $K_d$

From figure 7.9, it may be seen that the THD of a grid current decreases to 3% from 5%, because of an increase in the value of a damping factor,  $K_d$ . If the  $K_d$  value is decreased to 700, then the value of  $K_1$  and  $K_2$  is calculated as:

$$K_1 = \frac{L_1 + \alpha K_d}{(L_1 + L_2)} = \frac{0.6e-3 + 0.6 * 0.4e-6 * 700}{(0.6 + 0.4)e-3} = 0.768 \text{ and } K_2 = \frac{L_2 - \alpha K_d}{(L_1 + L_2)} = \frac{0.6e-3 - 0.6 * 0.4e-6 * 700}{(0.6 + 0.4)e-3} = 0.232$$

Hence, with the decrease of the damping factor,  $K_d$  value, the inverter side current gain decreases to 0.768 from 0.84 and the grid side current gain increases to 0.232 from 0.16, shown in figure 6.10. Thus, the system stability decreases.

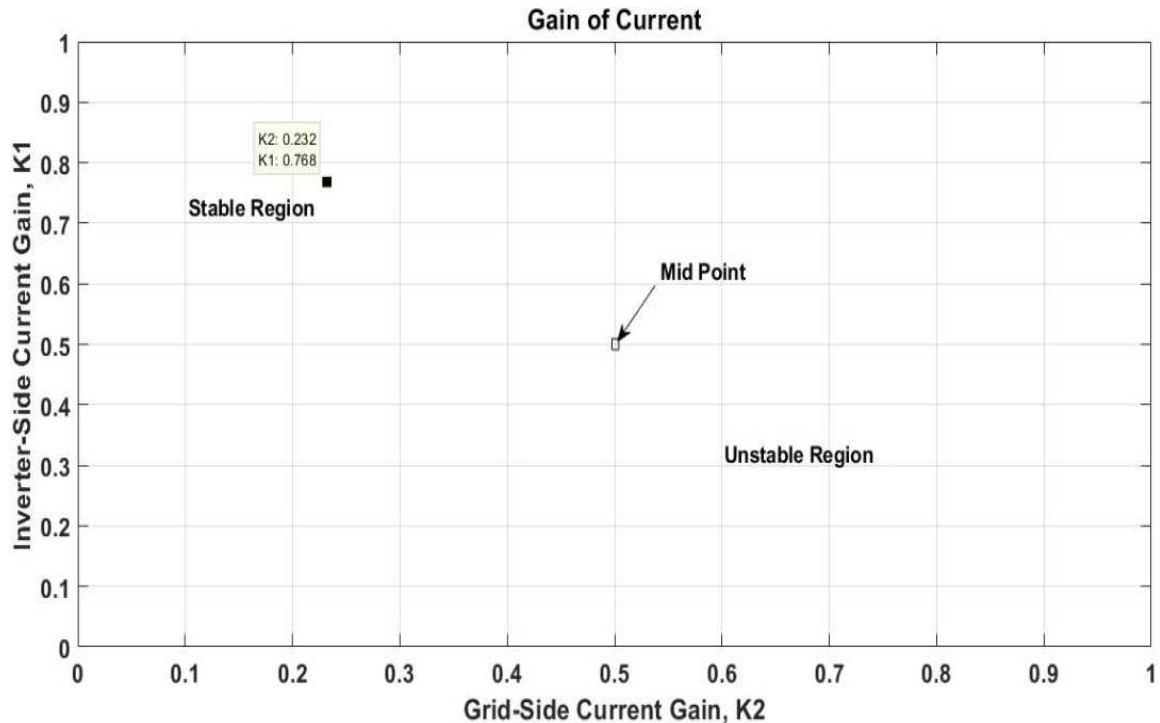
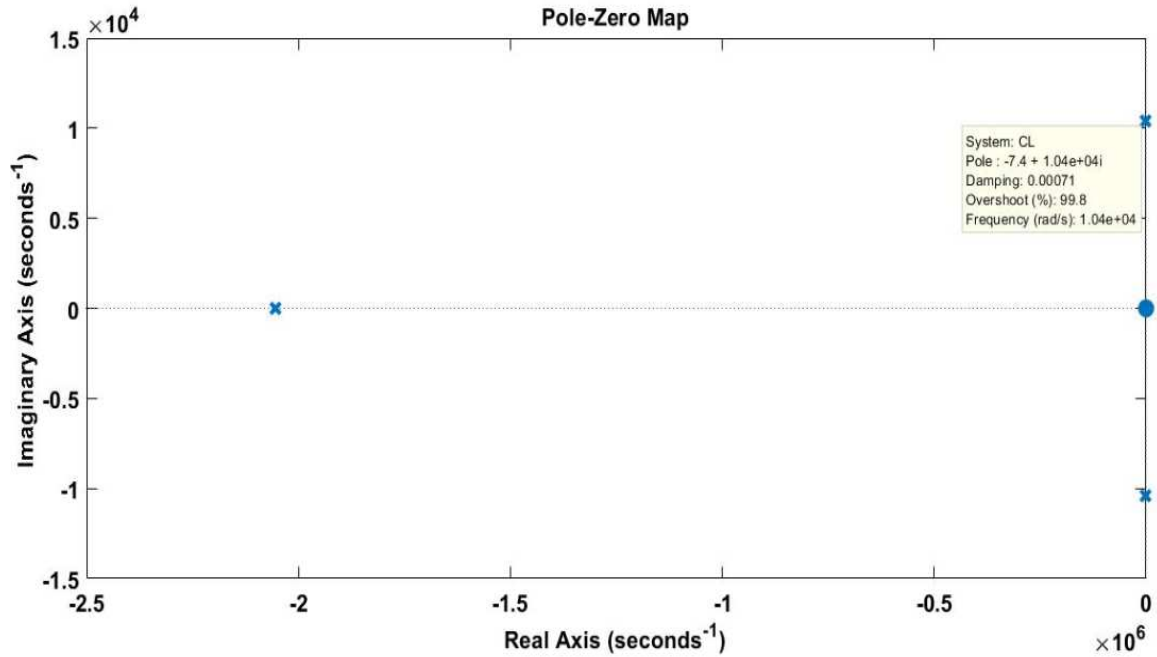
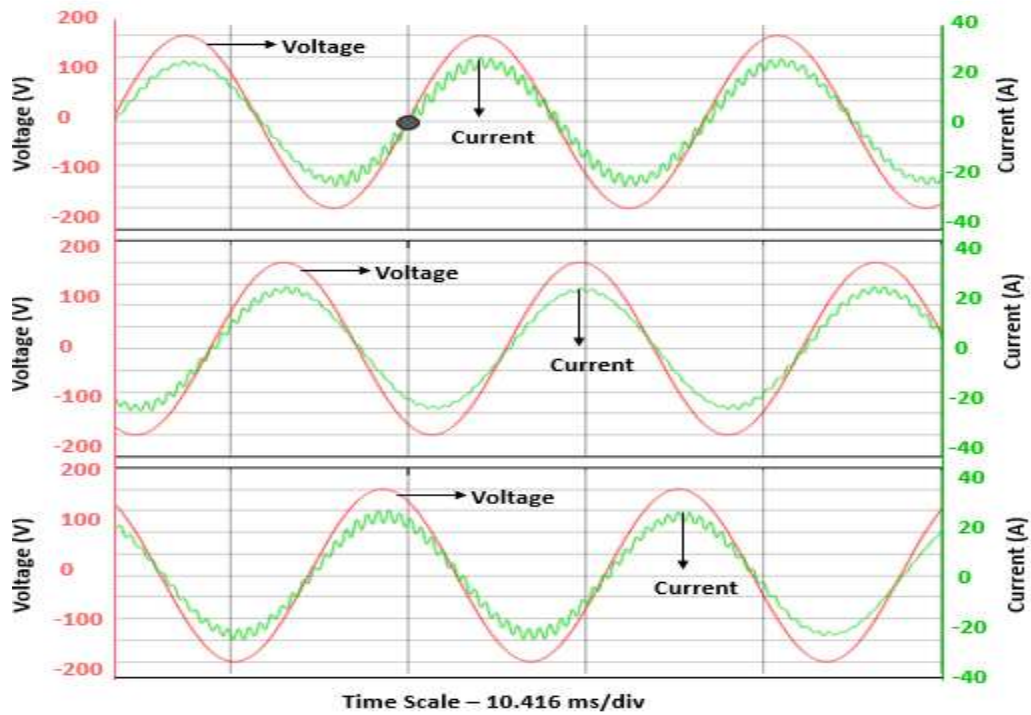


Figure 7.10: Graph of current gains for lower  $K_d$

From figure 7.10, it may be noticed that with the decrease of  $K_d$  value, the coordinate point of  $K_1$  and  $K_2$  shifted closer to the mid-point, which decreases the system stability. The closed loop poles for this case are found to be located at  $-7.4 + 1.04e4i$  and  $-7.4 - 1.04e4i$ , as shown in figure 7.11. Thus, the closed loop poles are shifted more towards the imaginary axis.

Figure 7.11: Pole-Zero plot for a lower  $K_d$ 

0.08

THD

Figure 7.12: Grid Voltage and Grid Current – Lower  $K_d$

From figure 7.12, it may be seen that the THD of a grid current increases to 8% from 5%, because of a decrease in the value of a damping factor,  $K_d$ .

**Table 7.2: Performance of a system for various damping factor,  $K_d$**

Damping Factor, $K_d$ .	Inverter Side Current Gain, $K_1$	Grid Side Current Gain, $K_2$	Stability of a system	Harmonics of an injected grid current (THD)
1000	0.84	0.16	System is stable	5%
1200	0.888	0.112	System stability increases	3%
700	0.768	0.232	System stability decreases	8%

## CHAPTER 8: DYNAMIC STIFFNESS

### 8.1. Introduction

To evaluate the robustness of the three-phase grid-tied LCL filtered inverter system, their dynamic stiffness characteristic for various current control methods has been examined. The dynamic stiffness of a voltage source system such as Uninterruptible Power System (UPS) inverter is defined as the transfer function from the grid voltage to grid current of the system [57]. However, the dynamic stiffness of a current controlled grid-tied inverter system is the inverse of the transfer function from the grid voltage to grid current of the system. The dynamic stiffness of a current controlled system is also defined as the magnitude of output grid voltage that causes a unit deviation in the injected grid current [58]. The stiffness of the controlled variable of the system for all frequencies may be determined from the dynamic stiffness characteristics. This analysis also helps us to know the harmonic behavior of the controlled variable [57]. High dynamic stiffness of a controlled variable leads to its low total harmonic distortion (THD) [58].

### 8.2. Dynamic stiffness characteristic of a WACC method

The dynamic Stiffness of a three phase grid-tied LCL filtered inverter system for a WACC method has been derived in (8.1).

$$\frac{V_g}{I_g} = \frac{s^3 L_1 L_2 C + s^2 C K_1 G_c k_{pwm} L_2 + s(L_1 + L_2) + k_{pwm} G_c (K_1 + K_2)}{s^2 L_1 C + s C K_1 G_c k_{pwm} + 1} \quad (8.1)$$

After substituting the equation of  $K_1$  and  $K_2$  of WACC method in (8.1), the dynamic stiffness of a system has been derived in (8.2).

$$\frac{V_g}{I_g} = \frac{s^3 L_1 L_2 C (L_1 + L_2) + s^2 C K_1 G_c k_{pwm} L_2 (L_1 + L_2) + s (L_1 + L_2)^2 + k_{pwm} G_c (L_1 + L_2)}{s^2 L_1 C (L_1 + L_2) + s C L_1 G_c k_{pwm} + (L_1 + L_2)} \quad (8.2)$$

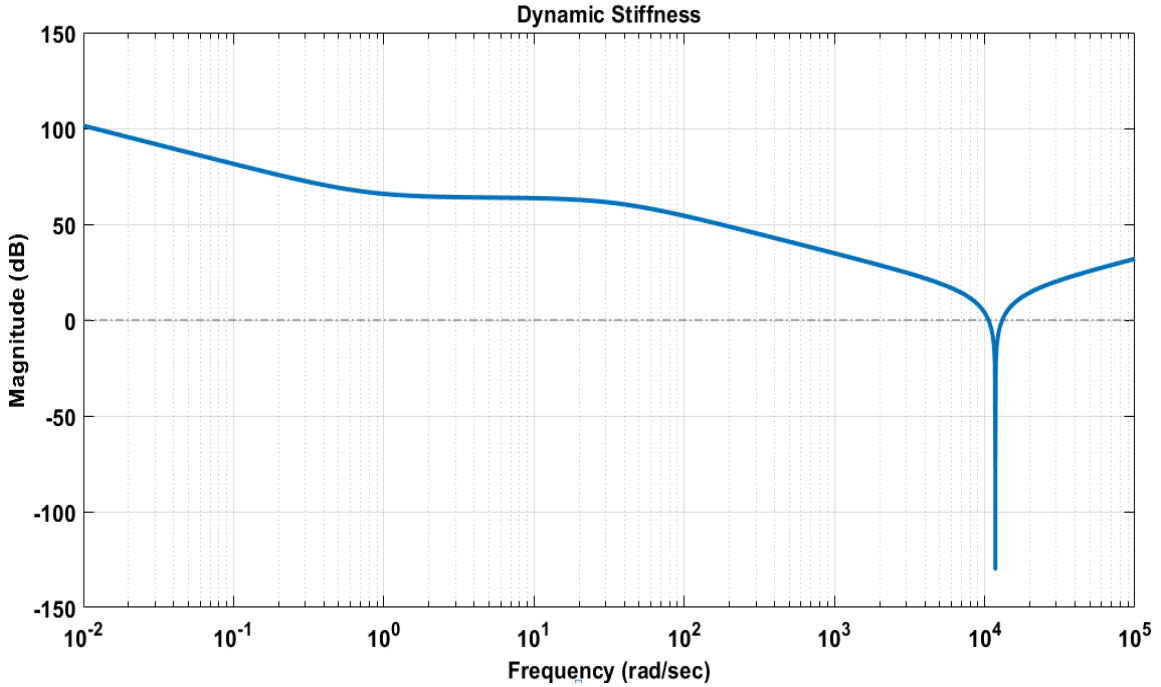


**Figure 8.1: Dynamic stiffness (Magnitude plot) of a three-phase grid-tied LCL filtered inverter system – WACC (Undamped)**

From the dynamic stiffness characteristic of a system for WACC (undamped) method shown in figure 8.1, it has been noticed that the system is undamped in nature, which leads to high total harmonic distortion of injected grid current. Damping methods like passive damping and active damping improves the dynamic stiffness characteristic of the system. However, due to power loss issue, passive damping is less efficient method. Hence, the dynamic stiffness characteristic of a WACC with Active Damping method has been examined.

### 8.3. Dynamic stiffness characteristic of a WACC with Active Damping method

The dynamic Stiffness of a three phase grid-tied LCL filtered inverter system for a WACC with Active Damping method has been derived in (8.2).

$$\frac{V_g}{I_g} = \frac{s^4 L_1^2 L_2 C^3 + 2s^3 L_1 L_2 C^3 (k_c + K_1 G_c) + s^2 [L_2 \{C^3 k_{pwm}^2 (K_c + K_1 G_c)^2 + L_1 C^2\} + L_1^2 C^2] + s [L_2 C^2 k_{pwm} (K_c + K_1 G_c) + L_1 C^2 k_{pwm} \{G_c (2K_1 + K_2) + K_c\}] + C^2 k_{pwm} G_c (K_c + K_1 G_c) (K_1 + K_2)}{s^3 L_1^2 C^3 + 2s^2 L_1 C^3 k_{pwm} (K_c + K_1 G_c) + s \{C^3 k_{pwm}^2 (K_c + K_1 G_c)^2 + L_1 C^2\} + C^2 k_{pwm} (K_c + K_1 G_c)} \quad (8.3)$$

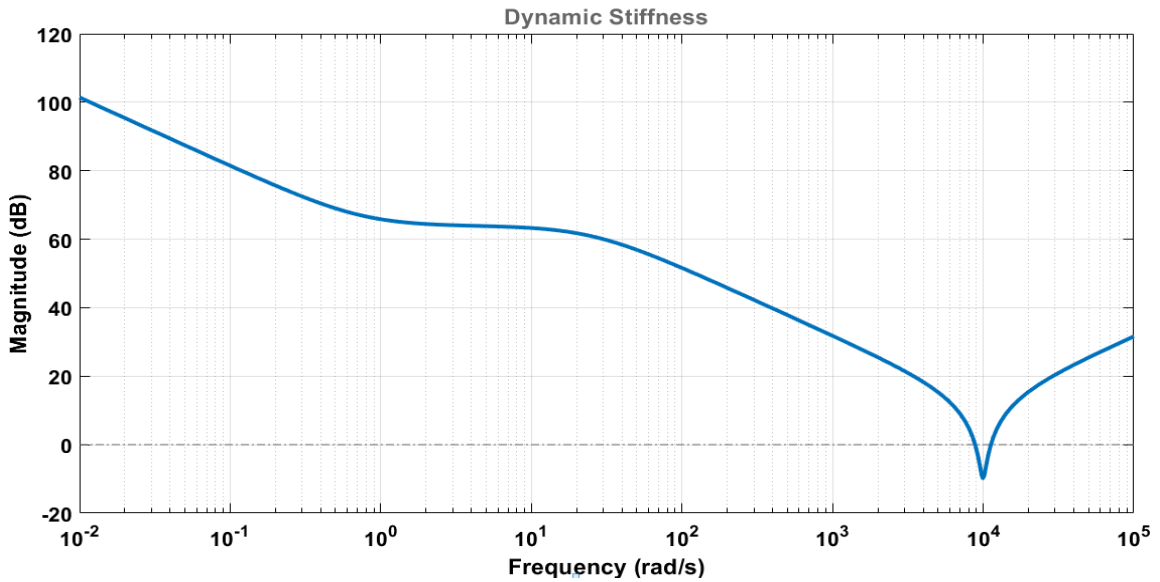


**Figure 8.2: Dynamic stiffness (Magnitude plot) of a three-phase grid-tied LCL filtered inverter system – WACC with Active Damping**

From the dynamic stiffness characteristic of a system for WACC with Active Damping method shown in figure 8.2, it has been inferred that the extra-feedback loop of capacitor current damps the LCL resonance. Therefore, the dynamic stiffness of a system has been improved, which leads to low total harmonic distortion of injected grid current. However, the controller design of the system is complex. Hence, the dynamic stiffness characteristic of a WACC\_EAD method has been examined.

#### 8.4. Dynamic stiffness characteristic of a WACC\_EAD method

$$\frac{V_g}{I_g} = \frac{s^3 L_1 L_2 C + s^2 C K_1 G_c k_{pwm} L_2 + s(L_1 + L_2) + k_{pwm} G_c (K_1 + K_2)}{s^2 L_1 C + s C K_1 G_c k_{pwm} + 1} \quad (8.4)$$

$$\frac{V_g}{I_g} = \frac{s^3 L_1 L_2 C (L_1 + L_2) + s^2 C K_1 G_c k_{pwm} L_2 (L_1 + L_2) + s(L_1 + L_2)^2 + k_{pwm} G_c (L_1 + L_2)}{s^2 L_1 C (L_1 + L_2) + s C (L_1 + L_1 L_2 K_d) G_c k_{pwm} + (L_1 + L_2)} \quad (8.5)$$

After substituting the equation of  $K_1$  and  $K_2$  of WACC\_EAD method in (8.4), the dynamic stiffness of a system has been derived in (8.5).

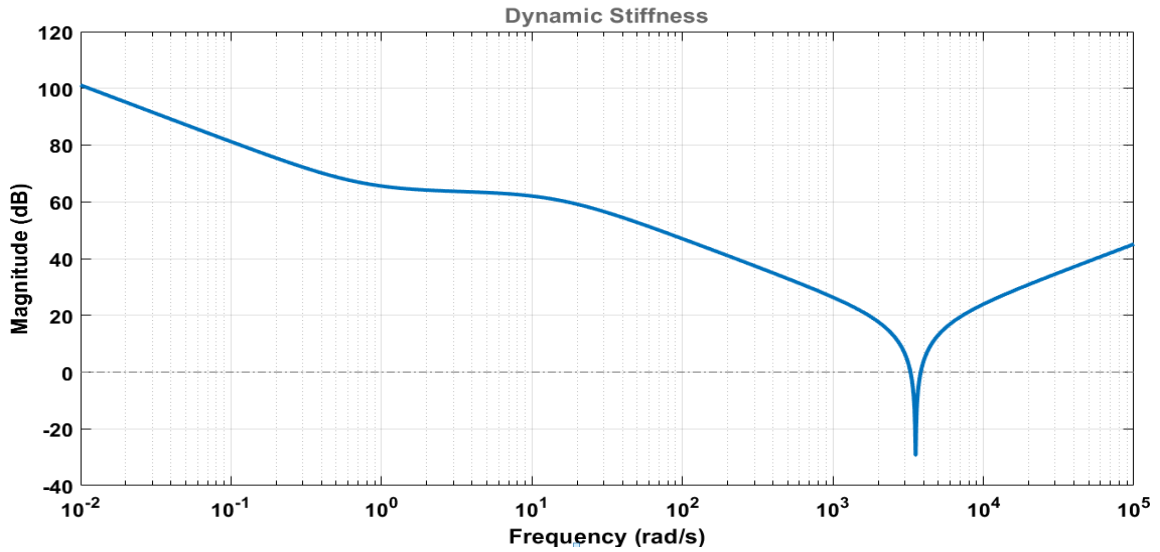


**Figure 8.3: Dynamic stiffness (Magnitude plot) of a three-phase grid-tied LCL filtered inverter system – WACC\_EAD**

From the dynamic stiffness characteristic of a system for WACC\_EAD shown in figure 8.3, it has been observed that the inverter-side current gain and the grid-side current gain is providing damping to the system. Therefore, the dynamic stiffness of a system has been improved, compared to a system for WACC (undamped) method. Here, the harmonic of injected grid current has been reduced without adding any extra-feedback loop.

## CHAPTER 9: CONCLUSION AND FUTURE WORK

### 9.1. Introduction

It has been observed that LCL filter is a more widely used filter, as compared to other filters because it may reduce high-frequency current harmonics, with more accuracy. However, it has stability issues because it triggers the resonance between the inverter and the grid. In addition to stability issues, this filter also makes the controller design of the system complex, if the grid-side current is used for the feedback control like in CCC method. In order to simplify the controller design of the system, WACC method was introduced. This method stabilizes the weighted average current but not the grid current. The grid current is marginally stable. Hence, the WACC method helps in making the controller design of the system simpler but the system is not stable. Therefore, this method has been improved by implementing various damping methods like passive damping and active damping. Execution of a passive damping method, where only a resistor is connected in series with the capacitor of an LCL filter is very simple and convenient to implement. With the increase of this resistance value, the system becomes more damped and stable, but it also faces power loss issues. This decreases the efficiency of the entire system. To avoid this issue of power loss, the active damping method has been applied, where an extra-feedback loop of capacitor current or voltage state damps LCL resonance. Although this method is more efficient and flexible as compared to passive damping

method, the controller design of this method is complex because of an extra-feedback loop. From the simulation and the hardware results, it has been inferred that the harmonics of the injected grid current of the system is reduced by implementing passive damping or active damping method.

## 9.2. Contributions

It has been noticed that in passive damping method, there is a limitation of less efficiency and in active damping method, there is a drawback of complex controller design. In order to overcome both the disadvantages, a new current control method has been proposed. In this new method, the equation of the gain of the inverter-side current and that of the grid-side current is modified. In this way, the inverter-side current gain will always be higher than the grid-side current gain. This new equation of the current gains provides damping and stability to the system, without implementing any external damping methods. Hence, the system becomes stable without altering the power circuit and without adding any extra-feedback loop in the controller design of the system. Here, with the help of the current gains, the system becomes actively damped. Due to this reason, this method is called as the Weighted Average Current Controller with Embedded Active Damping (WACC\_EAD). By implementing this new method, the harmonics of the injected grid current is also reduced like in active damping case. The system is also found to be robust. The robustness of the system has been tested for various grid conditions and damping factor values. In case of a strong grid, the system stability has been improved. Whereas, the system stability has been reduced in the case of a weak grid. It has also been deduced that with the increase of the damping factor value, the inverter-side

current gain increases and the grid-side current gain decreases. Therefore, the system stability increases with the increase of the damping factor. From the dynamic stiffness characteristics, it is found that the grid current for the WACC\_EAD method is stiffer, when compared to an undamped system, without adding any extra-feedback loop.

### 9.3. Future Work

WACC method simplifies the controller design of the three-phase grid-tied LCL filtered inverter system but to make the system stable, current control methods like WACC with passive damping, WACC with active damping and WACC\_EAD has been implemented in this dissertation. For all these current control methods, the system is using 6 current sensors in a three-phase system (3 sensors each for inverter-side current and grid-side current). Whereas, the system becomes highly unstable, when the CCC method is in use but the number of sensors used in this method is 3, which is less than that of the other current control methods. Thus, with the use of WACC, WACC with passive damping, WACC with active damping and WACC\_EAD methods, the cost of the system also increases. In order to overcome this drawback, the current in the inverter-side may be estimated. Thus, to make the system more economical, all the currents in the inverter-side of the system must be estimated, which will reduce the number of sensors, used in the entire system.

The WACC\_EAD methods may also be applied to a system where the grid is connected to multiple inverters with LCL filter. The stability of the system may be analyzed, and the harmonics of the injected grid current may be examined with the increase of the inverters in the system.

## REFERENCES

- [1] B Kurian and R Liyanapathirana, "Renewable Energy Resources Development in the EU Zone," in 2018 4th International Conference on Electrical Energy Systems (ICEES), 2018, pp. 635-639.
- [2] Franz Christange and Thomas Hamacher, "Analytical Modeling Concept for Weather Phenomena as Renewable Energy Resources," in 2016 IEEE International Conference on Renewable Energy Research and Applications (ICRERA), 2016, pp. 273-278.
- [3] A. Etxeberria, J.M. Vinassa, I. Vechiu and H. Camblong, "Hybrid Energy Storage Systems for Renewable Energy Sources Integration in Microgrids: A Review," IPEC, 2010 Conference Proceedings, 2010, pp. 532-537.
- [4] S. Narendiran, "Grid tie inverter and MPPT - A review," 2013 International Conference on Circuits, Power and Computing Technologies (ICCPCT), 2013, pp. 564-567.
- [5] B. Blackstone, Y. Baghzouz and S. Premrudeepreechacharn, "Determining MPPT and anti-islanding techniques in a grid-tie PV inverter," 2012 IEEE 15th International Conference on Harmonics and Quality of Power, 2012, pp. 409-413.
- [6] Md. Nahid Hossain, Tushar Kanti Routh, Abdul Hamid Bin Yousuf, Miah Md. Asasduzzaman, Md. Iqbal Hossain and Ummul Husnaeen, "Design and development of a grid tied solar inverter," 2012 International Conference on Informatics, Electronics & Vision (ICIEV), 2012, pp. 1054-1058.
- [7] B. Gu, J. Dominic, J. S. Lai, C. L. Chen, T. LaBella, and B. Chen, "High reliability and efficiency single-phase transformerless inverter for grid-connected photovoltaic systems," IEEE Trans. Power Electron., vol. 28, no. 5, pp. 2235–2245, May 2013.
- [8] C. Zou, B. Liu, S. Duan, and R. Li, "Influence of Delay on System Stability and Delay Optimization of Grid-Connected Inverters with LCL Filter," IEEE Transactions on Industrial Informatics, vol. 10, pp. 1775-1784, August 2014.
- [9] M. Lindgren and J. Svensson, "Control of a voltage-source converter connected to the grid through an LCL-filter-application to active filtering," in Proc. Rec. 29th Annu. IEEE Power Electron. Spec. Conf. (PESC'98), vol. 1, 1998, pp. 229–235.
- [10] C. Xie, Y. Wang, X. Zhong, and C. Chen, "A novel active damping method for LCL-filter-based shunt active power filter," in Proc. IEEE Int. Symp. Ind. Electron. (ISIE'12), 2012, pp. 64–69.

- [11] W. Wu, Y. He, T. Tang and F. Blaabjerg, "A New Design Method for the Passive Damped LCL and LLCL Filter-Based Single-Phase Grid-Tied Inverter," *IEEE Transactions on Industrial Informatics*, vol. 60, pp. 4339-4350, October 2013.
- [12] Y. Tang, P. C. Loh, P. Wang, F. H. Choo, F. Gao and F. Blaabjerg, "Generalized design of high-performance shunt active power filter with output LCL filter," *IEEE Trans. Ind. Electron.*, vol. 59, pp. 1443-1452, March 2012.
- [13] I. J. Gabe, J. R. Massing, V. F. Montagner and H. Pinheiro, "Stability Analysis of Grid-Connected Voltage Source Inverters with LCL-Filters using Partial State Feedback," in *European Conference on Power Electronics and Applications, 2007*, pp. 1-10.
- [14] B. Wang, Y. Xu, Z. Shen, J. Zou, C. Li and H. Liu, "Current Control of Grid-Connected Inverter with LCL Filter Based on Extended-State Observer Estimations Using Single Sensor and Achieving Improved Robust Observation Dynamics," *IEEE Trans. Ind. Electron.*, vol. 64, pp. 5428-5439, July 2017.
- [15] J. Xu and S. Xie, "Optimization of Weighted Current Control for Grid-Connected LCL-Filtered Inverters," in *IEEE ECCE Asia Downunder, 2013*, pp. 1170-1175.
- [16] G. Shen, X. Zhu, J. Zhang and D. Xu, "A new feedback method for PR current control of LCL-filter-based grid-connected inverter," *IEEE Trans. Ind. Electron.*, vol. 57, no. 6, pp. 2033-2041, June 2010.
- [17] G. Shen, J. Zhang, X. Li, C. Du, and D. Xu, "Current Control Optimization for Grid-tied Inverters with Grid Impedance Estimation," in *Proc. IEEE Applied Power Electronics Conference and Exposition, 2010*.
- [18] N. He, D. Xu, Y. Zhu, J. Zhang, G. Shen, Y. Zhang and J. Ma, C. Liu, "Weighted Average Current Control in a Three-Phase Grid Inverter with an LCL Filter," *IEEE Transactions on Power Electronics*, vol. 28, pp. 2785-2797, August 2013.
- [19] N. He, J. Zhang, Y. Zhu, G. Shen, and D. Xu, "Weighted average current control in three-phase grid inverter with LCL-filter," in *Proc. IEEE 7th Int. Power Electron. Motion Control Conf., Harbin, China, Jun. 2012*, pp. 826-830.
- [20] D. Pan, X. Ruan, X. Wang, H. Yu and Z. Xing, "Analysis and Design of Current Control Schemes for LCL-Type Grid-Connected Inverter Based on a General Mathematical Model," *IEEE Transactions on Power Electronics*, vol. 32, pp. 4395-4410, June 2017.

- [21] Z. Li, P. Yang, C. Wang, L. Xu, J. M. Guerrero and Y. Han, "Analysis and Design of Improved Weighted Average Current Control Strategy for LCL-Type Grid-Connected Inverters," *IEEE Transactions on Energy Conversion*, vol. 32, pp. 941-952, September 2017.
- [22] M. Liserre, F. Blaabjerg, and S. Hansen, "Design and control of an LCLfilter-based three-phase active rectifier," *IEEE Trans. Ind. Appl.*, vol. 41, no. 5, pp. 1281–1291, Sep./Oct. 2005.
- [23] T. C. Y. Wang, Y. Zhihong, S. Gautam, and Y. Xiaoming, "Output filter design for a grid-interconnected three-phase inverter," in *Proc. IEEE 34th Annu. Power Electron. Spec. Conf. (PESC'03)*, 2003, vol. 2, pp. 779–784.
- [24] R. Pena-Alzola et al., "Analysis of the passive damping losses in LCL-filter based grid converters," *IEEE Trans. Power Electron.*, vol. 28, no. 6, pp. 2642–2646, Jun. 2013.
- [25] P. Channegowda and V. John, "Filter optimization for grid interactive voltage source inverters," *IEEE Trans. Ind. Electron.*, vol. 57, no. 12, pp. 4106–4114, Dec. 2010.
- [26] K. H. Ahmed, S. J. Finney, and B. W. Williams, "Passive filter design for three-phase inverter interfacing in distributed generation," in *Proc. Compat. Power Electron. Conf.*, May/June. 2007, pp. 1–9.
- [27] R. Turner, S. Walton, and R. Duke, "Stability and bandwidth implications of digitally controlled grid-connected parallel inverters," *IEEE Trans. Power Electron.*, vol. 57, no. 11, pp. 3685–3694, Nov. 2010.
- [28] C. Xie, Y. Wang, X. Zhong, and C. Chen, "A novel active damping method for LCL-filter-based shunt active power filter," in *Proc. IEEE Int. Symp. Ind. Electron. (ISIE'12)*, 2012, pp. 64–69.
- [29] J. Dannehl, M. Liserre, and F. W. Fuchs, "Filter-based active damping of voltage source converters with LCL filter," *IEEE Trans. Ind. Electron.*, vol. 58, no. 8, pp. 3623–3633, Aug. 2011.
- [30] M. Liserre, A. D. Aquila, and F. Blaabjerg, "Genetic algorithm-based design of the active damping for an LCL-filter three-phase active rectifier," *IEEE Trans. Power Electron.*, vol. 19, no. 1, pp. 76–86, Jan. 2004.
- [31] M. Malinowski, W. Szczygiel, M. P. Kazmierkowski, and S. Bernet, "Sensorless operation of active damping methods for three-phase PWM converters," in *Proc. IEEE Int. Symp. Ind. Electron.*, Dubrovnik, Croatia, Jun. 20–23, 2005, pp. 775–780.

- [32] J. L. Agorreta, M. Borrega, J. Lopez, and L. Marroyo, "Modeling and control of N-paralleled grid-connected inverters with LCL filter coupled due to grid impedance in PV plants," *IEEE Trans. Power Electron.*, vol. 26, no. 3, pp. 770–785, Mar. 2011.
- [33] Y. Tang, P. C. Loh, P. Wang, F. H. Choo, and F. Gao, "Exploring inherent damping characteristic of LCL-filters for three-phase grid-connected voltage source inverters," *IEEE Trans. Power Electron.*, vol. 27, no. 3, pp. 1433–1443, Mar. 2012.
- [34] J. He and Y. W. Li, "Generalized closed-loop control schemes with embedded virtual impedances for voltage source converters with LC or LCL filters," *IEEE Trans. Power Electron.*, vol. 27, no. 4, pp. 1850–1861, Apr. 2012.
- [35] F. Liu, Y. Zhou, S. Duan, J. Yin, B. Liu, and F. Liu, "Parameter design of a two-current-loop controller used in a grid-connected inverter system with LCL filter," *IEEE Trans. Ind. Electron.*, vol. 56, no. 11, pp. 4483–4491, Nov. 2009.
- [36] Q. Zhang, L. Qian, C. Zhang, and D. Cartes, "Study on grid connected inverter used in high power wind generation system," in *Proc. IEEE Ind. Appl. Conf.*, Tampa, FL, Oct. 2006, pp. 1053–1058.
- [37] Y. Han, Z. Li, and J. M. Guerrero, "Dynamic evaluation of LCL type grid-connected inverters with different current feedback control schemes," in *Proc. 9th Int. Conf. Power Electron. ECCE Asia*, 2015, pp. 391–396.
- [38] A. Reznik, M. G. Simoes, A. Al-Durra, and S. M. Muyeen, "LCL Filter Design and Performance Analysis for Grid-Interconnected Systems," *IEEE Trans. Ind. Appl.*, vol. 50, pp. 1225–1232, Mar–Apr 2014.
- [39] Jinbang Xu, Jun Yang, Jie Ye, Zhixiong Zhang, Anwen Shen, "An LTCL Filter for Three-Phase Grid-Connected Converters," *IEEE Trans. Power Electron.*, vol. 29, no. 8, pp. 4322–4338, Aug. 2014.
- [40] 519-1992 IEEE Recommended Practices and Requirements for Harmonic Control in Electrical Power Systems, IEEE Std 519-1992, 1993.
- [41] 1547.1 IEEE Standard Conformance Test Procedures for Equipment Interconnecting Distributed Resources with Electric Power Systems, IEEE Std 1547.1-2005, 2005.
- [42] V. Blasko and V. Kaura, "A novel control to actively damp resonance in input LC filter of a three-phase voltage source converter," *IEEE Trans. Ind. Appl.*, vol. 33, no. 2, pp. 542–550, Mar./Apr. 1997.

- [43] R. Pena-Alzola, M. Liserre, F. Blaabjerg, M. Ordonez, and T. Kerekes, "A self-commissioning notch filter for active damping in a three-phase LCLfilter-based grid-tie converter," *IEEE Trans. Power Electron.*, vol. 29, no. 12, pp. 6754–6761, Dec. 2014. doi:10.1109/TPEL.2014.2304468.
- [44] Zhen Xin, Xiongfei Wang, Poh Chiang Loh, Frede Blaabjerg, "Grid-Current-Feedback Control for LCL-Filtered Grid Converters with Enhanced Stability," *IEEE Trans. Power Electron.*, vol. 32, no. 4, pp. 3216-3228, April 2017.
- [45] Jinwei He, Yun Wei Li, Dehong Xu, Xiaodong Liang, Beihua Liang, Chengshan Wang, "Deadbeat Weighted Average Current Control with Corrective Feed-Forward Compensation for Microgrid Converters with Nonstandard LCL Filter," *IEEE Transactions on Power Electronics.*, vol. 32, no. 4, pp. 2661-2674, April 2014.
- [46] G. Shen, D. Xu, L. Cao, and X. Zhu, "An improved control strategy for grid-connected voltage source inverters with an LCL filter," *IEEE Trans. Power Electron.*, vol. 23, no. 4, pp. 1899–1906, Jan. 2008.
- [47] Jianjun Sun, Yi Wang, Jinwu Gong, Xiaoming Zha, Shangsheng Li, "Adaptability of weighted average current control to the weak grid considering the effect of grid-voltage feedforward," in *2017 IEEE Applied Power Electronics Conference and Exposition (APEC)*, 26-30 March 2017, pp. 3530-3535.
- [48] Weimin Wu, Yuan Liu, Yuanbin He, Henry Shu-Hung Chung, Marco Liserre, Frede Blaabjerg, "Damping Methods for Resonances Caused by LCL-Filter-Based Current-Controlled Grid-Tied Power Inverters: An Overview," *IEEE Transactions on Industrial Electronics.*, vol. 64, no. 9, pp. 7402-7413, Sept. 2017.
- [49] R. N. Beres, X. Wang, F. Blaabjerg, M. Liserre, and C. L. Bak, "Optimal design of high-order passive-damped filters for grid-connected applications," *IEEE Trans. Power Electron.*, vol. 31, no. 3, pp. 2083–2098, Mar. 2016.
- [50] B. Bolsens, K. De Brabandere, J. Van den Keybus, J. Driesen, and R. Belmans, "Model-based generation of low distortion currents in grid coupled PWM-inverters using an LCL output filter," *IEEE Trans. Power Electron.*, vol. 21, no. 4, pp. 1032–1040, Jul. 2006.
- [51] Weimin Wu, Yunjie Sun, Min Huang, Xiongfei Wang, Huai Wang, Frede Blaab, "A Robust Passive Damping Method for LLCL-Filter-Based Grid-Tied Inverters to Minimize the Effect of Grid Harmonic Voltages," *IEEE Transactions on Power Electronics.*, vol. 29, no. 7, pp. 3279-3289, July 2014.

- [52] J. Dannehl, F. W. Fuchs, S. Hansen, and P. B. Thøgersen, "Investigation of active damping approaches for PI-based current control of grid-connected pulse width modulation converters with LCL filters," *IEEE Trans. Ind. Appl.*, vol. 46, no. 4, pp. 1509–1517, Jul.–Aug. 2010.
- [53] Roner André Liston, Emerson Giovanni Carati, Rafael Cardoso, Jean P, "A Robust Design of Active Damping with a Current Estimator for Single-Phase Grid-Tied Inverters," *IEEE Transactions on Industry Applications*, vol. 54, no. 5, pp. 4672-4681, Sept.-Oct 2018.
- [54] S. G. Parker, B. P. McGrath, and D. G. Holmes, "Regions of active damping control for LCL filters," *IEEE Trans. Ind. Appl.*, vol. 50, no. 1, pp. 424–432, Jan. 2014.
- [55] Aratrik Sarkar, Karan Puttannaiah, Armando A. Rodriguez, "Inner-Outer Loop based Robust Active Damping for LCL Resonance in Grid-Connected Inverters using Grid Current Feedback," in *2018 Annual American Control Conference (ACC)*, 27-29 June 2018, pp. 6766-6771.
- [56] C. Wessels et al., "Active damping of lcl-filter resonance based on virtual resistor for pwm rectifiers & stability analysis with different filter parameters," *IEEE Power Electronics Specialists Conference*, pp 3532-3538, 2008.
- [57] Michael J. Ryan and Robert D. Lorenz, "A High-Performance Sine Wave Inverter Controller with Capacitor Current Feedback and "Back-EMF" Decoupling," in *Proceedings of PESC '95*, 2002, pp. 507-513.
- [58] Michael J. Ryan, William E. Brumsickle, and Robert D. Lorenz, "Control Topology Options for Single-Phase UPS Inverters," *IEEE TRANSACTIONS ON INDUSTRY APPLICATIONS*, VOL. 33, pp. 493-501, MARCH/APRIL 1997.

## APPENDIX

In this section, the coding in C language for designing the controller of the three-phase grid-tied inverter system with LCL filter has been presented for WACC\_EAD method.

The coding for the controller design is shown as:

```

#define GLOBAL_Q 20
long GlobalQ = GLOBAL_Q; // Used for legacy GEL & Graph Debug.
#include "IQmathLib.h"
#include "PS_bios.h"
#define GetCurTime() PS_GetSysTimer()
#define PWM_IN_CHECK // To lower PWM value setting time, comment out
this line if PWM duty cycle values are strictly limited in the range.
interrupt void Task();
void TaskS4(_iq20 fIn0, _iq30 fIn1, _iq20 *fOut0);
void TaskS2(_iq20 fIn0, _iq30 fIn1, _iq20 *fOut0);
const Uint16 PSD_CpuClock = 60; // MHz
extern _iq fGbla;
extern _iq fGblb;
extern _iq fGbld_Vg;
extern _iq fGblq_Vg;
extern _iq fGbl0_Vg;
extern _iq fGbltheta;
extern _iq fGblVgd_a;
extern _iq fGblVgd_b;
extern _iq fGblVgd_c;
extern _iq fGblIgd_a;
extern _iq fGblIgd_b;
extern _iq fGblIgd_c;
extern _iq fGblInvd_a;
extern _iq fGblInvd_b;
extern _iq fGblInvd_c;
extern _iq fGbld_Ig0;
extern _iq fGblq_Ig0;
extern _iq fGblsinwt;
extern _iq fGblS4_Ui;
extern _iq fGblS4_Up;
extern _iq fGblS4_SatErr;
extern _iq fGblS2_Ui;
extern _iq fGblS2_Up;
extern _iq fGblS2_SatErr;
_iq fGbla = 0;
_iq fGblb = 0;

```

```

_iq    fGblD_Vg = 0;
_iq    fGblq_Vg = 0;
_iq    fGbl0_Vg = 0;
_iq    fGbltheta = 0;
_iq    fGblVgd_a = 0;
_iq    fGblVgd_b = 0;
_iq    fGblVgd_c = 0;
_iq    fGblIgd_a = 0;
_iq    fGblIgd_b = 0;
_iq    fGblIgd_c = 0;
_iq    fGblIinvd_a = 0;
_iq    fGblIinvd_b = 0;
_iq    fGblIinvd_c = 0;
_iq    fGblD_Ig0 = 0;
_iq    fGblq_Ig0 = 0;
_iq    fGblsinwt = 0;
interrupt void Task()
{
    _iq20 fSIN_R4, fAB_ABC1_2, fAB_ABC1_1, fAB_ABC1, fDQ_AB1_1,
fDQ_AB1, fFunVar132;
    _iq20 fSUM2, fFunVar130, fSUM1, fAB_DQ1_1, fAB_DQ1, fABC_AB2_1,
fABC_AB2;
    _iq20 fSUMP3, fP6, fP5, fSUMP2, fP4, fP3, fSUMP1, fP2, fP1, fZOH10,
fSUM5;
    _iq20 fZOH12, fSUM6, fZOH11, fSUM7, fZOH13, fSUM8, fZOH14, fSUM9,
fZOH15;
    _iq20 fSUM10, fABC2_2, fABC2_1, fABC2, fSUMP13, fMULT2, fATAN22,
fABC_AB1_1;
    _iq20 fABC_AB1, fZOH16, fSUM11, fZOH17, fSUM12, fZOH18, fSUM13;
    _iq21 fPSM_F2803x_ADC1_9, fPSM_F2803x_ADC1_10,
fPSM_F2803x_ADC1_11;
    _iq22 fPSM_F2803x_ADC1, fPSM_F2803x_ADC1_1,
fPSM_F2803x_ADC1_2, fPSM_F2803x_ADC1_3;
    _iq22 fPSM_F2803x_ADC1_4, fPSM_F2803x_ADC1_5, fC12;
    _iq23 fC11;
    _iq26 fC6;
    _iq29 fC14;
    _iq30 fC7, fC3, fC13;
    fPSM_F2803x_ADC1_11 = PS_GetDcAdc(11);
    fC12 = _IQ22(400);
    fSUM13 = ((fPSM_F2803x_ADC1_11) >> 1) - ((fC12) >> 2);
    fZOH18 = fSUM13;
    fPSM_F2803x_ADC1_10 = PS_GetDcAdc(10);
    fSUM12 = ((fPSM_F2803x_ADC1_10) >> 1) - ((fC12) >> 2);
    fZOH17 = fSUM12;
    fPSM_F2803x_ADC1_9 = PS_GetDcAdc(9);

```

```

fSUM11 = ((fPSM_F2803x_ADC1_9) >> 1) - ((fC12) >> 2);
fZOH16 = fSUM11;
fC13 = _IQ30(-(1.0));
// ABC to alpha/beta transformation
fABC_AB1 = _IQ20mpyIQX(_IQ30(1.0/3.0), 30, ((fZOH18) << 1) - fZOH17 -
fZOH16, 20);
fABC_AB1_1 = _IQ20mpyIQX(_IQ30(0.57735027), 30, fZOH17 - fZOH16, 20);
// uvw2ab
#ifdef _DEBUG
fGbla = fABC_AB1;
#endif

#ifdef _DEBUG
fGblb = fABC_AB1_1;
#endif

fATAN22 = _IQ20atan2(fABC_AB1, fABC_AB1_1);
fMULT2 = _IQ20mpyIQX(fC13, 30, fATAN22, 20);
fC14 = _IQ29(22.0/7.0);
fSUMP13 = fMULT2 + ((fC14) >> 9);
{
// ABC to DQ transformation
_iq20 angle1 = fSUMP13 - _IQ20(2*3.14159265/3);
_iq20 angle2 = fSUMP13 + _IQ20(2*3.14159265/3);
fABC2 = _IQ20mpyIQX(_IQ20cos(fSUMP13), 20, fZOH18, 20);
fABC2 += _IQ20mpyIQX(_IQ20cos(angle1), 20, fZOH17, 20);
fABC2 += _IQ20mpyIQX(_IQ20cos(angle2), 20, fZOH16, 20);
fABC2 = _IQ20mpyIQX(fABC2, 20, _IQ30(2.0/3.0), 30);
fABC2_1 = _IQ20mpyIQX(_IQ20sin(fSUMP13), 20, fZOH18, 20);
fABC2_1 += _IQ20mpyIQX(_IQ20sin(angle1), 20, fZOH17, 20);
fABC2_1 += _IQ20mpyIQX(_IQ20sin(angle2), 20, fZOH16, 20);
fABC2_1 = _IQ20mpyIQX(fABC2_1, 20, _IQ30(2.0/3.0), 30);
fABC2_2 = (fZOH18 + fZOH17 + fZOH16);
fABC2_2 = _IQ20mpyIQX(fABC2_2, 20, _IQ30(1.0 / 3.0), 30);
}
#ifdef _DEBUG
fGbld_Vg = fABC2;
#endif
#ifdef _DEBUG
fGblq_Vg = fABC2_1;
#endif
#ifdef _DEBUG
fGbl0_Vg = fABC2_2;
#endif
#ifdef _DEBUG
fGbltheta = fSUMP13;

```

```

#endif
#ifdef _DEBUG
    fGblVgd_a = fZOH18;
#endif
#ifdef _DEBUG
    fGblVgd_b = fZOH17;
#endif
#ifdef _DEBUG
    fGblVgd_c = fZOH16;
#endif
    fPSM_F2803x_ADC1_5 = PS_GetDcAdc(5);
    fC11 = _IQ23(165);
    fSUM10 = ((fPSM_F2803x_ADC1_5) >> 2) - ((fC11) >> 3);
    fZOH15 = fSUM10;
#ifdef _DEBUG
    fGblIgd_a = fZOH15;
#endif
    fPSM_F2803x_ADC1_4 = PS_GetDcAdc(4);
    fSUM9 = ((fPSM_F2803x_ADC1_4) >> 2) - ((fC11) >> 3);
    fZOH14 = fSUM9;
#ifdef _DEBUG
    fGblIgd_b = fZOH14;
#endif
    fPSM_F2803x_ADC1_3 = PS_GetDcAdc(3);
    fSUM8 = ((fPSM_F2803x_ADC1_3) >> 2) - ((fC11) >> 3);
    fZOH13 = fSUM8;
#ifdef _DEBUG
    fGblIgd_c = fZOH13;
#endif
    fPSM_F2803x_ADC1_2 = PS_GetDcAdc(2);
    fSUM7 = ((fPSM_F2803x_ADC1_2) >> 2) - ((fC11) >> 3);
    fZOH11 = fSUM7;
#ifdef _DEBUG
    fGblInvd_a = fZOH11;
#endif
    fPSM_F2803x_ADC1_1 = PS_GetDcAdc(1);
    fSUM6 = ((fPSM_F2803x_ADC1_1) >> 2) - ((fC11) >> 3);
    fZOH12 = fSUM6;
#ifdef _DEBUG
    fGblInvd_b = fZOH12;
#endif
    fPSM_F2803x_ADC1 = PS_GetDcAdc(0);
    fSUM5 = ((fPSM_F2803x_ADC1) >> 2) - ((fC11) >> 3);
    fZOH10 = fSUM5;
#ifdef _DEBUG
    fGblInvd_c = fZOH10;

```

```

#endif
    fC3 = _IQ30(0);
    fP1 = _IQ20mpyIQX(fZOH11, 20, _IQ30(0.84), 30); // fZOH11 * 0.84
    fP2 = _IQ20mpyIQX(fZOH15, 20, _IQ30(0.16), 30); // fZOH15 * 0.16
    fSUMP1 = fP1 + fP2;
    fP3 = _IQ20mpyIQX(fZOH12, 20, _IQ30(0.84), 30); // fZOH12 * 0.84
    fP4 = _IQ20mpyIQX(fZOH14, 20, _IQ30(0.16), 30); // fZOH14 * 0.16
    fSUMP2 = fP3 + fP4;
    fP5 = _IQ20mpyIQX(fZOH10, 20, _IQ30(0.84), 30); // fZOH10 * 0.84
    fP6 = _IQ20mpyIQX(fZOH13, 20, _IQ30(0.16), 30); // fZOH13 * 0.16
    fSUMP3 = fP5 + fP6;
    // ABC to alpha/beta transformation
    fABC_AB2 = _IQ20mpyIQX(_IQ30(1.0/3.0), 30, ((fSUMP1) << 1) - fSUMP2 -
fSUMP3, 20);
    fABC_AB2_1 = _IQ20mpyIQX(_IQ30(0.57735027), 30, fSUMP2 - fSUMP3,
20); // uvw2ab
    {
        // alpha/beta to DQ transformation
        _iq20 sinv, cosv;
        sinv = _IQ20sin(fSUMP13);
        cosv = _IQ20cos(fSUMP13);
        fAB_DQ1 = _IQ20mpyIQX(cosv, 20, fABC_AB2, 20) +
_IQ20mpyIQX(sinv, 20, fABC_AB2_1, 20);
        fAB_DQ1_1 = _IQ20mpyIQX(cosv, 20, fABC_AB2_1, 20) -
_IQ20mpyIQX(sinv, 20, fABC_AB2, 20); // ab2dq
    }
#ifdef _DEBUG
    fGblD_Ig0 = fAB_DQ1;
#endif
#ifdef _DEBUG
    fGblQ_Ig0 = fAB_DQ1_1;
#endif
    fSUM1 = ((fC3) >> 10) - fAB_DQ1;
    fC7 = _IQ30(0);
    TaskS4(fSUM1, fC7, &fFunVar130);
    fC6 = _IQ26(-(27.5));
    fSUM2 = ((fC6) >> 6) - fAB_DQ1_1;
    TaskS2(fSUM2, fC7, &fFunVar132);
    { // ab2dq
        // DQ to alpha/beta transformation
        _iq20 sinv = _IQ20sin(fSUMP13);
        _iq20 cosv = _IQ20cos(fSUMP13);
        fDQ_AB1 = _IQ20mpyIQX(cosv, 20, fFunVar130, 20) -
_IQ20mpyIQX(sinv, 20, fFunVar132, 20);
        fDQ_AB1_1 = _IQ20mpyIQX(sinv, 20, fFunVar130, 20) +
_IQ20mpyIQX(cosv, 20, fFunVar132, 20);
    }

```

```

    }
    {
        // alpha/beta to ABC transformation
        _iq20 temp1, temp2;
        temp1 = ((fDQ_AB1) >> 1);
        temp2 = _IQ20mpyIQX(_IQ30(0.86602540), 30, fDQ_AB1_1, 20);
        fAB_ABC1 = fDQ_AB1; // ab2uvw
        fAB_ABC1_1 = temp2 - temp1;
        fAB_ABC1_2 = -(temp1 + temp2);
    }
    fSIN_R4 = _IQ20sin(fSUMP13);
#ifdef _DEBUG
    fGblsinwt = fSIN_R4;
#endif
    // Start of changing PWM1(3ph) registers
    // Set Duty Cycle of U
#ifdef PWM_IN_CHECK
    if (fAB_ABC1 <= _IQ20((-1.0))) {
        PWM_CMPA(1) = PWM_TBPRD(1);
    } else if (fAB_ABC1 >= _IQ20(2 + (-1.0))) {
        PWM_CMPA(1) = 0;
    } else {
#else
    {
#endif
        _iq24_val = _IQ24mpyIQX(_IQ20(2 + (-1.0))) - fAB_ABC1, 20,
        _IQ30(1.0/2), 30);
        PWM_CMPA(1) = _IQ1mpyIQX(PWM_TBPRD(1), 1, _val, 24);
    }
    // Set Duty Cycle of V
#ifdef PWM_IN_CHECK
    if (fAB_ABC1_1 <= _IQ20((-1.0))) {
        PWM_CMPA(1+1) = PWM_TBPRD(1);
    } else if (fAB_ABC1_1 >= _IQ20(2 + (-1.0))) {
        PWM_CMPA(1+1) = 0;
    } else {
#else
    {
#endif
        _iq24_val = _IQ24mpyIQX(_IQ20(2 + (-1.0))) - fAB_ABC1_1, 20,
        _IQ30(1.0/2), 30);
        PWM_CMPA(1+1) = _IQ1mpyIQX(PWM_TBPRD(1), 1, _val, 24);
    }
    // Set Duty Cycle of W
#ifdef PWM_IN_CHECK
    if (fAB_ABC1_2 <= _IQ20((-1.0))) {

```

```

        PWM_CMPA(1+2) = PWM_TBPRD(1);
    } else if (fAB_ABC1_2 >= _IQ20(2 + (-(1.0)))) {
        PWM_CMPA(1+2) = 0;
    } else {
#else
    {
#endif
        _iq24_val = _IQ24mpyIQX(_IQ20(2 + (-(1.0))) - fAB_ABC1_2, 20,
        _IQ30(1.0/2), 30);
        PWM_CMPA(1+2) = _IQ1mpyIQX(PWM_TBPRD(1), 1, _val, 24);
    }
    // End of changing PWM1(3ph) registers
    PS_ExitAdcIntr(1, M__INT1);
}

// Parameter list for S4
// Parameter list for S4
#define S4_fsamp 10E3
#define S4_Kp 0.004
#define S4_Ki 0.1
#define S4_Kd 0.0001
#define S4_Kc 0.0
#define S4_Umax 1.0
#define S4_Umin (-(1.0))
_iq fGblS4_Ui = 0;
_iq fGblS4_Up = 0;
_iq fGblS4_SatErr = 0;
void TaskS4(_iq20 fIn0, _iq30 fIn1, _iq20 *fOut0)
{
    _iq20 fS4_SatErr, fS4_SUM1_1, fS4_Up, fS4_Ui, fS4_OutPreSat,
fS4_MUX229;
    _iq20 fS4_SUM31, fS4_Kc, fS4_Ki, fS4_Kd, fS4_SUM2, fS4_Kp;
    _iq30 fS4_VCC41;
    fS4_Ui = fGblS4_Ui;
    fS4_Up = fGblS4_Up;
    fS4_SatErr = fGblS4_SatErr;
    fS4_Kp = _IQ20mpyIQX(fIn0, 20, _IQ30(S4_Kp), 30); // fIn0 * S4_Kp
    fS4_SUM2 = fS4_Kp - fS4_Up;
    fS4_Kd = _IQ20mpyIQX(fS4_SUM2, 20, _IQ30(S4_Kd), 30); // fS4_SUM2
* S4_Kd
    fS4_Ki = _IQ20mpyIQX(fS4_Kp, 20, _IQ30(S4_Ki), 30); // fS4_Kp * S4_Ki
    fS4_Kc = _IQ20mpyIQX(fS4_SatErr, 20, _IQ30(S4_Kc), 30); // fS4_SatErr *
S4_Kc
    fS4_SUM31 = fS4_Ui
        + fS4_Ki
        + fS4_Kc;

```

```

fS4_VCC41 = _IQ30(0);
fS4_MUX229 = (fIn1 > _IQ30(0.5)) ? ((fS4_VCC41) >> 10) : fS4_SUM31;
fS4_OutPreSat = fS4_Kd
                + fS4_Kp
                + fS4_MUX229;
*fOut0 = (fS4_OutPreSat > _IQ20(S4_Umax)) ? _IQ20(S4_Umax) :
((fS4_OutPreSat < _IQ20(S4_Umin)) ? _IQ20(S4_Umin) : (fS4_OutPreSat));
fGblS4_Ui = fS4_MUX229;
fGblS4_Up = fS4_Kp;
fS4_SUM1_1 = *fOut0 - fS4_OutPreSat;
fGblS4_SatErr = fS4_SUM1_1;
}

// Parameter list for S2
// Parameter list for S2
#define S2_fsamp 10E3
#define S2_Kp 0.004
#define S2_Ki 0.1
#define S2_Kd 0.0001
#define S2_Kc 0.0
#define S2_Umax 1.0
#define S2_Umin (-(1.0))
_iq fGblS2_Ui = 0;
_iq fGblS2_Up = 0;
_iq fGblS2_SatErr = 0;
void TaskS2(_iq20 fIn0, _iq30 fIn1, _iq20 *fOut0)
{
    _iq20 fS2_SatErr, fS2_SUM1_1, fS2_Up, fS2_Ui, fS2_OutPreSat,
fS2_MUX229;
    _iq20 fS2_SUM31, fS2_Kc, fS2_Ki, fS2_Kd, fS2_SUM2, fS2_Kp;
    _iq30 fS2_VCC41;

    fS2_Ui = fGblS2_Ui;

    fS2_Up = fGblS2_Up;

    fS2_SatErr = fGblS2_SatErr;

    fS2_Kp = _IQ20mpyIQX(fIn0, 20, _IQ30(S2_Kp), 30); // fIn0 * S2_Kp
    fS2_SUM2 = fS2_Kp - fS2_Up;
    fS2_Kd = _IQ20mpyIQX(fS2_SUM2, 20, _IQ30(S2_Kd), 30); // fS2_SUM2
* S2_Kd
    fS2_Ki = _IQ20mpyIQX(fS2_Kp, 20, _IQ30(S2_Ki), 30); // fS2_Kp * S2_Ki
    fS2_Kc = _IQ20mpyIQX(fS2_SatErr, 20, _IQ30(S2_Kc), 30); // fS2_SatErr *
S2_Kc

```

```

    fS2_SUM31 = fS2_Ui
                + fS2_Ki
                + fS2_Kc;
    fS2_VCC41 = _IQ30(0);
    fS2_MUX229 = (fIn1 > _IQ30(0.5)) ? ((fS2_VCC41) >> 10) : fS2_SUM31;
    fS2_OutPreSat = fS2_Kd
                + fS2_Kp
                + fS2_MUX229;
    *fOut0 = (fS2_OutPreSat > _IQ20(S2_Umax)) ? _IQ20(S2_Umax) :
    ((fS2_OutPreSat < _IQ20(S2_Umin)) ? _IQ20(S2_Umin) : (fS2_OutPreSat));
    fGblS2_Ui = fS2_MUX229;
    fGblS2_Up = fS2_Kp;
    fS2_SUM1_1 = *fOut0 - fS2_OutPreSat;
    fGblS2_SatErr = fS2_SUM1_1;
}
void Initialize(void)
{
    PS_SysInit(0, 10, 12);
    PS_StartStopPwmClock(0); // Stop Pwm Clock
    PS_InitTimer(0, 0);
    PS_AdInit();
    {
        int i;
        /* TAdcAttr: Channel No., Soc No., Trig Src, INTADC#, Window Size, Gain
*/
        const TAdcAttr aryAdcInit[9] = {{0, 0, ADCTRIG_PWM1, 1, 6,
_IQ22(165.0/1.5)},
                {1, 1, ADCTRIG_PWM1, 1, 6, _IQ22(165.0/1.5)},
                {2, 2, ADCTRIG_PWM1, 1, 6, _IQ22(165.0/1.5)},
                {3, 3, ADCTRIG_PWM1, 1, 6, _IQ22(165.0/1.5)},
                {4, 4, ADCTRIG_PWM1, 1, 6, _IQ22(165.0/1.5)},
                {5, 5, ADCTRIG_PWM1, 1, 6, _IQ22(165.0/1.5)},
                {9, 6, ADCTRIG_PWM1, 1, 6, _IQ21(300.0/1.5)},
                {10, 7, ADCTRIG_PWM1, 1, 6, _IQ21(300.0/1.5)},
                {11, 8, ADCTRIG_PWM1, 1, 6, _IQ21(300.0/1.5)}};
        const TAdcAttr *p = aryAdcInit;
        for (i = 0; i < 9; i++, p++) {
            PS_SetAdcChn(p->nIntrNo, p->nChnNo, p->nSocNo, p->nTrigSrc, p-
>nWindSz, p->nGain);
        }
    }

    PS_InitPwm3ph(1, 3, _IQ8(1.0e6/((double)10000*1)), _IQ24((0E-6) * 1.0e6));
    // pwnNo, waveType, frequency, deadtime
    PS_SetPwm3ph1AdcIntr(ePwmIntrAdc, 1, _IQ24(0));
    PS_SetPwm3ph1Vector(ePwmIntrAdc, 8, 0, Task);

```

```
PS_SetPwm3ph1TzAct(eTZHighImpedance);  
PS_SetPwm3ph1UvwSL(_IQ24(0), _IQ24(0), _IQ24(0));  
PS_StartPwm3ph1();
```

```
PS_StartStopPwmClock(1); // Start Pwm Clock
```

```
}
```

```
void main()
```

```
{
```

```
Initialize();
```

```
PS_EnableIntr(); // Enable Global interrupt INTM
```

```
PS_EnableDbgm();
```

```
for (;) {
```

```
}
```

```
}
```